UNIVERSITY OF SÃO PAULO
INSTITUTE OF GEOSCIENCES

# Investigation of luminescence signals of quartz and their application for provenance analysis and extending dating range of Brazilian fluvial sediments

**Pontien Niyonzima**

Project Supervisor: Prof. Dr. André Oliveira Sawakuchi

Doctoral Thesis

Program of Post-Graduate in Geochemistry and Geotectonics

São Paulo

2022

UNIVERSITY OF SÃO PAULO
INSTITUTE OF GEOSCIENCES

# Investigation of luminescence signals of quartz and their application for provenance analysis and extending dating range of Brazilian fluvial sediments

**Pontien Niyonzima**

Thesis submitted to the Institute of Geosciences, University of São Paulo, in fulfilment of the requirements of the degree of Doctor (Ph.D.) of Science in Geosciences.

Area of concentration: Geochemistry and Geotectonics

Supervisor: Prof. Dr. André Oliveira Sawakuchi

São Paulo

2022

# Dedication

This thesis is dedicated to my wife

Belyse Ingabire Niyonzima,

My Daughters

Belinda Shami Niyonzima,

Abby Liz Hayla Niyonzima

Gabby Julia Kayla Niyonzima

Serviço de Biblioteca e Documentação do IGc/USP

Ficha catalográfica gerada automaticamente com dados fornecidos pelo(a) autor(a)via programa desenvolvido pela Seção Técnica de Informática do ICMC/USP

Bibliotecários responsáveis pela estrutura de catalogação da publicação: Sonia Regina Yole Guerra - CRB-8/4208 | Anderson de Santana - CRB-8/6658

Niyonzima, Pontien
Investigation of luminescence signals of quartz and their application for provenance analysis and extending dating range of Brazilian fluvial sediments / Pontien Niyonzima; orientador Andre Oliveira Sawakuchi. -- São Paulo, 2022.
94 p.

Tese (Doutorado - Programa de Pós-Graduação em Geoquímica e Geotectônica) -- Instituto de Geociências, Universidade de São Paulo, 2022.

1. Radiofluorescence. 2. Optically stimulated luminescence. 3. Violet stimulated luminescence. 4. Ironstones. 5. Fluvial sediments. I. Sawakuchi, Andre Oliveira, orient. II. Título.

UNIVERSIDADE DE SÃO PAULO

INSTITUTO DE GEOCIÊNCIAS

# Investigation of luminescence signals of quartz and their application for provenance analysis and extending dating range of Brazilian fluvial sediments

**PONTIEN NIYONZIMA**

Orientador: Prof. Dr. André Oliveira Sawakuchi

Tese de Doutorado

**Nº 643**

COMISSÃO JULGADORA

Dr. André Oliveira Sawakuchi

Dra. Priscila Emerich Souza

Dra. Sonia Tatumi

Dr. Carlos Conforti Ferreira Guedes

Dr. Daniel Rodrigues do Nascimento Junior

SÃO PAULO

2022

# Acknowledgement

I would like to express my gratitude to the Almighty God for the gift of life and his guidance during this journey of four years of doctoral studies.

First and foremost, I would like to thank my supervisor Prof. Dr. André Oliveira Sawakuchi, who has been a tremendous support, since the first time I contacted him to start this project. Despite André´s busy and hectic work life, he has always prioritised finding the time for me, regardless of importance of the issue at hand. I owe a debt of gratitude to André, but I do not have any idea of how I will pay but for sure I pay it on the due time. André, thank you for being such a good supervisor for me, Almighty God bless you abundantly.

I would also like to thank Raquel for all help I have received from you since my first day in Brazil, particularly your support in the struggles for my visa registration, looking for accommodation. I will cherish all your support during this period of my PhD studies.

I also wish to express my gratitude to Dr. Naomi Porat (Luminescence Dating Laboratory, Israel Geological Survey) for her support throughout this entire work. I am very grateful for her willingness to share with us her knowledge in revising, commenting, suggesting on the articles in this thesis for them to meet the publication standards.

Grateful acknowledgement is made the my colleagues of Luminescence and Gamma Spectrometry Laboratory (LEGaL), Institute of Geosciences, University of São Paulo, for the warm manner by which they welcomed me there. I thank them for the many useful discussions and suggestions, and for the great time before, in between and after scientific sessions. Acknowledging and thanking everyone that have helped and supported me during the last four years.

I am very grateful to National Council for Science and Technology Development (CNPq), The World Academy of Sciences (TWAS) (CNPq/TWAS grant 154507/2017-2) and The São Paulo Research Foundation (FAPESP grant 2019/04059-6) for funding my PhD fellowship at the University of São Paulo.

# Abstract

This work investigates the feasibility of applying quartz radiofluorescence (RF) as provenance proxy, carried out experiments to evaluate if violet stimulated luminescence (VSL) of quartz is able to extend the dating age range of fluvial sediments in Brazil, and performed optically stimulated luminescence (OSL) dating to establish formation ages of ferruginous deposits (ironstones) of the Xingu River in Eastern Amazonia. The focus on luminescence properties of quartz from fluvial deposits is motivated by their widespread occurrence across Brazil, land of large rivers, thus, representing the most important continental record of landscape changes during the Quaternary.

Firstly, the work examines RF emissions in quartz from parent rocks (igneous plutonic and volcanic) and sediments of different provenances. After deconvolution of RF spectra into its emission bands, emission band intensities were plotted versus OSL (first 1s) and 110°C thermoluminescence (TL) peak sensitivies to investigation whether RF emission band intensity can be used as sediment provenance. It has been shown that ultraviolet (UV) RF intensity correlates with both OSL and TL sensitivities of quartz from sediments. This correlation supported the suggestion that both 110°C TL peak and OSL of quartz use the same recombination centers rather than the same electron trap and that sensitization processes in nature of two signals might be due to the changes in recombination probability instead of changes in charge trapping probability. It is concluded that UV-RF intensity measured using X-ray sources can also be used for provenance analysis of sediments in the same way as the OSL and TL sensitivities.

Characteristics of VSL signals of quartz from major fluvial systems from Western Brazil (Pantanal), Southeastern Brazil (Paraná River basin) and Central and Eastern Amazonia were investigated to assess if the VSL signal is suitable to extend the age range of luminescence dating of fluvial sediments. Single-aliquot regenerative dose (SAR), multiple aliquots regenerative dose (MAR) and multiple aliquots additive dose (MAAD) protocols were used to estimate the maximum dose that can be estimate by VSL signals for Brazilian sediments. Quartz VSL was found to significantly increase the dating limit to the Early Pleistocene (~800 ka to 1.6 Ma for the $2D_0$ MAAD) even with the relatively lower characteristic doses ($D_0$) observed in dose response curves of the studied samples. Despite the improvement in luminescence age range of Brazilian

fluvial sediments using VSL dating relative to the conventional OSL dating, the behavior of VSL appears to be sample dependent, with natural VSL signal missing in samples from Amazonian settings.

In the estimation of formation ages of ironstones from the Xingu River, ages between ~60 ka and 3 ka were obtained using the SAR OSL dating protocol. This indicates that ironstones of the Xingu River result from a Late Pleistocene and Holocene surface geochemical system able to precipitate goethite and cement fluvial sediments under transport. The high dose rates (2.7-12.3 Gy $ka^{-1}$) of these fluvial deposits limits the OSL dating to the last ~60 ka, assuming maximum doses of ~200 Gy estimated using quartz OSL applied to fluvial deposits across Brazil.

The performed investigations improve the applicability of luminescence signals (RF, OSL and VSL) to obtain provenance and depositional age data from a variety of fluvial deposits occurring over Brazil. This is a contribution to expand the application of luminescence methods to study fluvial deposits.

**Keywords**: Radiofluorescence; Optically stimulated luminescence, Ironstones; Violet stimulated luminescence; Fluvial sediments.

# Resumo

Este trabalho investigou a viabilidade da aplicação de radiofluorescência (RF) do quartzo como indicador (*proxy*) de proveniência, realizou experimentos para avaliar se a luminescência do quartzo estimulada por luz violeta (VSL, em inglês) é capaz de estender o intervalo temporal da datação de sedimentos fluviais no Brasil e realizou datações por luminescência opticamente estimulada (OSL, em inglês) para estabelecer idades de formação de depósitos ferruginosos (*ironstones*) do rio Xingu na Amazônia Oriental. Assim, esta tese de doutoramento buscou desenvolver aplicações das características de luminescência do quartzo no estudo de depósitos fluviais quaternários. Isto foi motivado pela ampla ocorrência de depósitos fluviais no Brasil, terra dos grandes rios, os quais geraram importante registro continental de mudanças de paisagem e do clima durante o Quaternário.

Inicialmente, o trabalho examinou as emissões de RF em quartzo de rochas fonte (ígneas plutônicas e vulcânicas) e sedimentos de diferentes proveniências. Após a deconvolução dos espectros de RF em suas bandas de emissão, as intensidades das bandas de emissão foram comparadas com as sensibilidades OSL (primeiro 1s) e termoluminescência (TL, pico a 110°C) para investigar se a intensidade da banda de emissão de RF pode ser usada como indicador de proveniência sedimentar. Foi demonstrado que a intensidade de RF ultravioleta (UV) se correlaciona com as sensibilidades OSL e TL do quartzo de sedimentos. Essa correlação apoiou a sugestão de que tanto o pico TL de 110°C quanto o OSL de quartzo usam os mesmos centros de recombinação em vez da mesma armadilha de elétrons e que a sensibilização natural dos sinais OSL e TL pode ocorrer devido às mudanças na probabilidade de recombinação em vez de mudanças na probabilidade de captura de cargas. Conclui-se que a intensidade de UV-RF medida com fonte de raios X também pode ser utilizada para análise de proveniência de sedimentos da mesma forma que as sensibilidades OSL e TL.

Características dos sinais VSL de quartzo dos principais sistemas fluviais do Oeste do Brasil (Pantanal), Sudeste do Brasil (bacia do Rio Paraná) e Amazônia Central e Oriental foram investigadas para avaliar se o sinal VSL é adequado para estender o intervalo de tempo da datação por luminescência de sedimentos fluviais brasileiros . Os protocolos de dose regenerativa de alíquota única (SAR, em inglês), dose regenerativa

de alíquotas múltiplas (MAR, em inglês) e dose aditiva de alíquotas múltiplas (MAAD, em inglês) foram usados para estimar a dose máxima que pode ser medida por sinais VSL do quartzo presente em sedimentos quaternários brasileiros. Conclui-se que o sinal VSL do quartzo pode aumentar significativamente o limite de datação até o Pleistoceno Inicial (~800 ka a 1,6 Ma para $2D_0$ obtida por MAAD), mesmo com doses características relativamente mais baixas ($D_0$) observadas nas curvas de dose-resposta das amostras estudadas, se comparadas com outros estudos da literatura. Apesar da VSL ampliar o intervalo de tempo da datação por luminescência dos sedimentos fluviais brasileiros, em relação à datação OSL convencional, o comportamento do sinal VSL parece ser dependente da origem amostra. Isto é sustentado pela ausência de sinal VSL natural em amostras de quartzo derivadas dos depósitos fluviais amazônicos estudados.

Na estimativa das idades de formação dos *ironstones* do rio Xingu, idades entre ~60 ka e 3 ka foram obtidas por meio do protocolo de datação SAR OSL em alíquotas de quartzo. Isso indica que as rochas ferruginosas do rio Xingu resultam de sistema geoquímico superficial do Pleistoceno Tardio e Holoceno, capaz de precipitar goethita e aprisionar sedimentos detríticos em transporte no canal do rio Xingu. As altas taxas de dose (2,7-12,3 Gy $ka^{-1}$) desses depósitos fluviais limitam a datação OSL para os últimos ~60 ka, assumindo doses máximas de ~200 Gy estimadas a partir da dose característica ($D_0$) das curvas de dose resposta.

As investigações realizadas contribuem para entender a sensibilização natural de sinais OSL e TL, processo ainda pouco compreendido, e ampliam as aplicaçoes dos sinais de luminescência (RF, OSL e VSL) do quartzo para análise de proveniência e geocronlogia de depósitos fluviais no Brasil.

**Palavras-chave**: Radiofluorescência; Luminescência opticamente estimulada, Rochas sedimentares ferruginosas; Luminescência estimulada por luz violeta; Sedimentos fluviais.

# Table of Contents

# Introduction

## Motivation and purpose

Human excellence is nurtured by inherent curiosity to know about the past (Gould, 1987). The age determination of geological and archeological events in the last ~2.6 million years (The Quaternary period) is critical for understanding past climate and environmental changes, landscape evolution, and human evolution and dispersal. This understanding is important for future predictions of climate, environmental changes and resource planning.

In this connection, the luminescence dating technique, a novel and rapidly developing application in geochronology, has played an important role in age determination of the archaeological and geological events in the Quaternary timespan (Aitken, 1998; Rhodes, 2011; Liritzis *et al*., 2013; Roberts *et al*., 2015; Duller, 1997). In particular, it has proven to be a highly useful and widely applicable technique for obtaining chronologies for the Late and Middle Pleistocene (Buylaert *et al*., 2008; Rittenour, 2008; Cunha *et al*., 2012; Herman *et al*., 2013; Guralnik et al., 2015; Henshilwood *et al*., 2002; Singhvi and Porat, 2008; Fattahi and Walker, 2007; Wallinga, 2002).

Luminescence dating is an interdisciplinary research field based on solid state physics, radiation physics, and Earth and archaeological sciences; all these areas have contributed to the development of the luminescence dating technique. Despite the immense success of the luminescence technique, there are continuous attempts from laboratories across the world to further improve the technique for wider application. Some of the active research areas are: use of luminescence as a sediment tracer and provenance tool (Sawakuchi *et al*., 2018; Gray *et al*., 2019), extending the age range to cover the full Quaternary (Ankjaergaard et al., 2013), investigating the feasibility of luminescence method to shed the light on the formation age of Quaternary rocks (Niyonzima *et al*., 2022), and modelling charge build up in thermally and optically dynamic environments (King *et al*., 2016). Even a slight improvement in the method

can have a significant positive impact on the application of the technique in the Geosciences or Archaeology fields, and on the age resolution of the past events.

The researchers rely on the fact that natural minerals such as quartz and feldspar, which are widely used in dating, are rich in luminescent defects and have complex charge transfer processes. It is expected that a better understanding of these defects and processes will give rise to more robust dating methods, and help to place the existing dating protocols on a solid foundation.

Hence, the first overriding objective of this thesis, therefore, was to investigate luminescence signals of quartz extracted from Brazilian fluvial sediments for better understanding of charge transfer process, and the application of the technique for age resolution and improving of its dating range. This consisted of investigating the variation of the radiofluorescence (RF) emission spectra in quartz extracted from different igneous rocks and sediments of different geological settings. We investigated the difference in RF emission spectra between quartz extracted from igneous rocks and sediments for better understanding the mechanisms involved in thermoluminescence (TL) and optically stimulated luminescence (OSL) sensitivities, properties successfully used in sediment provenance analysis (e.g. Sawakuchi *et al*., 2018; Mendes *et al*., 2019). The possibility of use of RF of quartz for sediment provenance analysis was also investigated by studying the correlation between the ultraviolet (UV) RF emission intensity and sensitivity of both TL and OSL emissions.

Besides the widespread unconsolidated sandy fluvial deposits, some bedrock rivers in eastern Amazonia host sandy and gravelly deposits cemented by goethite. These deposits form rocks over the riverbed and represent unique riverine landscape features. This is the case of the Xingu River draining shield areas in eastern Amazonia. Additionally, it has been reported that the original oxygen isotopes ratio of iron minerals such as goethite and hematite is generally preserved, thereby providing information about weathering and climate conditions at the time of formation (Giral-Kacmarcik *et al*., 1998; Girard *et al*., 2002). The formation ages of ironstones (fluvial sands and gravels cemented by goethite) of the Xingu River are unknown and their formation process is still poorly understood despite their relevance as substrate for the aquatic ecosystem (Fitzgerald *et al*., 2018). Different dating methods of ironstones were applied in Brazilian settings, including (U-Th)/He of goethite (Riffel *et al.*, 2016),

electron paramagnetic resonance of matrix kaolinite (Allard *et al*., 2018) and cosmogenic nuclides of trapped quartz grains ($^{10}$Be) (Pupim *et al*., 2015). These methods are suitable to obtain ages in the hundred thousand to million years timescale and dating of ironstones is still challenging for the thousand years timescale necessary to cover the late Pleistocene and Holocene age range. In this thesis, we checked the feasibility of OSL dating on detrital quartz grains within ironstones to shed light on the timing and processes of formation over the riverbed of the Xingu River. This was the second objective of this thesis.

The third objective aimed to extend the age range of luminescence dating to tackle research problems beyond the late Pleistocene, which is usually the age limit for quartz OSL dating. In this way, deposition ages of fluvial sediments have a fundamental role to constrain the landscape changes in Amazonia during the middle and early Pleistocene, when most species representing the modern Amazonian biota appeared (Smith *et al*., 2014). Geochronological methods to determine reliable burial ages for the middle and early Pleistocene fluvial sedimentary record of Amazonia are crucial to understand the role of the physical landscape for the biota diversification (Hoorn *et al*., 2017). So far, most successful dating studies of Amazonian Quaternary sedimentary deposits are based on radiocarbon dating of rare organic material (e.g. Rossetti *et al*., 2005) or quartz optically stimulated luminescence (OSL) (e.g. Rossetti *et al*., 2015). However, the use of quartz for OSL dating is typically limited to the last 100–150 ka due to saturation of the OSL signal around 150-200 Gy (Wintle and Adamiec, 2017). The violet stimulated luminescence (VSL) from quartz, which probes traps deeper than those accessible by blue light, has been observed to grow with doses up to about 1000 Gy (Jain, 2009), ~10 times higher than the OSL from the same grains. Further studies confirmed that VSL signal originates from thermally stable with lifetime of $10^{11}$ years at 10°C (Ankjaergaard *et al*.,2013, 2015) with no athermal loss (Ankjaergaard *et al*.,2013); thus giving the potential to extend the age range of quartz luminescence dating to cover the full quaternary period. Therefore, we explored the VSL single aliquot regenerative dose (SAR), multiple aliquots regenerative (MAR), multiple aliquots additive dose (MAAD) protocols, and investigated the behavior of the VSL signal under different measurement conditions with the aim of extending the dating range of luminescence dating for Brazilian fluvial sediments.

## Thesis outline

The thesis is outlined in five chapters. Chapter 1 introduces the basic concepts of dating based on luminescence methods. The physical basics of luminescence, principal of luminescence, environments suitable for luminescence dating, and explanation of how the phenomenon can be used for dating is presented.

Chapters 2, 3 and 4 describe three manuscripts, where two are published (Niyonzima *et al*., 2020, 2022) and other is in preparation for submission in peer-reviewed scientific journal. Each article is individually understandable. They are structured so that they describe the motivation, experimental procedures, results and discussion. They all address the subject of using luminescence signals from quartz extracted from Brazilian fluvial sediments for provenance analysis and dating.

The work presented in Chapter 2 is based on the article *"Radiofluorescence of quartz from rocks and sediments and its correlation with thermoluminescence and optically stimulated luminescence sensitivities",* published in *Ancient TL* (Niyonzima et al., 2020). This study investigates radiofluorescence (RF) emissions in quartz from parent rocks and sediments of different provenances and different optically stimulated luminescence (OSL) and thermoluminescence (TL) sensitivities. The correlation of OSL and TL (110°C peak) sensitivities were compared to RF emission peak sensitivities in order to understand the sensitivity variations in terms of charge traps and recombination centers. We investigate the relationships between intensities of RF emission peaks and OSL and TL sensitivities in order to investigate the possibility of RF emission band sensitivity to be used as a provenance proxy as in the way as OSL and TL sensitivities for quartz from sediments.

The work presented in Chapter 3 is based on manuscript: "*Testing the potential of quartz violet stimulated luminescence (VSL) for dating of Brazilian fluvial sediments" (Niyonzima et al., in preparation).* On this chapter, VSL properties of quartz from major fluvial systems in South America, represented by fluvial terraces from western Brazil, southeastern Brazil and central and eastern Amazonia. Firstly, we investigated the presence of VSL signals in quartz from the studied samples under different preheating temperatures. Afterwards, dose recovery test of SAR-VSL protocol and thermal stability test were performed to evaluate dose estimation capacity. We also estimated

equivalent dose ($D_e$) and characteristic doses ($D_0$) of samples that showed VSL signal using a single aliquot regenerative dose (SAR), multiple aliquots regenerative doses (MAR), and multiple aliquots additive doses (MAAD) protocols. Considerations about the use of VSL to extend the age limit of quartz dating beyond the late Pleistocene were addressed in this chapter.

The work presented in Chapter 4 is based on the article "*Luminescence dating of quartz from ironstones of the Xingu River, Eastern Amazonia"*, published in Quaternary Geochronology (Niyonzima *et al*., 2022). In this study, OSL dating method was applied for first time in establishing formation ages of ferruginous deposits (ironstones) of the Xingu River in Eastern Amazonia, Brazil. Equivalent doses, environmental dose rates and hence luminescence ages were determined. Equivalent dose distributions were also evaluated in order to inform about how quartz grains are incorporated into ironstones. Additionally, the organic content of some samples was dated by radiocarbon ($^{14}C$) for comparison with quartz OSL ages.

In Chapter 5, we summarize the main conclusions based on outcomes from the thesis. It this chapter also, we clarified the possible work to be done in the future in order to support some arguments raised in this work.

# Chapter 1. Essential of luminescence

## 1.1. The physical basis of luminescence

Simple band gap energy model of OSL is presented in Figure 1 below. Light-sensitive OSL electron traps are shown in red, light-insensitive (thermoluminescence) traps in blue. (*a*) Under typical initial conditions, low thermal stability traps close to the conduction band are kept empty by thermal eviction at ambient temperature, but other traps are filled; luminescence centers are available. (*b*) On light exposure, electrons in OSL traps are evicted and may become trapped in other available trapping sites or may recombine at hole centers (luminescence centers).

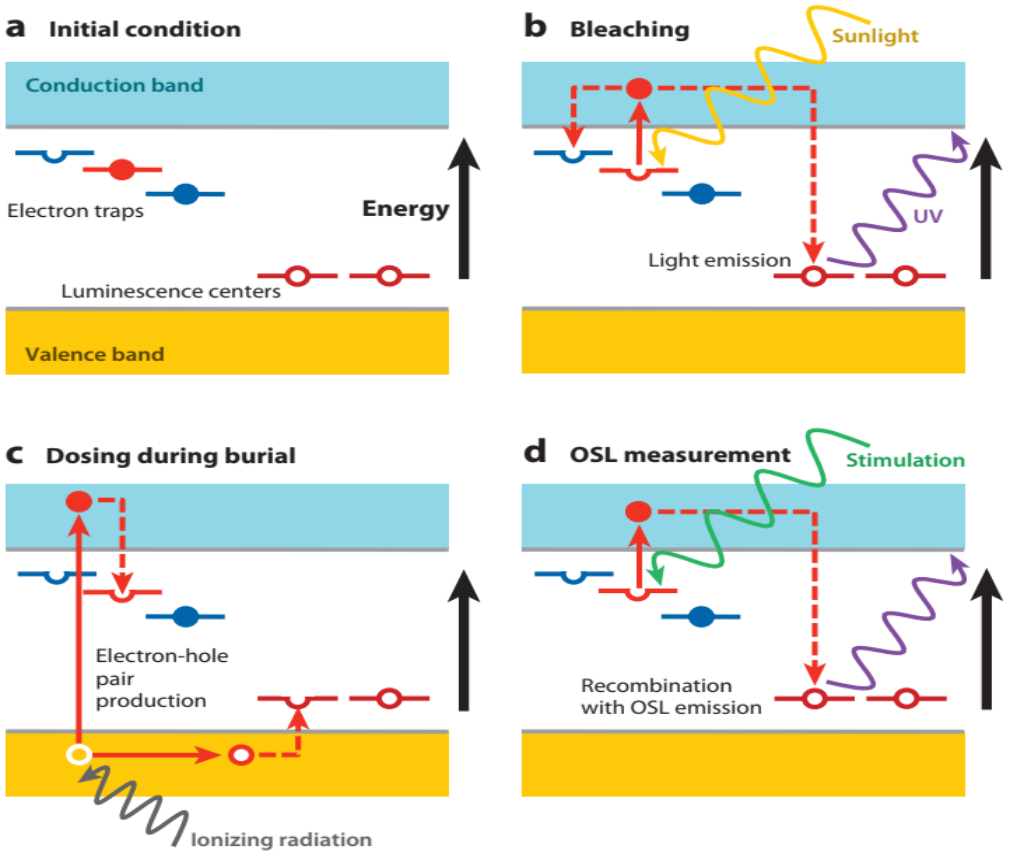


Figure 1: Simple band gap energy model of optically stimulated luminescence (OSL) for the insulators and semi-conductors (Taken from Rhodes, 2011).

After brief light exposure, all OSL traps are emptied. (*c*) During subsequent burial, ionizing radiation gradually produces electron-hole pairs, some of which may become trapped, increasing the OSL trap population. (*d*) Following collection and

mineral separation, the trapped electrons stored within minerals can be released in the laboratory using a number of methods that cause them to produce a luminescence signal.

Heating the sample at a fixed heating rate from room temperature to 500°C releases the trapped electrons and the resulting signal is termed Thermoluminescence (TL). A second means of releasing the electrons stored within the mineral is the exposure to the stimulating light (Huntley *et al*., 1985). As soon as the light is switched on luminescence is emitted by the mineral grains. As the measurement continues, the electrons in the trap are emptied and the signal decreases. The signal is termed Optically Stimulated Luminescence (OSL), Figure 2 (b). For thermoluminescence, typically the TL signal (commonly known as a glow curve) comprises a series of peaks, Figure 2 (a). Each peak may be due to a single type of trap within the mineral being measured, but more commonly the signal is a composite of several traps. In the other hand for OSL, the signal initially decreases rapidly, and then at a slower rate, Figure 2 (b).

,

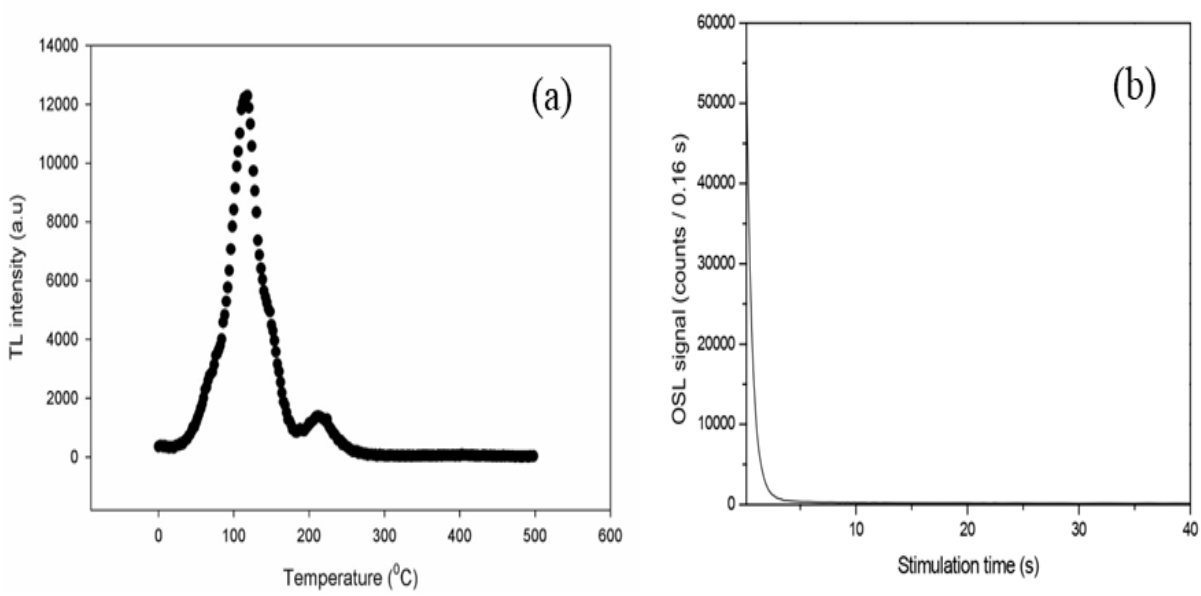


Figure 2: (a) typical thermoluminescence (TL) signal from an aliquot of quartz as it is heated from room temperature to 450°C at a rate of 5°C per second. (b) Typical OSL signal observed from a quartz aliquot – the OSL signal drops rapidly as the trapped electrons in the quartz are used up to produce the luminescence signal.

## 1.2. Introduction to luminescence dating

Luminescence dating is based on the process called 'stimulated luminescence' from naturally occurring minerals such as quartz and feldspar. The most commonly used form of this technique is optically stimulated luminescence (OSL), where the term 'optical' usually refers to visible light which is commonly used to date quartz (e.g. violet, blue or green light). In case of feldspar, near infra-red light is used for stimulation giving rise to the infra-red stimulated luminescence (IRSL).

The OSL process was first used for age determination by Huntley *et al*. (1985), and has been used extensively in archeology and the Earth sciences (Aitken, 1998). It has since then became one of the most important methods for dating the Late Quaternary (e.g. Rhodes, 2011; Roberts *et al*., 2015; Duller, 1996). OSL is a two-step process: a) ionization of the lattice by interaction with high-energy radiation, creation of free electrons and holes and subsequent trapping of these charge carriers at the lattice defects (traps), and b) optical eviction of trapped charge from light sensitive traps followed by radiative electron-hole recombination resulting in the OSL. The charge trapping centers from localized energy states within the bandgap of the feldspar (~ 7.7–7.8 eV; Malins *et al*., 2004) and quartz (~ 8.3–8.7 eV; Itoh, 1989), thereby providing metastable states to the electrons and holes released by exposure of ionizing radiation. Some of these states depending on the energy potential (trap depth) may have a lifetime of millions of years, which makes them useful for geochronology.

The OSL clock in quartz and feldspar is zeroed by exposure to daylight during erosion and sediments transport prior to burial. After burial, the population of trapped charge increases over time due to the impact of ionizing radiation from the environment ($^{238}$U, $^{232}$Th, $^{40}$K and cosmic rays). The geological age (a = annum) of the sample is estimated as the ratio between the absorbed ionizing radiation dose (also known as palaeodose or equivalent dose; unit Gy) and the environmental dose rate (unit Gy $a^{-1}$), acquired since the sample was last buried and blocked from daylight (Aitken, 1985, 1994).

## 1.3. Environnements suitable for luminescence dating

Figure 3 is the cartoon illustrating different types of environment in which luminescence dating can be applied. One very common, application is the dating of sediments, and in this case the event being dated is the last exposure of the mineral grains to the daylight. The age range over which the method can be applied is from a century or less to over five hundred thousand years (Prescott and Robertson, 1997). On the application of luminescence to dating archeological or geological materials relies on the determining two quantities. The first is the amount of radiation absorbed by the sample during the period since the event being dated, measure as equivalent dose as $D_e$. To determine the age of the sample in years $D_e$ has to be divided by the radiation dose received by the sample each year, the dose rate.

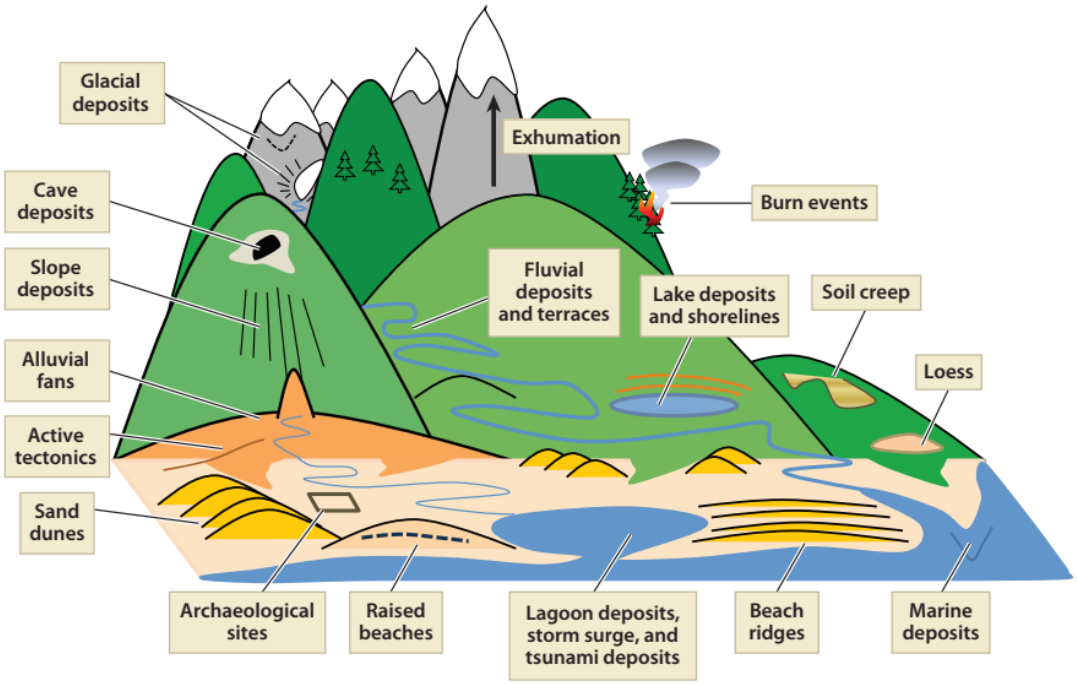


Figure 3: Cartoon illustration of the main environments in which optically stimulated luminescence (OSL) can be applied (Rhodes, 2011).

Radioactivity is the common phenomenon in the natural environment. Luminescence dating exploits the presence of the radioactive isotopes of elements such as uranium (U), thorium (Th) and potassium (K). Naturally occurring minerals such as quartz and feldspar act as dosimeters, recording the amount of radiation to which they have been exposed. The common property of some naturally occurring minerals is that

when they are exposed to emissions released by radioactive decay, they are able to store within their crystal structure a small proportion of the energy delivered by the radiation. This energy accumulates as exposure to radioactive decay continues through time. At some later date this energy may be released, and in some minerals this energy is released in the form of light. This is termed luminescence.

## 1.4. Principle of luminescence dating

A rechargeable battery provides a useful analogy for how mineral grains behave and how luminescence dating works. When mineral grains are exposed to light or heated, trapped electrons are released, much like depleting a battery. Once this heating or exposure to daylight stops, re-exposure to natural radioactivity begins to recharge the mineral grains, much like recharging a battery, Figure 4. In the laboratory, the mineral grains are stimulated to release their stored energy in the form of light emission. Using this analogy, the date can be calculated by dividing the total accumulated energy during burial time by the rate of energy accumulation. The brightness of this luminescence signal can be related to the amount of energy that has been stored in the minerals.

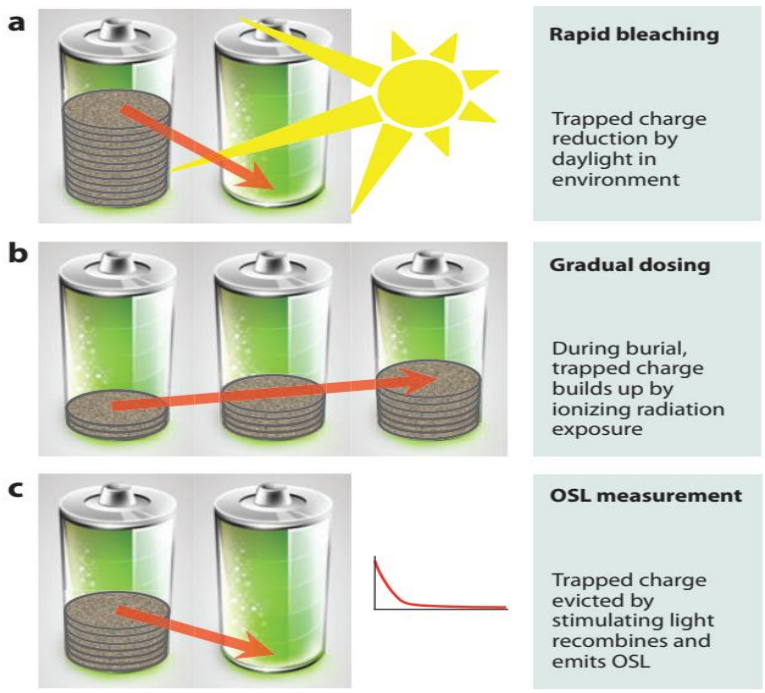


Figure 4: The rechargeable battery analogy to help understand optically stimulated luminescence (OSL) dating; gray circles show charge level (Rhodes, 2011).

The potential for luminescence dating of quartz from sediments has been increasingly realized since the 1980s (Aitken, 1998). Many minerals, including quartz and most feldspar, store energy within their crystal structure that has been deposited by ionizing radiation from the environment and in addition, cosmic rays. The amount of stored energy increases with the amount of radiation to which a crystal has been exposed (Duller, 2004). Luminescence dating provides direct ages of the time that has elapsed since this trapped charges was last zeroed, either thermally, or as in the case for loess from exposure to sunlight (Aitken, 1998). By measuring the stored energy in the crystal through sample stimulation in the laboratory, an estimate of the dose of radiation a sample has experienced since zeroing can be obtained. By dividing this value by the measured annual dose rate at the sample´s location, age in years since sample burial can be obtained.

## 1.5. References


Aitken, M. J., 1985. Thermoluminescence dating. **Academic press, London.**

Aitken, M. J., 1994. Optical dating: a non-specialist review. **Quaternary Science Reviews**, 13(5-7), 503-508.

Aitken, M. J., 1998. An Introduction to Optical Dating. Oxford: **Oxford University Press**.

Allard, T., Gautheron, C., Riffel, S. B., Balan, E., Soares. B. F., Pinna-Jamme, R., Derycke, A., Morin, G., Bueno, G. T., do Nascimento, N., 2018. Combined dating of goethites and kaolinites from ferruginous duricrusts. Deciphering the Late Neogene erosion history of Central Amazonia. **Chemical Geology,** 479, 136–150.

Ankjærgaard, C., Guralnik, B., Porat, N., Heimann, A., Jain, M., Wallinga, J., 2015. Violet stimulated luminescence: geo-or thermochronometer? **Radiation Measurement**, 81, 78–84.

Ankjærgaard, C., Jain, M., Wallinga, J., 2013. Towards dating quaternary sediments using the quartz violet stimulated luminescence (VSL) signal. **Quaternary Geochronology**, 18, 99–109.

Buylaert, J. P., Murray, A. S., Vandenberghe, D., Vriend, M., De Corte, F., 2008. Optical dating of Chinese loess using sandsized quartz: establishing a time frame for Late Pleistocene climate changes in the western part of the Chinese Loess Plateau. **Quaternary Geochronology**, 3(1), 99-113.

Cunha, P. P., Almeida, N. A., Aubry, T., Martins, A. A., Murray, A. S., Buylaert, J.P., Sohbati, R., Raposo, L., Rocha, L., 2012. Records of human occupation from Pleistocene river terrace and aeolian sediments in the Arneiro depression (Lower Tejo River, central eastern Portugal). **Geomorphology**, 165, 78-90.

Duller, G. A. T., 1996. Recent developments in luminescence dating of Quaternary sediments. **Progress in Physical Geography**, 20(2), 127-145.

Duller, G. A. T., 1997. Behavioural studies of stimulated luminescence from feldspars. **Radiation Measurements**, 27(5), 663-694.

Duller, G. A. T., 2014. Luminescence dating of Quaternary sediments: recent advances. **Journal of quaternary science**, 19, 183–192.

Fattahi, M., Walker, R. T., 2007. Luminescence dating of the last earthquake of the Sabzevar thrust fault, NE Iran. **Quaternary Geochronology**, 2(1), 284-289.

Fitzgerald, D. B., Sabaj Perez, M. H., Sousa, L. M., Gonçalves, A. P., Rapp Py-Daniel, L., Lujan, N. K., Zuanon, J., Winemiller, K. O., Lundberg, J. G., 2018. Diversity and community structure of rapids-dwelling fishes of the Xingu River: Implications for conservation amid large-scale hydroelectric development. **Biological Conservation**, 222, 104–112.

Giral-Kacmarkcik, S., Savin, S. M., Nahon, D., Girard, J.-P., Lucas, Y., and Abel, L., 1998. Oxygen isotope geochemistry of kaolinite in laterite-forming processes, Manaus, Amazonas, Brazil. **Geochimica et Cosmochimica Acta,** 62, 1865–1879.

Girard, J. P., Freyssinet, P., Morillon, A. C., 2002. Oxygen isotope study of Cayenne duricrust paleosurfaces: implications for past climate and laterization processes over French Guiana. **Chemical Geology,** 191, 329–343.

Gould, S. J., 1987. Time's arrow, time's cycle: Myth and metaphor in the discovery of geological time (Vol. 2). **Harvard University Press**.

Gray, H. J., Jain, M., Sawakuchi, A. O., Mahan, S. A., Tucker, G. E., 2019. Luminescence as a sediment tracer and provenance tool. **Reviews of Geophysics**, 57, 987–1017.

Guralnik, B., Jain, M., Herman, F., Ankjærgaard, C., Murray, A. S., Valla, P. G., Kook, M., 2015. OSL-thermochronometry of feldspar from the KTB borehole, Germany. **Earth and Planetary Science Letters**, 423, 232-243.

Henshilwood, C. S., d'Errico, F., Yates, R., Jacobs, Z., Tribolo, C., Duller, G.A., Mercier, N., Sealy, J.C., Valladas, H., Watts, I., Wintle, A. G., 2002. Emergence of modern human behavior: Middle Stone Age engravings from South Africa. **Science**, 295(5558), 1278-1280.

Herman, F., Seward, D., Valla, P. G., Carter, A., Kohn, B., Willett, S. D., Ehlers, T. A., 2013. Worldwide acceleration of mountain erosion under a cooling climate. **Nature**, 504(7480), 423-426.

Hoorn, C., Bogotá-A., G.R., Baez, M.R., Lammertsma, E.I., Flantua, S.G.A., Dantas, E.L., Dino, R., Carmo, D.A., Chemale, F.Jr. 2017. The Amazon at sea: Onset and stages of the Amazon River from a marine record, with special reference to Neogene plant turnover in the drainage basin. **Global and Planetary Change,** 153, 51-65.

Huntley, D. J., Godfrey-Smith, D. I., Thewalt, M. L., 1985. Optical dating of sediments. **Nature**, 313, 105-107.

Itoh, C., Tanimura, K., Itoh, N., Itoh, M., 1989. Threshold energy for photogeneration of self-trapped excitons in Si O 2. **Physical Review B**, 39(15), 11183.

Jain, M., 2009. Extending the dose range: probing deep traps in quartz with 3.06 eV photons. **Radiation Measurements**, 44, 445–452.

King, G. E., Herman, F., Lambert, R., Valla, P. G., Guralnik, B., 2016a. Multi-OSL thermochronometry of feldspar. **Quaternary Geochronology,** 33, 76–87.

Liritzis, I., Singhvi, A. K., James, K. (2013). Luminescence dating in archaeology, anthropology, and geoarchaeology: an overview; Heidelberg, Germany: **Springer.**

Malins, A. E. R., Poolton, N. R. J., Quinn, F. M., Johnsen, O., Denby, P. M., 2004. Luminescence excitation characteristics of Ca, Na and K-aluminosilicates (feldspars) in the stimulation range 5–40 eV: determination of the band-gap energies. **Journal of Physics D: Applied Physics**, 37(10), 1439.

Mendes, V. R., Sawakuchi, A. O., Chiessi, C. M., Giannini, P.C. F., Rehfeld, K., Mulitza, S., 2019. Thermoluminescence and optically stimulated luminescence measured in marine sediments indicate precipitation changes over northeastern Brazil. **Paleoceanography Paleoclimatology,** 2019PA003691.

Niyonzima, P., Sawakuchi, A. O., Bertassoli Jr. D. J., Pupim, F. N., Porat, N., Freire, M. P., Goes, A. M., Rodrigues, F. C. G. Luminescence dating of quartz from ironstones of the Xingu River, astern Amazonia. **Quaternary Geochronology,** 67101241.

Prescott, J. R., Robertson, G. B., 1997. Sediment dating by luminescence: a review. **Radiation Measurements,** 27, 893-922.

Pupim, F. N., Bierman, P. R., Assine, M. L., Rood, D. H., Silva, A., Merino, E. R., 2015. Erosion rates and landscape evolution of the lowlands of the Upper Paraguay River basin (Brazil) from cosmogenic $^{10}$Be. **Geomorphology,** 234, 151–160.

Rhodes, E. J., 2011. Optically stimulated luminescence dating of sediments over the past 200,000 years. **Annual Review of Earth and Planetary Sciences**, 39, 461-488.

Riffel, S. B., Vasconcelos, P. M., Carmo, I. O., Farley, K. A., 2016. Goethite (U–Th)/He geochronology and precipitation mechanisms during weathering of basalts. **Chemical Geology,** 446, 18–32.

Rittenour, T. M., 2008. Luminescence dating of fluvial deposits: applications to geomorphic, palaeoseismic and archaeological research. **Boreas**, 37(4), 613-635.

Roberts, R. G., Jacobs, Z., Li, B., Jankowski, N. R., Cunningham, A. C., Rosenfeld, A. B., 2015. Optical dating in archaeology: thirty years in retrospect and grand challenges for the future. **Journal of Archaeological Science**, 56, 41-60.

Roberts, R. G., Lian, O. B., 2015. Dating techniques: Illuminating the past. **Nature**, 520(7548), 438-439.

Rossetti, D. F., Cohen, M. C. L., Tatumi, S. H., Sawakuchi, A. O., Cremon, É. H., Mittani, J. C. R., Bertani, T. C., Munita, C. J. A. S., Tudela, D. R. G., Yee, M., Moya, G. 2015. Mid-Late Pleistocene OSL chronology in western Amazonia and implications for the transcontinental Amazon pathway. **Sedimentary Geology,** 330, 1–15.

Rossetti, D. F, Toledo, P. M., Góes A. M. 2005. New geological framework for Western Amazonia (Brazil) and implications for biogeography and evolution. **Quaternary Research,** 63, 78–89.

Sawakuchi, A. O., Jain, M., Mineli, T. D., Nogueira, L., Bertassoli Jr, D. J., Häggi, C., Sawakuchi, H. O., Pupim, F. N., Grohmann, C. H., Chiessi C. M., M. Zabel c, Mulitza S., Mazoca, C. E. M., Cunha, D. F., 2018. Luminescence of quartz and feldspar fingerprints provenance and correlates with the source area denudation in the Amazon River basin. **Earth and Planetary Science Letters**, 492, 152–162.

Singhvi, A. K., Porat, N., 2008. Impact of luminescence dating on geomorphological and palaeoclimate research in drylands. **Boreas**, 37(4), 536-558.

Smith, B. T., McCormack, J. E., Cuervo, A. M., Hickerson, M. J., Aleixo, A., Cadena, C.D., Perez-Em an, J., Burney, C. W., Xie, X., Harvey, M. G., Faircloth, B. C., Glenn, T. C., Derryberry, E. P., Prejean, J., Fields, S., Brumfield, R., 2014. The drivers of tropical speciation. **Nature,** 515 (7527), 406-409.

Wallinga, J., 2002. Optically stimulated luminescence dating of fluvial deposits: a review. **Boreas**, 31(4), 303-322.

Wintle, A. G., Adamiec, G., 2017. Optically stimulated luminescence signals from a review. **Radiation Measurements,** 98, 10–33.

Wintle, A. G., Murray, A.S., 2006. A review of quartz optically stimulated luminescence characteristics and their relevance in single-aliquot regeneration dating protocols. **Radiation Measurements,** 41, 369-391.

# Chapter 2: Radiofluorescence of quartz from rocks and sediments and its correlation with thermoluminescence and optically stimulated luminescence sensitivities

P. Niyonzima, A. O. Sawakuchi, M. Jain, R. Kumar, T. D. Mineli, I. del Río, F. N. Pupim

## 2.1. Abstract

The present study examines radiofluorescence (RF) emissions in quartz from parent rocks (igneous plutonic and volcanic) and sediments of different provenances, which represent a range of optically stimulated luminescence (OSL) and thermoluminescence (TL) sensitivities observed in nature. OSL and TL (110 $^{o}$C peak) sensitivities of quartz have been successfully used for sediment provenance analysis, but the considerable sensitivity variations are still poorly understood in terms of charge traps and recombination centers. In the studied samples, the RF spectra obtained at room temperature and using X-ray irradiation consist of two broad emission bands: the first emission band is centered at ~1.9 eV (blue) and has a higher intensity compared to the second emission band centered at ~3.5 eV (ultraviolet, UV). The deconvolution analysis confirms that the quartz RF spectrum is at least the sum of four emission bands located between 1.5 eV (827 nm) and 4.0 eV (310 nm). The general observation is that the RF intensity differs between quartz from rocks and sediments, and among quartz from sediments with different provenances. Generally, quartz from sediments showed higher RF intensity compared to quartz from rocks, rendering the same pattern observed for OSL and TL sensitivities. For quartz from sediments, we observed strong correlations between the UV-RF band intensity and the OSL or 110°C TL sensitivities. We argue that these correlations may be attributed to the fact that both 110°C TL peak and OSL of quartz use the same recombination centers rather than the same electron trap. The UV-RF intensity measured using X-ray sources can also be used for provenance analysis of sediments in the same way as the OSL and TL sensitivities.

## 2.2. Introduction

Since the first proposals for the use of thermoluminescence (TL) (e.g., Grögler *et al*., 1958; Fleming, 1970; Mejdahl, 1979; Wintle and Huntley, 1979) and optically stimulated luminescence (OSL) in quartz (Huntley *et al*., 1985) as dating techniques, it appears that both TL and OSL signals are not merely due to charge eviction from traps after stimulation with consequent luminescence recombination. However, more complex mechanisms are involved (Martini *et al*., 2009). Aitken and Smith (1988) reported parallel changes in the OSL sensitivity and the sensitivity of the 110 °C TL peak and suggested that this might be related to a common mechanism. Most researchers agree on the involvement of the same recombination centers of these two processes (e.g., Chen *et al*., 2000). Radiofluorescence (RF), the light emission during irradiation, has been investigated in quartz samples from rocks and sediments as well as in artificially growing $SiO_2$ crystals (Marazuev *et al*., 1995; Krbetschek and Trautmann, 2000; Martini *et al*., 2012b) for dosimetry and dating purposes. RF has also been investigated for a better understanding of the luminescence dynamics in quartz (Martini *et al*., 2012a; 2012b; Chithambo and Niyonzima, 2017) by comparing the 3.44 eV RF peak intensity measured after series of irradiation and thermal treatments in order to understand the specific role of various defect centers. Different from TL and OSL, the RF emission seems to correspond predominantly to the direct recombination of electrons from the conduction band with the holes at the recombination centers during irradiation (*e.g*., Schmidt *et al*., 2015, Friedrich *et al*., 2017).

Deconvolution of the RF spectra showed the presence of the same emission bands from both natural and "artificial" (laboratory crystal growth) quartz crystals, indicating that the same luminescence processes are involved (Martini *et al*., 2012a, 2012b; Chithambo and Niyonzima, 2017). The similarity among RF, TL and OSL emission spectra (Huntley *et al*., 1991; Krbetschek *et al*., 1997; Schilles *et al*., 2001) provided evidence that these luminescence signals share the same recombination centers (Friedrich *et al*., 2017). This similarity suggests that changes in OSL and TL sensitivities in nature, as observed in quartz from sediments (*e.g*., Pietsch *et al*., 2008; Zular *et al.,* 2015) are probably related to the recombination process rather than trapping process. In this way, investigation of the relationship between RF and OSL and TL sensitivities can shed light on the role of recombination centers for the natural

sensitization processes. In addition to its widespread application for dating of Quaternary sediments (Aitken, 1998), luminescence signals from quartz are used for tracing the provenance of sediments (e.g., Lü and Sun, 2011, Gray *et al*., 2019). In the previous works, TL spectra (Rink *et al*., 1993), the proportion of OSL components (Tsukamoto *et al*., 2011), the OSL and TL sensitivities (Sawakuchi *et al*., 2012; Zular *et al*., 2015, Mendes *et al*., 2019) and OSL signal components (Nian *et al*., 2019) of quartz have been used in discriminating sediment sources and provenance analysis. Thus, several luminescence properties (*e.g*., sensitivity, thermal activation, spectral variation, and signal components) can be used to discriminate quartz from different provenances. A general pattern is that quartz extracted from different types of igneous and metamorphic rocks has a relatively low luminescence sensitivity (Chithambo *et al*., 2007; Guralnik *et al*., 2015) compared to quartz from sediments, which shows a wide range of OSL sensitivity variation (Sawakuchi *et al*., 2011). Thus, recent studies have successfully applied OSL sensitivity in sediment provenance analysis through discrimination of sediments with different transport histories since their parent rocks (*e.g*., Sawakuchi *et al*., 2018; Mendes *et al*., 2019).

In this study, we investigate the variation of RF emission spectra in quartz extracted from different igneous rocks, which are primary sources of terrigenous sediments, and sediments of different geological settings, ranging from tectonic active mountain ranges to stable craton areas in South America. This suite of samples has a broad range in natural TL and OSL sensitivities, as presented in Sawakuchi *et al*. (2020) and Mineli *et al*. 2021 and summarized in Table 1. Correlation between UV-RF and sensitivity of both TL and OSL is also investigated in this study. We hypothesis that, this correlation would support the use of RF of quartz for sediment provenance analysis.

## 2. 3. Experimental details

### 2.3.1. Samples description and preparation

Samples used in this investigation were quartz from igneous rocks (granite, rhyolite, and hydrothermal vein) representing different conditions of quartz crystallization and sediments (alluvial, fluvial and coastal sands) of different depositional environments from South American sites (Table 1). OSL and TL sensitivities of these samples were previously studied in Mineli *et al*. 2021 and they are summarized in Table 1.

Rock samples were crushed to release quartz crystals, which were manually picked for careful grinding using a pestle and ceramic mortar. Quartz crystals from igneous rocks and quartz grains from sediments in the range of 180–250 μm were extracted by wet sieving. The target fraction was treated with hydrogen peroxide ($H_2O_2$, 27%) and hydrochloric acid (HCl, 10%) to remove organic matter and carbonate minerals, respectively. Heavy minerals and feldspar grains were removed by heavy liquid separation with lithium metatungstate solutions with densities of 2.75 g/cm$^3$ and 2.62 g/cm$^3$, respectively. To purify and concentrate the quartz fraction, samples were etched in 38% hydrofluoric acid (HF) for 40 min. Infrared stimulation (IR) was performed to confirm the absence of feldspar contamination in the HF treated quartz fraction. Samples with remaining feldspar were subjected to steps of HF 5% etching for 24 hours followed by wet sieving (180 μm sieve), and in some cases, samples were repeatedly HF-etched until a negligible infrared signal was achieved, compared with blue stimulation signal.

Table 1: Description of studied samples, indicating types of rocks and sediments, approximate age of crystallization (rocks) or deposition (sediments), location of the sampling sites, and average TL and OSL sensitivities and standard deviation as presented in Mineli *et al*. 2021. Aliquots used to measure TL, and OSL sensitivities contained approximately 150 to 200 grains, as observed under an optical microscope, with an average mass of 8.1 ± 0.9 mg. TL and OSL sensitivities data were not obtained for sample L0680, which was collected in the same geological setting of sample L0674. Both samples are examples of sediments with low sensitivity quartz. For both TL and OSL measurements, 2 to 6 aliquots were measured for each sample and results presented in the table are average with standard deviation. Values without standard deviation imply only one aliquot with detectable OSL or TL signals.

| | Code | Name | Age | Location | TL 110°C (cts $Gy^{-1}$) | OSL (cts $Gy^{-1}$) |
|---|---|---|---|---|---|---|
| Rocks | VR12 | Granite | Neoproterozoic | Ribeira Fold Belt, Guaraú Massif, (Cajati, São Paulo, Brazil) | 1865 ± 1851 | 67 ± 70 |
| | ITA1 | Granite | Neoproterozoic | Ribeira Fold Belt, Itacoatiara Massif (Niterói, Rio de Janeiro, Brazil) | 2019 ± 261 | 4.4 |
| | LA1 | Rhyolite | Pleistocene | Los Alamos (New Mexico, USA) | 1795 ± 319 | 63 ± 25 |
| | IP22 | Hydrothermal quartz | Permian | Teresina Formation, Paraná Basin (Anhembi, São Paulo, Brazil) | 108 | 2.2 |
| Sediments | L0001 | Coastal sand | Pleistocene | South Atlantic Coast (Southern Brazil) | 128760 ± 42674 | 23152 ± 9361 |
| | L0017 | Fluvial sand | Pleistocene | Central Amazon (Northern Brazil) | 22426 ± 5354 | 1390 ± 502 |
| | L0698 | Fluvial sand | Holocene | Western Amazon (Northern Brazil) | 12396 ± 4036 | 2432 ± 1309 |
| | L0229 | Fluvial sand | Pleistocene | Pantanal Wetland (Western Brazil) | 308683 ± 51341 | 53520 ± 9522 |
| | L0688 | Fluvial sand | Holocene | Paraná River Basin (Southern Brazil) | 433092 ± 53278 | 89544 ± 53278 |
| | L0572 | Fluvial sand | Pleistocene | Central Amazon (Northern Brazil) | | |
| | L0674 | Alluvial sand | Pleistocene | Mejillones Peninsula, Andes (Chile) | 266 ± 44 | 17 ± 9 |
| | L0680 | Colluvial sand | Pleistocene | Salar Del Carmen, Andes (Chile) | * | * |

### 2.3.2. Instrumentation

Radiofluorescence measurements were carried out using the Risø station for CryOgenic Luminescence Research COLUR at Center for Nuclear Technologies, Technical University of Denmark (DTU), Risø campus. It consists of a Horiba Fluorolog-3 spectrometer expanded to include multi-excitation and detection ports, an X-ray irradiator (40 kV anode voltage, 100 µA anode current, and ca 0.06 Gy/s dose rate to quartz), and a temperature-controlled closed-loop He cryostat (7-300 K) (Prasad *et al*., 2016).

All the radiofluorescence measurements reported in this paper were obtained using X-ray irradiation at room temperature and a CCD detector. Quartz grains were mounted on a steel cup using double-sided tape. Measurements were performed with a constant dose rate (ca. 0.06 Gy/s), integration times of 30 s (~1.8 Gy) for quartz sediment grains (samples L0001, L0017, L0229, L0572, L0674, L0680, L0688, and L0698) and 300 s (~18 Gy) for quartz rock crystals (samples VR12, ITA1, LA1, and IP22) and full-range detection (300-1,000 nm). Integration times were higher for quartz from rocks to acquire significant RF spectra. Background emission was acquired by measuring empty cups with tape. Samples were exposed to daylight, but they were not submitted to any thermal or irradiation treatment before the acquisition of RF spectra. RF spectra were deconvoluted into Gaussian components using the least square method with the Levenberg – Marquardt algorithm (Origin software 2018).

The same quartz samples used for RF measurements were previously submitted to OSL and TL sensitivity measurements performed in the two Risø TL/OSL DA-20 readers at the Luminescence and Gamma Spectrometry Laboratory (LEGaL) of the Institute of Geosciences, University of São Paulo, Brazil. The OSL and TL sensitivity data are presented in Mineli et al. 2020 and summarized in Table 1. The measurement protocol is described in Table 2. Aliquots of similar masses were used in order to minimize the effect of aliquot size on luminescence signal sensitivity. The readers are equipped with a beta-radiation source ($^{90}Sr/^{90}Y$) with dose rates of ca. 0.132 Gy/s and ca. 0.077 Gy/s, blue (470 nm, max. 80 mW $cm^{-2}$) and infrared (870 nm, max. 145 mW $cm^{-2}$) LEDs for stimulation and Hoya U-340 filters (200–400 nm) for light detection in the ultraviolet band. Regarding the instrument response spectra correction, RF and OSL/TL measurements were done on different equipment, and the absolute counts of

RF and OSL sensitivities are not directly comparable. However, the main goal of this study is the relative comparison between RF and OSL/TL. In the TL and OSL measurements carried out in Mineli *et al*. 2021, quartz aliquots were mounted on 9.7 mm diameter stainless steel discs using silicone oil. Each aliquot contained approximately 150 to 200 grains, as observed under an optical microscope, with an average mass of 8.1 ± 0.9 mg (see procedures for aliquot preparation in Sawakuchi *et al*., (2018).

Table 2: Measurement protocol used by Mineli *et al.* 2021 for determination of TL (step 3) and OSL (step 4) sensitivities. The 110$^{o}$C TL sensitivity was determined through the integration of the 75-125$^{o}$C interval of the TL glow curve and the OSL sensitivity through the first second of light emission of the OSL decay curve.

| Step | OSL and TL sensitivities [a] |
|---|---|
| 1 | Bleach with blue LEDs at 125° C for 100 s |
| 2 | Dose: 10 Gy |
| 3 | TL up to 190°C (5°C/s) (110$^{o}$C TL sensitivity) |
| 4 | Blue stimulation at 125°C for 100 s (OSL sensitivity) |
| 5 | Blue stimulation at 125°C for 100 s (background) |

## 2.4. Results

The comparison between RF spectra of quartz from rocks and sediments is shown in Fig. 1. Both types of quartz show similar RF in higher energy part of the spectrum (2.5-4.0 eV), despite the difference in their intensities and number of overlapping peaks, while in the lower part of the spectrum (1.5-2.5 eV), non-similarity in the RF spectra was observed.

The luminescence spectra of quartz samples used in this study showed a broad unstructured emission ranging from 1.5 eV (827 nm) to 4.1 eV (310 nm), with maximum RF intensity close to 2.0 eV (620 nm) for quartz from rocks (Figure 1a) and 3.6 eV (354 nm) for quartz from sediments (Figure 1b). For the emission spectra of quartz from rocks (Figure 1a), we identified five different emission bands represented by a broader band in the range of 1.6-2.1 eV (red), a narrow emission band centered at 2.3 eV and bands at 2.4–2.8 eV (blue), 3.0-3.4 eV (UV-violet) and 3.4-3.8 eV (UV). The visual analysis of the emission spectra of quartz from sediments resulted in the

identification of four different emissions at 1.6-2.2 eV (red), around 2.3-2.7 eV (blue), 3.0-3.3 eV (UV-violet) and 3.5-3.8 eV (UV) (Figure 1b). The RF intensity in some samples was not strong enough to perform a curve fitting analysis (Figure 1).

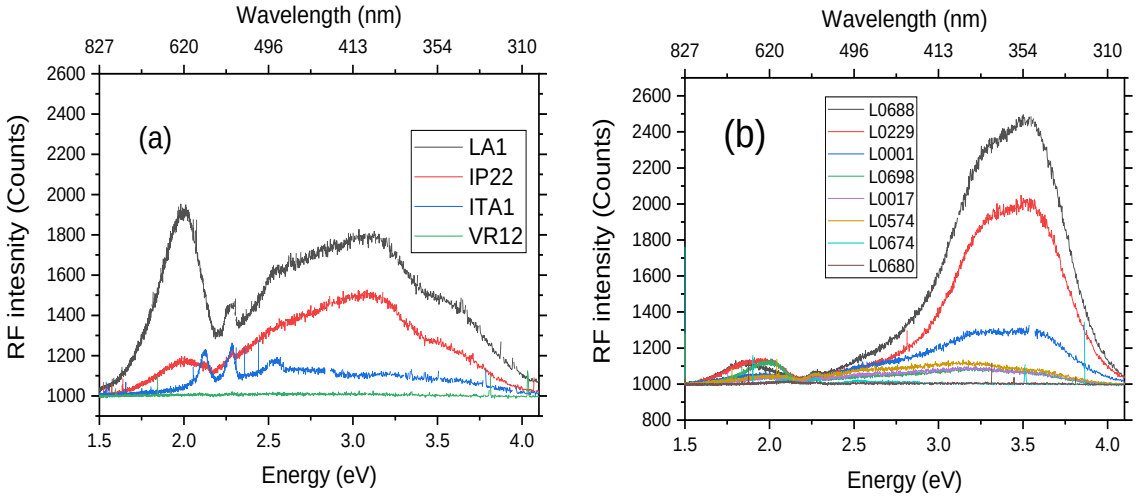


Figure 1. Comparison of the RF emission spectra measured in quartz from rocks (a) and sediments (b).

Generally, quartz from sediments of central and southern Brazil, represented by samples from the Paraná River (L0688), Southern Atlantic coast (L0001) and Pantanal Wetland (L0229), showed high UV-RF emission intensity compared to sediments from Chilean Andes, i.e., Mejillones Peninsula (L0674) and Salar Del Carmen (L0680). For quartz from Brazilian sediments, the exceptions are the samples from northern Brazil, i.e., central Amazon (L0572) and western Amazon (L0017 and L0698), that showed low RF intensity compared to that of quartz from central and southern Brazil used in this study. For the samples from rocks, quartz from granite (VR12 and ITA1) shows low RF intensity compared to quartz from rhyolite (LA1) and hydrothermal vein (IP22). Figure 2 shows the main characteristics of RF spectra recorded for quartz from rocks (LA1 and IP22) and sediments with higher (L0688) and lower (L0572) RF intensities.

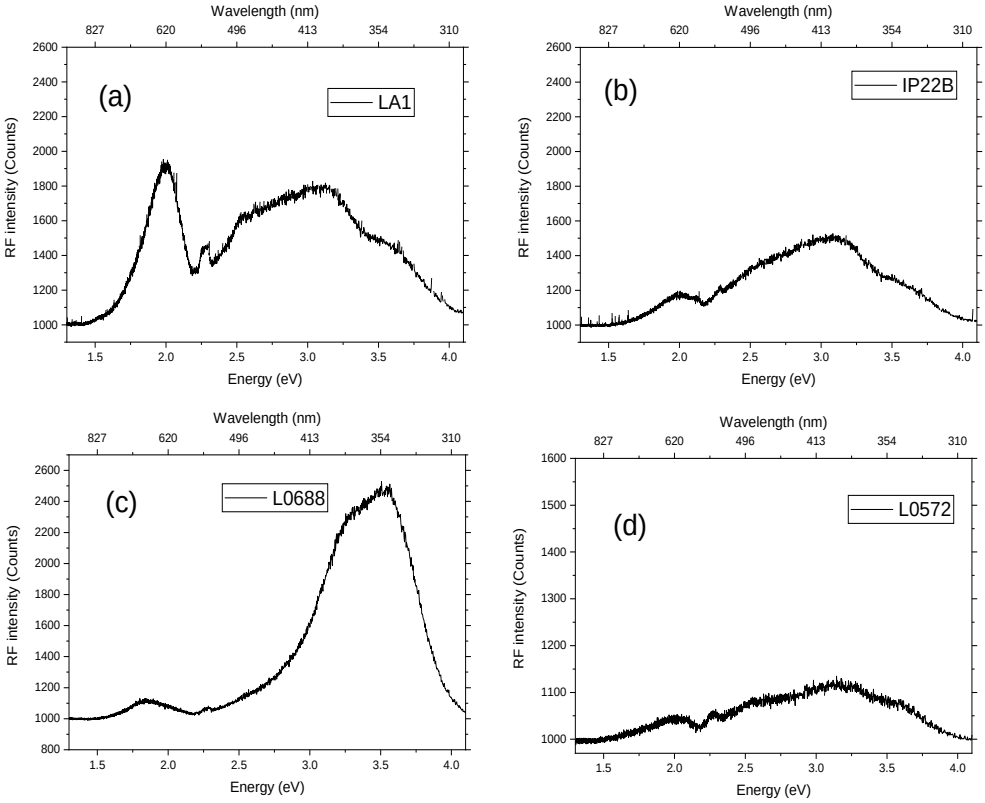


Figure 2. Spectra to illustrate the differences in RF intensities for quartz from rocks and sediments. RF spectra of quartz from rhyolite (a) and hydrothermal vein (b) have relatively low RF intensity compared to quartz from sediments of stable tectonic areas in southern Brazil (c). However, quartz from sediments of the Chilean Andes (d) has low RF intensity, comparable to quartz from rocks. The sample description can be found in Table 1.

All the RF emission spectra from quartz extracted from both rocks and sediments have been deconvoluted into their main components (Fig. 3). The fitting of the RF emission spectra was performed assuming four bands, and the Gaussian fitting agrees with experimental curves for samples with high RF intensity (Figure 3a).

The energy and full width at half-maximum for the four emission bands used in the deconvolution of the RF spectra are presented in Table 3, i.e., 1.87 eV (0.32 eV), 2.55 eV (0.99 eV), 3.36 eV (0.37 eV), 3.62 eV (0.42 eV) for quartz from sediments (L0688) and 1.97 eV (0.34 eV), 2,53 eV (0.48 eV), 3.07 eV(0.71 eV) and 3.7 eV (0.49 eV) for quartz from rocks (LA1). Martini *et al*. (2012b) reported five emission bands in natural quartz, i.e., 1.95 eV (0.48 eV), 2.53 eV (0.46 eV), 2.80 eV (0.45 eV), 3.44 eV (0.58 eV) and 3.94 eV (0.49 eV). Values within brackets are full width at half-maximum of the emission bands. More studies are needed to investigate the reasons

behind the difference in the number of RF emission bands and values of their full width at half-maximum for quartz from Brazil and quartz from other regions.

For the quartz from rocks and quartz from sediment samples (e.g., L0572, Figure 3c) with low RF intensity, Gaussian fittings are not entirely satisfactory in the energy region ranging from 2.1 eV to 2.4 eV (Figure 3b, c, and d), where small and sharp peaks might be sample related or instrumental artifacts. Other candidates to explain the presence of these sharp peaks are the presence of other mineral phases as inclusions in quartz, such as zircon or apatite. However, additional mineral inclusion analysis is required to confirm or reject this statement.

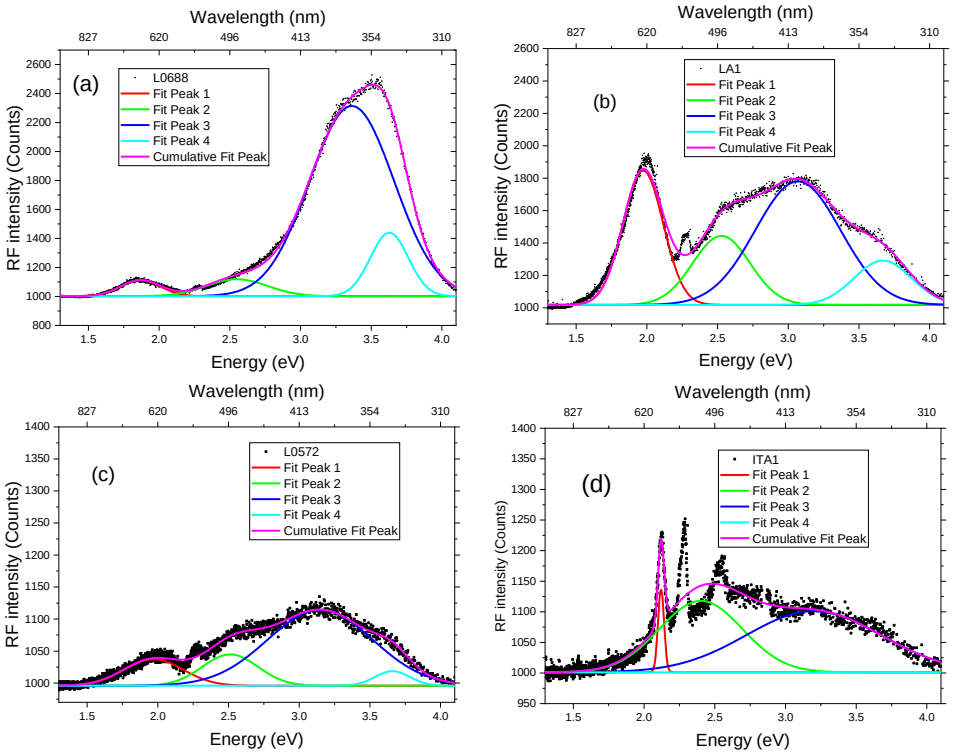


Figure 3. Gaussian components of high-intensity RF emission spectra of quartz from sediments of the Paraná River Basin (a) and rhyolite of Los Alamos (b). Gaussian components of low-intensity RF emission spectra of quartz from sediments of Central Amazon (c) and granite of the Ribeira Fold Belt (d).

Table 3: Energy values of the detected emission bands for quartz from rock (LA1) and sediment (L0688) samples.

| Bands | Sediment sample L0688 | | Rock sample LA1 | |
|---|---|---|---|---|
| | Energy (eV) | FWHM (eV) | Energy (eV) | FWHM (eV) |
| Peak 1 | 1.87 | 0.32 | 1.97 | 0.34 |
| Peak 2 | 2.55 | 0.99 | 2.53 | 0.48 |
| Peak 3 | 3.36 | 0.37 | 3.07 | 0.71 |
| Peak 4 | 3.62 | 0.42 | 3.70 | 0.49 |

Bands with peaks at 3.36 eV and 3.6 eV are the most intense in the sediment samples, and a band with a peak at 1.9 eV is the most intense for rock samples. Bands with peaks at 2.5 eV, 3.07 eV, and 3.7 eV are overlapping, as observed in quartz from rhyolite (Figure 3b). The RF intensities of bands with peaks at 3.07 eV and 3.70 eV for quartz from rocks and at 3.36 eV and 3.62 eV for quartz from sediments were used to investigate the relationship between UV-RF and the sensitivities of the 110°C TL peak and OSL (initial 1 s of light emission) assessed by Mineli *et al*. 2021 (Figure 4).

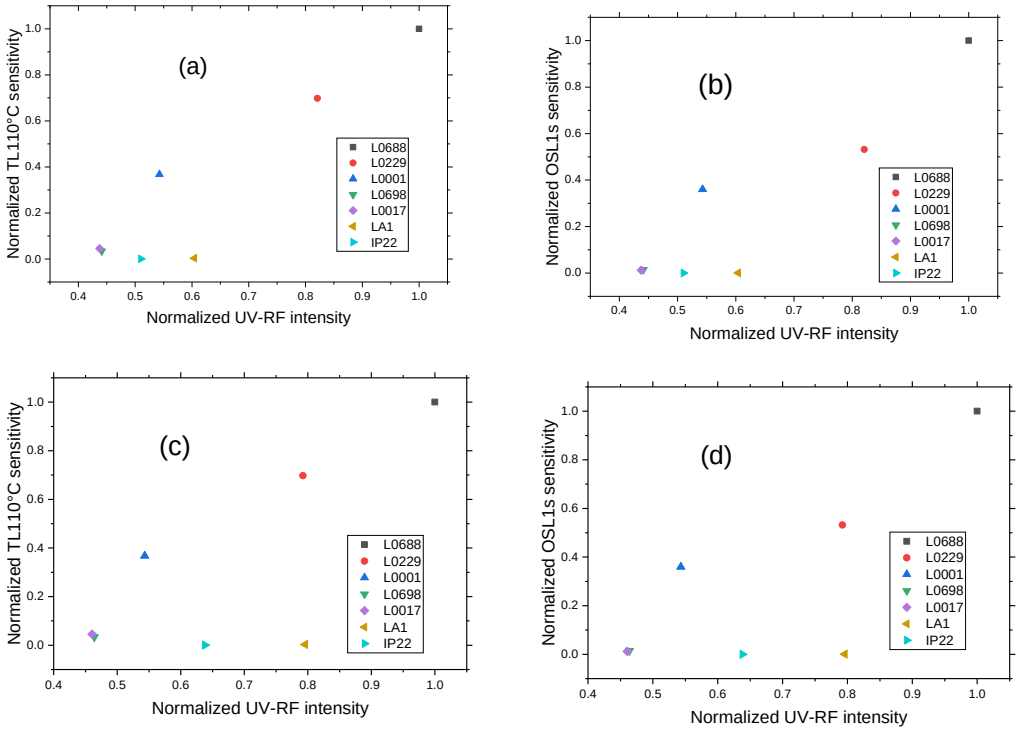


Figure 4. Relationship between 3.6 eV RF emission band intensity and sensitivities of 110°C TL peak (a) and OSL (b); and between 3.36 eV RF emission band intensity and sensitivities of 110°C TL peak (c) and OSL (d). The sensitivity of the OSL signal was taken from the integral of the initial second of the OSL decay curve divided by the given radiation dose**.** The sensitivity of the 110°C TL peak (heating rate of 5°C/s) was determined from the integration of the 75˚C-125$^{o}$C interval divided by the given dose. The TL and OSL sensitivities and UV-RF intensity were normalized to their corresponding highest signal for easy comparison.

A linear correlation, with a correlation coefficient (r) ranging from 0.95 to 0.99, between UV-RF and the sensitivities of the 110°C TL peak, and the OSL (first 1s) is observed for quartz extracted from sediments (Figure 5). However, no correlation was observed for quartz from rocks (LA1 and IP22) (Figure 4). The results from Fig. 5 indicate that samples with high UV-RF intensity are more sensitive in the case of both 110°C TL and OSL (first 1s).

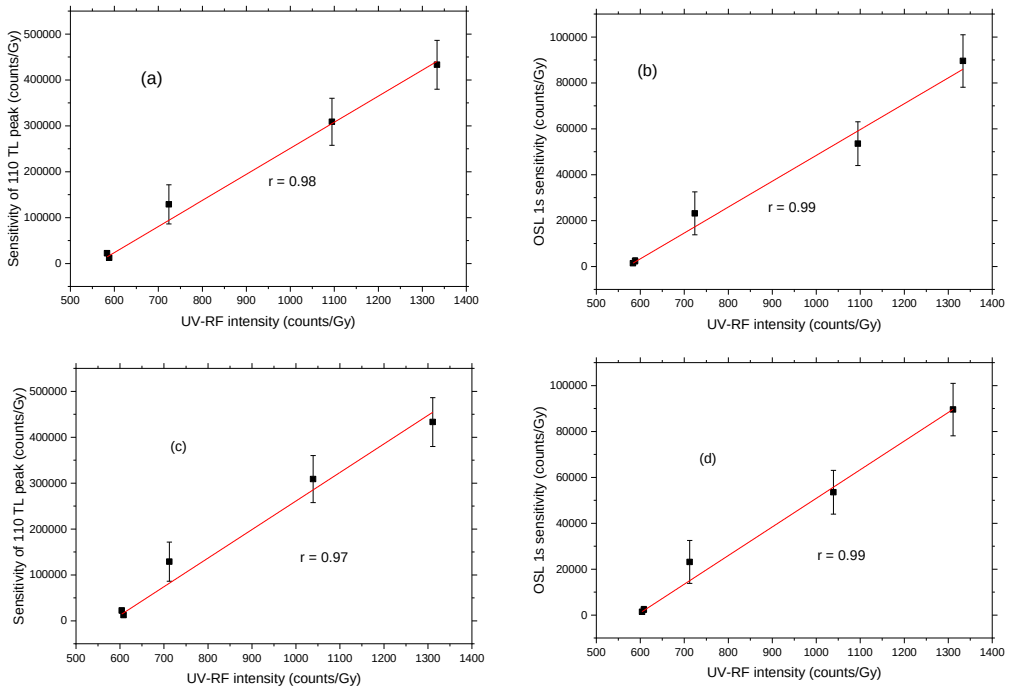


Figure 5. Correlation between 3.6 eV RF emission intensity and the 110ºC TL peak (a) and OSL (b) sensitivities of quartz from sediments. The intensity of the 3.36 eV emission band was also plotted for comparison with the 110ºC TL peak (c) and of OSL (d) sensitivities. The data for all graphs were fitted with a linear equation. For the UV-RF measurement, we only measured one aliquot for each sample.

## 2.5. Discussions and conclusions

In quartz, the correlation between the sensitivities of the 110°C TL peak and the first 1s of the OSL decay curve has been widely acknowledged, indicating that the fast OSL component and 110°C TL peak sensitize in a similar manner (Jain *et al*., 2003). In this study, we present the correlation between both OSL and TL sensitivities with RF intensity of quartz from sediments, which support the use of RF as provenance proxy in the same way as OSL and TL sensitivities.

The RF and TL emissions were found to be similar in the violet, blue, and red regions, suggesting that their recombination centers must be closely related to each other (Shimizu *et al*., 2006). According to Huntley *at al*. (1991), the OSL spectra of quartz have been observed in the ultraviolet region, so that the UV-RF (3.6 eV and 3.36 eV) emissions might also be related to the UV-OSL emission. In this study, we observed a linear correlation between the OSL sensitivity, presumably dominated by the fast component, and UV-RF (3.6 eV and 3.36 eV) intensity for quartz from sediments. We also observed a linear correlation between UV-RF and sensitivity of 110°C TL, which strongly supports the suggestion that sensitization processes in nature might be due to changes in recombination process (density of recombination centers for example) rather than changes in the charge trapping probability like proposed by Moska and Murray (2006).

In the present work, we also observe low RF intensity of quartz from rocks compared to quartz from sediments, which is a pattern also observed for the OSL sensitivity of quartz (Sawakuchi *et al*., 2011). The RF sensitization, when quartz is released from parent rocks to sedimentary systems, occurs mainly in the UV and blue emission bands (320–400 nm). However, quartz from sediments recently released from their parent rocks in active tectonic settings (L0017 and L0698) have RF intensity in the same range of quartz from rocks. Additional studies are needed to confirm that a single natural process is promoting the sensitization of quartz TL, OSL, and RF.

In conclusion, the results of this study indicate that quartz RF intensity mirrors sensitivity patterns observed for OSL and TL signals in nature and the UV-RF intensity measured using X-ray sources can also be used for provenance analysis of sediments in the same way as the OSL and TL sensitivities.

## 2.6. Acknowledgments

We appreciate the thoughtful and detailed comments and suggestions by Dr. Sebastian Kreutzer, who greatly contributed to improving the quality of our work. PN is grateful to the National Council for Science and Technology Development (CNPq), The World Academy of Sciences (TWAS) (CNPq/TWAS grant 154507/2017-2), and The São Paulo Research Foundation (FAPESP grant 2019/04059-6) for funding the Ph.D. fellowship at the University of São Paulo. AOS is supported by the National Council for Science and Technology Development (CNPq grant 304727/2017-2).

## 2.7. References


Aitken, M. J., 1998. An introduction to optical dating: the dating of quaternary sediments by the use of photon-stimulated luminescence. **Oxford University Press**.

Aitken, M. J., Smith, B. M., 1988. Optical dating: Recuperation after bleaching. **Quaternary Science Reviews**, 7, 387-393.

Chen, G., Li, S. H., Murray, A. S., 2000. Study of the 110°C TL peak sensitivity in optical dating of quartz. **Radiation Measurements**, 32, 641-645.

Chithambo, M. L., Preusser, F., Ramseyer, K., Ogundare, F. O., 2007. Time-resolved luminescence of low sensitivity quartz from crystalline rocks. **Radiation Measurements**, 42, 205–212.

Chithambo. M., Niyonzima. P., 2017. Radioluminescence of annealed synthetic quartz, **Radiation Measurements**, 106, 35-39.

Fleming, S. J., 1970. Thermoluminescence dating: refinement of the quartz inclusion method. **Archaeometry**, 12, 133-145.

Friedrich, J., Fasoli, M., Kreutzer, S., Schmidt, C., 2017. The basic principles of quartz radiofluorescence dynamics in the UV– analytical, numerical and experimental results. **Journal of Luminescence**, 192, 940–948.

Gray, H. J., Jain, M., Sawakuchi, A. O., Mahan, S. A., Tucker, G. E., 2019. Luminescence as a sediment tracer and provenance tool. **Reviews of Geophysics**, 57, 987-1017.

Grögler, N., Houtermans, F. G., Stauffer, H., 1958. Radiation damage as a research tools for geology and prehistory. Convengo sulle dotazioni con metodi nuclear. **5th Internazation Elettr Nucl Sezione Nuclear Roma**: 5-15.

Guralnik, B., Ankjærgaard, C., Jain. M., Murray, A. S., Müller, A., Wälle, M., Herman, F, 2015. OSL-thermochronometry using bedrock quartz: A note of caution. **Quaternary Geochronology**, 25, 37-48.

Huntley, D. J., Godfrey, S. D. I., Thewalt, M. L. W., 1985. Optical dating of sediments. **Nature**, 313, 105-107.

Huntley, D. J., Godfrey-Smith, D. I., Haskell, E. H., 1991. Light-induced emission spectra from some quartz and feldspars. **Nuclear Tracks Radiation Measurements**, 18, 127–131.

Jain, M., Murray, A. S., Bøtter-Jensen, L., 2003. Characterization of blue-light stimulated luminescence component in different quartz samples: Implications for dose measurement. **Radiation Measurements**, 37, 441-449.

Krbetschek, M. R., Götze, J., Dietrich, A., Trautmann, T., 1997. Spectral information from minerals relevant for luminescence dating. **Radiation Measurements**, 27, 695–748.

Krbetschek, M. R., Trautmann, T., 2000. A spectral radioluminescence study for dating and dosimetry. **Radiation Measurements**, 32, 853–857.

Lü, T., Sun. J., 2011. Luminescence sensitivities of quartz grains from eolian deposits in northern China and their implications for provenance. **Quaternary Research**, 76, 181-189.

Marazuev, Y. A., Brik, A. B., Degota, V. Y., 1995. Radioluminescent dosimetry of Alpha - quartz. **Radiation Measurements**, 24, 565-569.

Martini, M., Fasoli, M., Galli, A., 2009. Quartz OSL emission spectra and the role of [AlO4]° recombination centres. **Radiation Measurements**, 44, 458-461.

Martini, M., Fasoli, M., Galli, A., Villa, I., Guibert, P., 2012a. Radioluminescence of synthetic quartz related to alkali ions. **Journal of Luminescence**, 132, 1030-1036.

Martini, M., Fasoli, M., Villa, I., Guibert, P., 2012b. Radioluminescence of synthetic and natural quartz. **Radiation Measurements**, 47, 846-850.

Mehdahl, V., 1979. Thermoluminescence dating: Beta-dose attenuation in quartz grains. **Archaeometry**, 21, 61-72.

Mendes, V. R., Sawakuchi, A. O., Chiessi, C. M., Giannini, P .C. F.; Rehfeld, K., Mulitza, S., 2019. Thermoluminescence and optically stimulated luminescence measured in marine sediments indicate precipitation changes over northeastern Brazil. **Paleoceanography and Paleoclimatology**, 34.

Mineli, T. D., Sawakuchi, A. O., Guralnik, B., Lambert, R., Jain, M., Pupim, F. N., del Río, I. A. G., Nogueira, L., 2021. Variation of luminescence sensitivity, characteristic dose and trap parameters of quartz from rocks and sediments. **Radiation Measurements**, 144, 106583

Moska, P., Murray, A. S., 2006. Stability of the quartz fast-component in insensitive samples. **Radiation Measurements**, 41, 878-885.

Nian, X., Zhang, W., Qiu, F., Qin, J., Wang, Z., Sun, Q., Chen, J., Chen, Z., Liu, N., 2019. Luminescence characteristics of quartz from Holocene delta deposits of the

Yangtze River and their provenance implications. **Quaternary Geochronology**, 49, 131–137.

Pietsch, T. J., Olley, J. M., Nanson, G. C., 2008. Fluvial transport as a natural luminescence sensitizer of quartz. Quaternary Geochronology, 3, 365-391.

Prasad, A. K., Lapp, T., Kook, M. and Jain, M., 2016. Probing luminescence centers in Na rich feldspar. **Radiation Measurements**, 90, 292-297.

Rink, W. J., Rendell, H., Marseglia, E. A., Luff, B. J., Townsend, P. D., 1993. Thermoluminescence Spectra of Igneous Quartz and Hydrothermal Vein Quartz. **Physics and Chemistry of Minerals**, 20, 353-361.

Sawakuchi, A. O., Blair, M. W., DeWitt, R., Faleiros, F. M., Hyppolito, T., Guedes, C. C. F., 2011. Thermal history versus sedimentary history: OSL sensitivity of quartz grains extracted from rocks and sediments. **Quaternary Geochronology**, 6, 261–272.

Sawakuchi, A. O., Guedes, C. C. F., Dewitt, R., Giannini, P. C. F., Blair, M. W., Nascimento Jr., Faleiros, F. M., 2012. Quartz OSL sensitivity as a proxy for storm activity on the southern Brazilian coast during the Late Holocene. **Quaternary Geochronology**, 13, 92–102.

Sawakuchi, A. O., Jain, M., Mineli, T. D., Nogueira, L., Bertassoli Jr, D. J., Häggi, C., Sawakuchi, H. O., Pupim, F. N., Grohmann, C. H., Chiessi C. M., M. Zabel c, Mulitza S., Mazoca, C. E. M., Cunha, D. F., 2018. Luminescence of quartz and feldspar fingerprints provenance and correlates with the source area denudation in the Amazon River basin. **Earth and Planetary Science Letters**, 492, 152–162.

Sawakuchi, A. O., Rodrigues, F. C. G., Mineli, T. D., Mendes, V. R., Melo, D. B., Chiessi, C. M., Giannini, P. C. F., 2020. Optically stimulated luminescence sensitivity of quartz for provenance analysis. **Methods and Protocols**, 3(1), 6.

Schilles, T., Poolton, N. R. J., Bulur, E., Bøtter-Jensen, L., Murray, A. S., Smith, G. M., Riedi, P. C., and Wagner, G. A., 2001. A multi-spectroscopic study of luminescence sensitivity changes in natural quartz induced by high-temperature annealing. **Journal of Physics D: Applied Physics**, 34**,** 722–731.

Schmidt, C., Kreutzer, S., DeWitt, R., Fuchs, M., 2015. Radiofluorescence of quartz: A review. **Quaternary Geochronology**, 27, 66-77.

Shimizu, N., Mitamura, N., Takeuchi, A., Hashimoto, T., 2006. Dependence of radioluminescence on TL-properties in natural quartz. **Radiation Measurements**,

41, 831-835.

Tsukamoto, S., Nagashima, K., Murray, A. S., Tada, R., 2011. Variations in OSL components of quartz from Japan sea sediments and the possibility of reconstructing provenance. **Quaternary International**, 234, 182-189.

Wintle, A. G., Huntley, D. J., 1979. Thermoluminescence dating of deep sea sediments. **Nature**, 279, 710–712.

Zular, A., Sawakuchi, A. O., Guedes, C. C. F., Giannini, P. C. F., 2015. Attaining provenance proxies from OSL and TL sensitivities: coupling with grain size and heavy minerals data from southern Brazilian coastal sediments. **Radiation Measurements**, 81, 39–45.

# Chapter 3: Testing the potential of quartz violet stimulated luminescence for dating of Brazilian fluvial sediments

P. Niyonzima, A. O., Sawakuchi, N. Porat, F.N. Pupim, F. C. G. Rodrigues, I. S. A. A. Bezerra

## 3.1. Abstract

Brazil hosts large tropical rivers forming widespread quartz-rich sandy deposits recording landscape changes during the Quaternary. The optically stimulated luminescence (OSL) techniques have been applied in quartz to determine sediment deposition ages, but they are not suitable to obtain ages beyond 100–200 ka and potassium feldspar is lacking in most Pleistocene deposits due to intense tropical weathering. In the present study, we investigated the potential of post-blue violet stimulated luminescence (VSL) signals of quartz to extend the dating age range of fluvial sediments in Brazil. For this purpose, we appraised VSL properties of quartz from major fluvial systems in South America terraces from Western Brazil, Southeastern Brazil and Central and Eastern Amazonia. We estimated equivalent dose ($D_e$) and characteristic doses ($D_0$) of samples that showed natural VSL signal using a single aliquot regenerative dose (SAR) protocol, multiple aliquot regenerative doses (MAR) protocol and multiple aliquot additive doses (MAAD). Under preheat temperatures 200 to 340°C and blue bleach at 125°C for 100 s, the natural VSL signal is absent for samples from the Amazon basin, including samples with $D_e$ beyond OSL saturation. The natural VSL signal appears only in samples from Western and Southeastern Brazil when a lower preheat at 160°C is used, suggesting that the VSL signal in the studied samples is unstable over geological time scales. However, an isothermal decay experiment demonstrates that the VSL signal originates from a deep trap at about 2.3 eV, thermally stable for $10^{11}$ years at 10°C. The VSL SAR protocol poorly recovered a 500 Gy laboratory dose, indicating that VSL SAR poorly reproduces the natural dose growth. For a well bleached sample from the Paraná River basin, with OSL $D_e$ of 14.0 ± 0.3 Gy and characteristic dose of the second exponential function ($D_{0,2}$) of 146.4 ± 13.9 Gy, the VSL SAR protocol estimated $D_e$ of 85.4 ± 7.2 Gy for

regenerative doses in the range of 500–2500 Gy when the dose response curve (DRC) is fitted with exponential function. For an OSL saturated sample from the Pantanal wetland, the estimated $D_e$ using the VSL SAR protocol was 128.8 ± 18.5 Gy. The SAR VSL signal exhibits DRC with $D_0$ of about ~ 251 Gy, which is relatively low compared to previous VSL works. Applying MAAD protocol on the same sample, a characteristic dose ($D_{0,2}$) of ~821 Gy was estimated, higher than $D_0$ value for the SAR but still lower than previously reported values from Chinese loess samples ($D_{0,2}$ = 1334 Gy). In spite of $D_0$ lower than reported values from other sites, VSL protocols would allow a significant extension of quartz dating in Brazil, where Pleistocene sediments have common dose rates in the 0.5–1.0 Gy/ka range. The present study shows that the behavior of VSL signal appears to be sample dependent, indicating the need for further investigations on behavior of VSL signals of samples from different geological settings.

## 3.2. Introduction

Quartz optically stimulated luminescence (OSL) is widely used to establish the chronology of Quaternary sediments (Wintle and Adamiec, 2017), but its applicability is commonly limited to doses of 100–200 Gy (Wintle and Murray, 2006). Sedimentary deposits in Brazilian geological settings have typical dose rates of 1–2 Gy/ka. Hence, quartz OSL dating is limited to samples whose age does not exceed ~200 ka. There have been several attempts to extend the quartz luminescence dating range. Among the various techniques, thermally transferred optically stimulated luminescence (TT–OSL) signal has been reported for potentially extending the applicability of luminescence dating (Duller and Wintle, 2012) due to its ability to sample charges from traps deeper than the main OSL trap. Previous results suggested the potential for dating sediments of up to 1 Ma using quartz TT–OSL (Wang *et al*., 2006; Pickering *et al*., 2013; Arnold *et al*., 2015). While this methodology generated a large interest after promising results, following studies demonstrated that some characteristics of the quartz TT–OSL signal limit dating applications, such as slow signal resetting by sunlight (Tsukamoto *et al*., 2008; Kim *et al*., 2009; Porat *et al*., 2009) and low thermal stability (Hernandez *et al*., 2012). Quartz-rich sediments from Brazil are extensively used for luminescence dating using OSL and displayed excellent luminescence properties (Mineli *et al*., 2021), reaching ages up to 300 ka in relatively low dose rate environments (< 1 Gy/ka) (Guedes *et al*., 2013; Pupim *et al*., 2016).

The violet stimulated luminescence (VSL) signal from quartz was proposed by Jain (2009) to overcome the time limit for OSL dating. The method uses violet stimulation (402 nm), that is believed to sample deeper electron traps with higher saturation level than those accessible by blue light, offering the potential to extend the upper limit of luminescence dating using a stable, non-fading quartz luminescence signal saturating at higher doses. It was reported that the VSL saturation dose ($D_0$) values are 5–15 times larger than those of blue OSL (Jain, 2009; Ankjaergaard *et al*., 2013). The VSL signal obtained after blue stimulation, thus a “post-blue VSL”, originates from a deep trap with signal stability at the Ma timescale, which is bleachable by sunlight (Ankjaergaard *et al*., 2013; 2015, Hernandez and Mercier, 2015). Laboratory given doses were successfully recovered over a wide range between 300 Gy

and 2 kGy (Jain, 2009; Ankjaergaard *et al*., 2013; 2015; Colarossi *et al*., 2018) using VSL single-aliquot regenerative (SAR) dose protocols.

Several studies suggested that VSL SAR protocols can accurately estimate natural doses of up to ~300 Gy, resulting in ages that are in agreement with other independent ages (Ankjærgaard *et al*., 2013; Porat *et al*., 2018; Sontag-González *et al*., 2020). However, application of SAR VSL dating was not always successful. Several studies indicated an underestimation of ~50 % or more for samples with natural doses higher than 300 Gy (Ankjaergaard *et al*., 2015; 2016; Colarossi *et al*., 2018; Sontag-González *et al*., 2020). Ankjaergaard *et al*. (2016) concluded that the SAR protocols proposed for VSL dating are compromised by sensitivity changes induced by heating. Despite the fact that the SAR procedure is designed to monitor and correct potential sensitivity changes that occur during multiple regeneration cycles by measuring the response to a test dose, any sensitivity change that occurs before the first test dose measurement is not detected (Murray and Wintle, 2000). In attempting to overcome the sensitivity change obstacle, alternative approaches using multiple aliquots additive dose (MAAD) and multiple aliquots regenerative dose (MAR) (Aitken, 1998) protocols have been carried out (Ankjærgaard *et al*., 2016; Colarossi *et al*., 2018; Sontag-González *et al*., 2020; Ankjærgaard, 2019; Rahimzadeh *et al*., 2021). Ankjaergaard (2019) demonstrated good agreement between obtained VSL ages and independent chronology up to ~500 ka and 900 ka using the MAAD and MAR protocols, respectively. Despite the encouraging results using MAAD and MAR approaches, it was highlighted that proposed protocols need to be tested in samples from different geological settings, as the quartz VSL properties vary among samples (Ankjaergaard *et al*., 2013; Sontag-González *et al*., 2020), possibly mirroring the large variability observed in quartz OSL (Mineli *et al*., 2021).

In the present study, we investigated VSL signals of different quartz samples from major fluvial systems of Brazil, with equivalent doses ($D_e$) previously determined using other luminescence signals (Pupim *et al*., 2019; Mineli *et al*., 2021). Our aims are extending luminescence dating range for Brazilian sediments and providing additional data on the variation of quartz VSL signal characteristics relevant for sediment dating. In the first step, quartz sediment samples representative of Brazilian sediments were analyzed to investigate best suited parameters for measuring quartz VSL signals. Then,

trap energy and thermal lifetime are reported for the detected VSL signal. Finally, post-blue VSL SAR, MAR and MAAD protocols were tested by constructing dose response curves (DRC) and assessment of the maximum equivalent dose that could be estimated for the studied samples. The VSL data from Brazilian quartz are discussed in terms of VSL characteristics reported for quartz from other study settings.

## 3.3. Material and Methods

### 3.3.1. Sample description and preparation

For this study, a total of 13 sediment samples were collected from major fluvial systems of Brazil (Table 1 and Figure 1). Expected doses range from 14 Gy, previously determined using OSL (Mineli *et al*., 2021), to 1221.6 Gy, using TT-OSL (Bezerra *et al*., 2021) (Table 1). Sediments samples were wet sieved to isolate the 180–250 μm grain size fractions. Then, the samples were submitted to a treatment with $H_2O_2$ and HCl (10%) to remove organic matter and carbonate minerals, respectively. Quartz separation involved lithium metatungstate solution (LMT) to separate light materials from heavy minerals (LTM = 2.85 g/cm$^3$) and to separate quartz from feldspar grains (LMT = 2.62 g/cm$^3$). After this step, quartz concentrates were submitted to a treatment with 38% HF for 40 min to remove the external layer of quartz grains. The absence of significant feldspar contamination was confirmed by infrared stimulation, and in some cases, samples were repeatedly etched with HF 5% until a negligible (less than 10% of the blue OSL) infrared signal remained.

Table 1: Details of the studied fluvial sediment samples. Samples locations are showed in Figure 1. $D_e$ values were estimated using protocols proposed by Adamiec *et al*. (2010) for TT-OSL, Buylaert *et al*. (2012) for post-Infrared Infrared luminescence at 290°C (pIRIR290) and Murray and Wintle (2000) for OSL. For samples from Eastern and Central Amazonia, references were made for De values of samples collected from the neighbouring area.

| **Site** | **Laboratory code** | **Latitude/Longitude** | **Equivalent dose ($D_e$) estimation method** | **Expected $D_e$ (Gy)** | **Expected $2D_0$ (Gy)** | **Reference** |
|---|---|---|---|---|---|---|
| Fluvial terrace, Pantanal wetland, Western Brazil | L0229 | -20.0134/-55.9777 | OSL | Saturated | 128.2 ± 3.2 | Mineli *et al*. (2021) |
| Paraná River terrace, Southeastern Brazil | L0688 | -23.65694/-50.0350 | OSL | 14.0 ± 0.3 | | |
| Içá Formation, Solimões River, Western-Central Amazonia | L0477<br>L0496<br>L0693 | -3.4004/-64.6118<br>-4.0861/-63.0978<br>-4.3633/-70.9124 | OSL | 117.3 ± 6.6<br>97.3 ± 7.7<br>164.4 ± 33.6 | | Pupim *et al*. (2019) |
| Amazon River terrace, Eastern Amazonia | L1083<br>L1084<br>L1085 | -2.0092/-54.0941 | $pIRIR_{290}$ | 170.2 ± 24.4 | | Bezerra *et al*. (2021) |
| Amazon River terrace (sediment core), Central Amazonia | L1485<br>L1486<br>L1487<br>L1488 | -3.49425/-58.9736 | TT-OSL | Up to 1221.6 ± 117.3 | | |

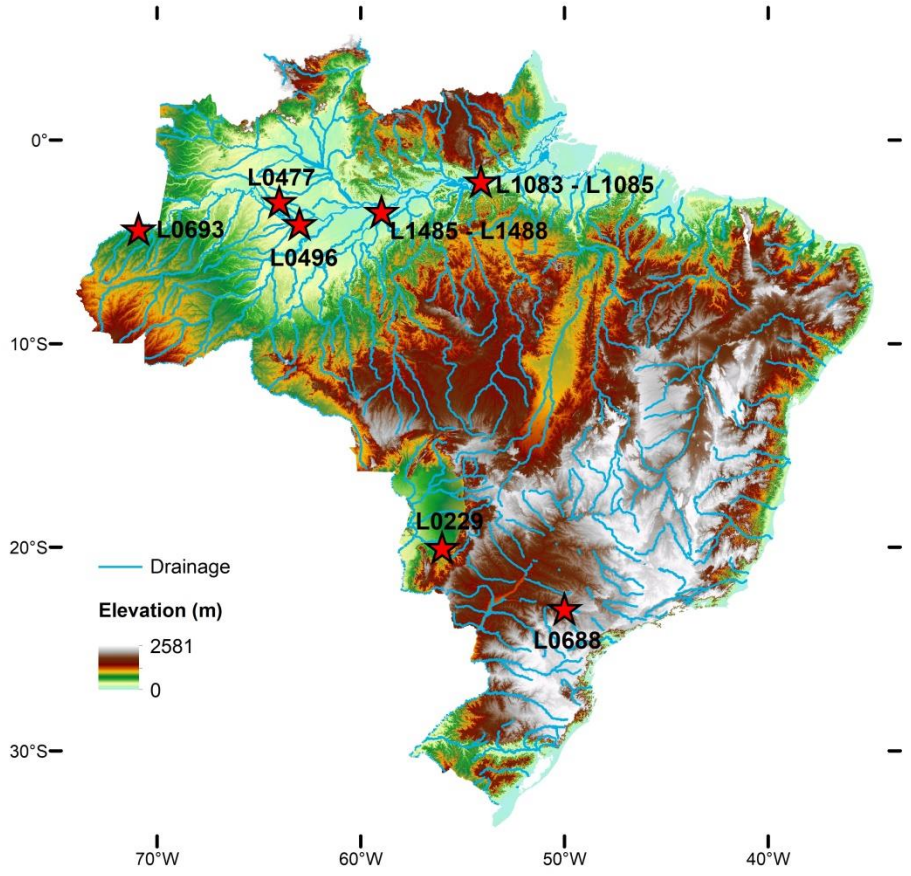


Figure 1: Digital elevation map of Brazil with the location of the studied samples (red stars). Samples characteristics are described in Table 1.

### 3.3.2. Luminescence instrumentation and measurements

All luminescence measurements were conducted using solid state violet (402 nm) laser diodes fitted onto an automated Risø TL/OSL-20 reader system equipped with $^{90}Sr/^{90}Y$ beta source delivering dose rate of 0.119 ± 0.002 Gy/s. The stimulation was made at 90% maximum power density (~100 mW/cm$^2$). Quartz VSL emissions were recorded in the ultraviolet spectra through a Thorn EMI 9235QB photomultiplier. The violet laser stimulation attachment is equipped with AHF F39–404, Brightline HC/405/10, ø45 mm, 2 mm detection filter. The quartz grains were mounted on aluminium discs using silicone spray. The presence of VSL signal in the samples was investigated after a range of preheat temperatures from 160 to 340°C for 100 s and blue stimulation at 125°C for 100 s followed by VSL at 30°C stimulation for 500 s. We have also studied the thermal stability of trapped electrons associated with VSL signals using an isothermal annealing experiment (Li and Chen, 2001).

Dose recovery test was performed using a given dose of 500 Gy to test whether the SAR VSL protocol can adequately correct for any sensitivity change during the first SAR cycle (Wintle and Murray, 2006). The signal was integrated between 0-8 s and the background between 475–500 s (Jain, 2009; Ankjaergaard *et al*., 2016). Dose response curves (DRCs) were fitted with single saturating exponential, exponential plus linear, and double saturating exponential functions in order to obtain the function that best fits the regenerated signals. Finally, we investigate the VSL dose response behavior using VSL SAR, MAR and MAAD protocols (Ankjaergaard *et al.*, 2016) (Table 2).

Table 2: VSL protocols used in this study. For the natural signal measurement, Ln/Tn, the irradiation dose in step 1 is x = 0 Gy. The experimental details for MAAD, MAR protocols are discussed in the main text of the corresponding sections.

| Step | SAR VSL (Ankjaergaard et al., 2016) | MAR (Ankjaergaard et al., 2016) | MAAD (Ankjaergaard, 2019) |
|---|---|---|---|
| 1 | Irradiation (x Gy) | Irradiation dose (x Gy) | Additive dose |
| 2 | Preheat (160-340ºC, 100s) | Preheat (160°C, 100s) | Preheat (160°C, 100s) |
| 3 | Blue bleach (125ºC, 100s) | Blue bleach (125°C, 100s) | Blue bleach (125°C, 100s) |
| 4 | VSL (30 ºC, 500s) ($L_x$) | VSL (30°C, 500s) ($L_x$) | VSL (30°C, 500 s) |
| 5 | Test dose (200 Gy) | Test dose (200 Gy) | Test dose (540 Gy) |
| 6 | Preheat (160ºC, 100s) | Preheat (160°C, 100s) | Preheat (160°C, 100s) |
| 7 | Blue bleach (125ºC, 100s) | Blue bleach (125°C, 100s) | Bleu bleach (125°C, 100s) |
| 8 | VSL (30 ºC, 500s) ($T_x$) | VSL (30°C, 500s) ($T_x$) | VSL (30°C, 500s) |
| 9 | TL (500°C for 20s) | | |

### 3.4. Results

#### 3.4.1. Characterization of VSL signal

In the initial measurements to estimate $D_e$, we first used the post-blue VSL-SAR protocol of Ankjaergaard *et al*. (2016) (Table 2) where a preheating step of 340°C followed by blue stimulation is used to reduce the contribution from both the slow decaying but early saturating OSL S3 component as well as the fast OSL component in the VSL signal. None of the samples in this study displayed natural VSL signals when measured after this preheat temperature (340°C). Following this, the presence of the VSL signal was investigated using preheat temperatures in the range between 160 and 320°C for 100 s. A natural VSL signal was observed only after a low preheat temperature of 160°C and only for the samples from the Paraná River basin (Southeastern Brazil) and Pantanal wetland (Western Brazil). Studied samples from the Amazon River basin did not display natural VSL signal even after using the lower preheat temperature. Figure 2 shows the decay curves for samples that displayed natural and regenerated (500 Gy) post-blue VSL signals measured using a preheat at 160°C for 100 s. Examples of VSL decay curves of samples from the Amazon River basin are shown in Figure S1.

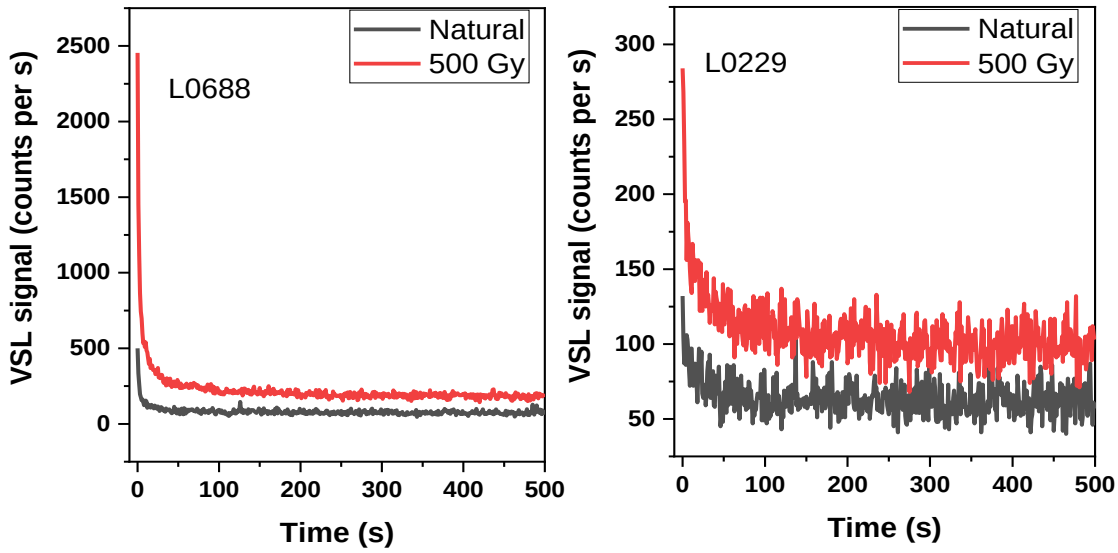


Figure 2: Natural VSL decay curves compared with VSL decay curves measured after irradiation dose of 500 Gy. VSL was recorded after preheat at 160°C for 100 s.

A second blue OSL stimulation (post-blue OSL) was added between the blue bleaching and VSL measurement steps to ensure the total bleach of OSL traps before VSL measurement. The post-blue OSL is much smaller compared to the OSL, and it shows almost no decay compared to either OSL or VSL (Figure S2), indicating that indeed the blue OSL is fully depleted prior to VSL measurements.

### 3.4.2. Thermal stability

The absence of the VSL signal in samples (L0229 and L0688) after a high temperature preheat might indicate thermal instability of the VSL signal. Thus, further investigation of VSL thermal stability was performed using sample L0229, which presented substantial VSL signal. The thermal stability of trapped electrons associated to VSL signals was measured using isothermal annealing experiment (Li and Chen, 2001). An aliquot was irradiated with 500 Gy, preheated to 160°C for 100 s, bleached by blue light at 125°C for 40 s, and held at a temperature that varied between 160 and 300°C (with 40°C increment) for various holding times up to 10000 s, followed by violet stimulation. The VSL response to a test dose of 200 Gy was used for sensitivity change correction. For storage temperatures of 160°C and 200°C, the VSL signals did not show any trend with respect to the isothermal storage time. Hence, these were removed for further analysis. We observed the decrease of VSL signal with isothermal storage time for temperatures of 240, 280 and 300°C. However, the scatter in data point was observed for the temperatures of 240°C and 280°C. The scatter might be due to the overall low VSL signal of the studied sample. Since the decay of the VSL signal does not follow first order kinetics, the effective lifetime ($\tau_{eff}$) was derived from the fit of VSL decay curve (Figure 3a) following Equation 1 (Ankjaergaard *et al*., 2013):

$$I(t) = \left(1 + ct/\tau_{eff}\right)^{-1/c}, c > 0 \qquad (1)$$

Where *I(t)* is the intensity of the VSL signal at time *t*, and *c* is a dimensionless parameter.

When the resultant curves are best fitted by stretched hyperbolic function from the fit, effective lifetime ($\tau_{eff}$) at each temperature is estimated. The slope and the intercept of a regressed straight line from the natural logarithm of the effective lifetime, ln($\tau_{eff}$), plotted against inverse of temperature, *1/kT*, corresponds respectively to the VSL

thermal trap depth, E[eV], and the natural logarithm of the frequency factor, s[$s^{-1}$]. The thermal lifetime of the VSL signal at mean air temperature of 10°C is calculated from Equation 2:

$$\tau = s^{-1} \exp\left(\frac{E}{kT}\right) \qquad (2)$$

The effective lifetime ($\tau_{eff}$) plotted against the inverse of temperature ($1/kT$) gave the values of E = 2.3 ± 0.2 eV and ln(s) = 43.3 ± 3.7 $s^{-1}$ (s = 6.4 x$10^{18}$ $s^{-1}$). When the values of E and s are inserted in Equation 2, a thermal lifetime of 2 x $10^{11}$ years at 10°C is obtained.

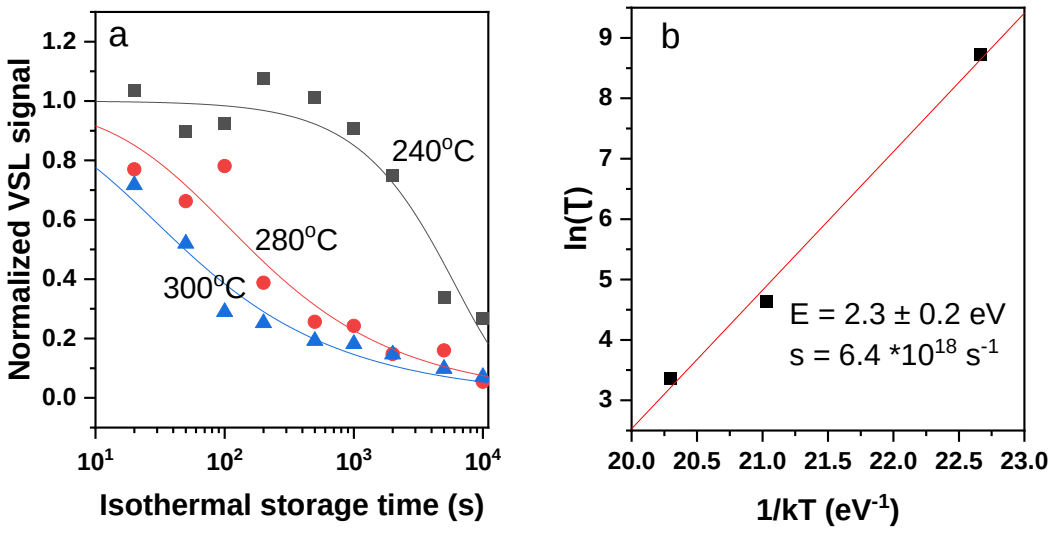


Figure 3: VSL signal lifetime estimation using isothermal experiment for sample L0229. The VSL signals were normalized using VSL signal from zero second heating isothermal temperature in order minimize the possible overlap of graphs from different isothermal temperature. (a) The change in the (normalized) VSL signal with isothermal storage time, fitted by a stretched hyperbolic function to estimate the lifetime. The x-axis is in log scale for clarity. (b) Natural logarithm of the lifetime as a function of the inverse of temperature fitted to a straight line to estimate the kinetic parameters (E and s).

### 3.4.3. Dose recovery tests under varied preheat temperatures

Sample L0688 was used for the dose recovery test over preheat temperatures of 160–280°C in 40°C intervals. Twelve medium-sized aliquots were prepared; with three aliquots measured for each preheat temperature. The VSL response to a test dose of 40 Gy was used for sensitivity correction. Each aliquot was initially bleached for 500 s at 380°C using violet laser at 90% power to remove the natural signal, followed by a beta

dose of 500 Gy that was considered as an unknown dose. Dose response curves were constructed using regenerative doses up to 1000 Gy, and fitted with a single saturating exponential function to estimate the known given dose. Figure 4 shows the ratios of the average calculated-to-the given dose as a function of preheat temperature.

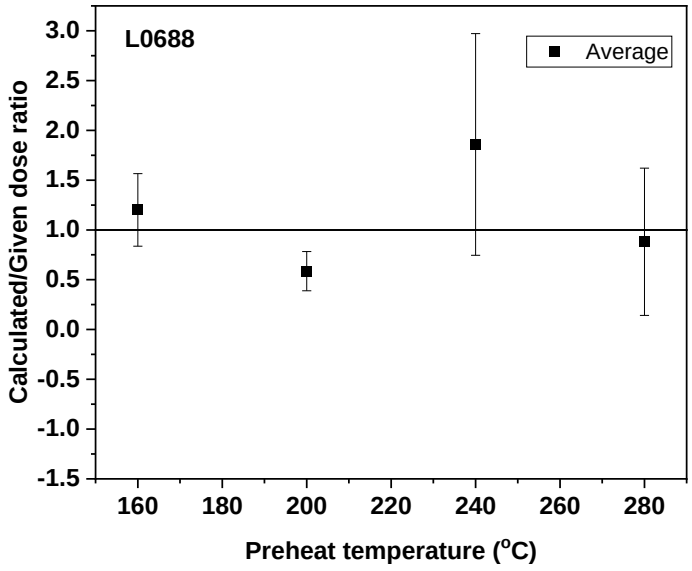


Figure 4: The average calculated-to-given dose ratios estimated using VSL and the SAR protocol as a function of preheat temperature. Each data point corresponds to the average of three aliquots.

Calculated-to-given dose ratios of the individual aliquots are very scattered especially when using preheat temperature higher than 200°C. This inter-aliquots scatter produced large standard deviation of the average calculated-to-given dose ratio for temperatures of 240°C and 280°C. The average values of calculated-to-given dose ratios are 1.20 ± 0.36, 0.58 ± 0.19, 1.86 ± 1.11 and 0.88 ± 0.74 for temperatures of 160°C, 200°C, 240°C and 280°C, respectively. The best and acceptable calculated-to-given dose ratio of 0.95 was observed on one aliquot for preheat temperature of 160°C.

In an attempt to identify the cause of the obtained poor dose recovery results, we tested the efficiency of this SAR VSL protocol in resetting the signal between cycles in order to examine the capacity of mid-SAR cycle VSL signal resetting. Colarossi *et al*. (2018) proposed a method of examining mid-SAR cycle signal resetting by plotting the luminescence signal from the first channel of a test dose measurement ($T_x$) as a function of the signal from the last channel of the preceding ($L_x$) for each cycle of the SAR

protocol. Efficiently resetting of the luminescence signal will be indicated by a slope of the linear regression close to zero.

The luminescence signal from the first channel of the test dose measurement ($T_x$) was plotted as a function of the signal from the last channel of the preceding regeneration measurement ($L_x$) for each cycle of the SAR protocol (Figure 5).

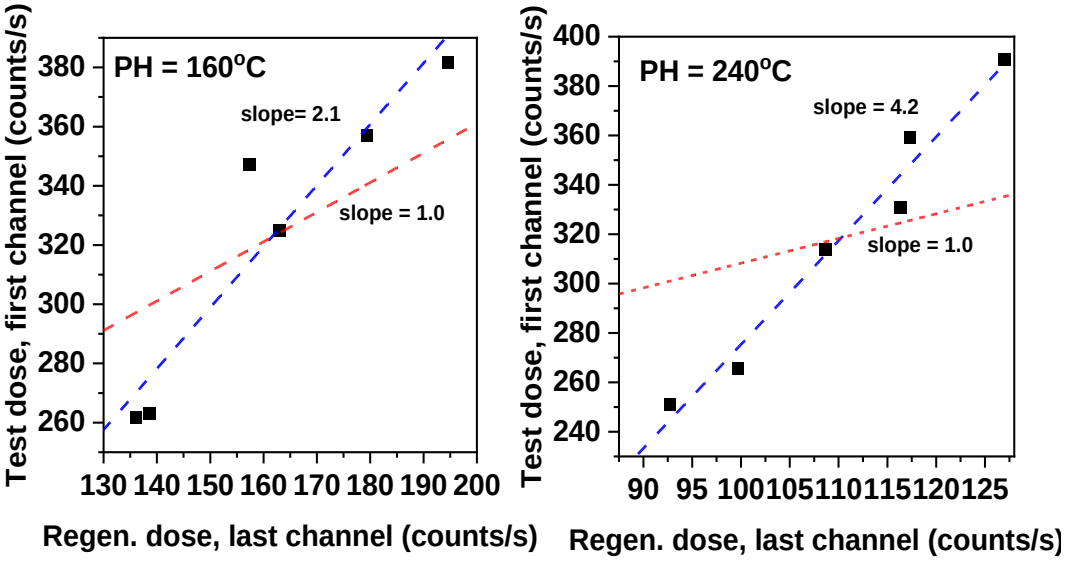


Figure 5: Investigation of the amount of signal carried over from the regeneration dose measurement ($L_x$) to the test dose measurement ($T_x$). The number in the linear fit is the corresponding slope. A linear relationship with slope of 1.0 is shown for comparison.

The data in Figure 5 have slopes greater than 1.0, implying the probability of charges being carried over from the $L_x$ measurement into the $T_x$ measurement. Here, low VSL signal and ineffective resetting between dose regeneration and test dose signal measurements may also be the cause of the poor recovery of the known dose.

### 3. 4. 4. Dose response behaviour

### 3.4.4.1. Single aliquot regenerative dose

SAR measurements were carried out on samples L0688 and L0229 that displayed a measurable natural VSL signal. These samples were previously dated by OSL and gave a central age model (CAM) $D_e$ and $2D_0$ respectively of 14.0 ± 0.3 Gy and 128.2 ± 3.2Gy (Table 1). The $D_e$ values estimated using the VSL SAR protocol and regeneration

doses up to 2500 Gy are shown in Table 3. The VSL signal of the aliquots was then measure and normalized to the VSL signal of a 200 Gy test dose (Table 3) to construct a SAR DRC (Figure 6).

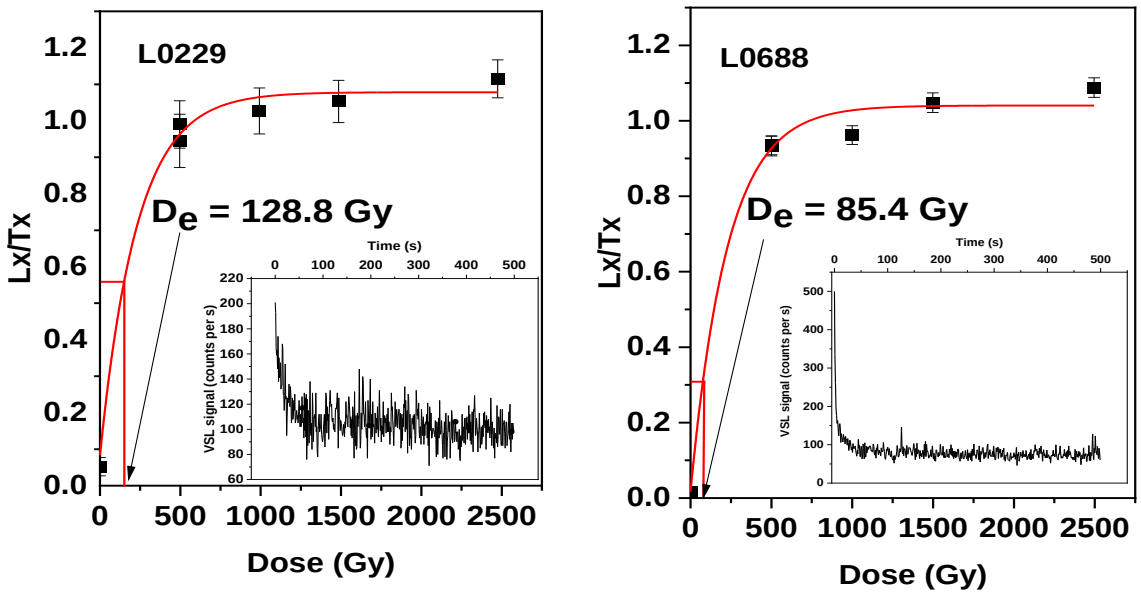


Figure 6: Example of dose response curves from single aliquot regenerative protocol for VSL signal fitted with a single saturating exponential for samples L0229 and L0688. The insets are the natural VSL decay curves for aliquots of each sample.

The intensity of the VSL signal (Figure 6, inset) is roughly 0.5% of the OSL signal measured prior to VSL measurement (Figure S2). Additionally, the VSL signal reaches a background level after ~100 s, while the OSL signal reaches a background level in the first seconds of the decay curve. The SAR DRC can be well fitted with a single saturating exponential function for L0688 ($R^2$ = 0.998) and L0229 ($R^2$ = 0.996) samples with higher values of $D_e$ compared to exponential plus linear function (Table 3). For Sample L0688, the sum of two saturating exponentials failed to fit the VSL RDC.

### 3. 4. 4.2. Multiple aliquots regenerative dose

VSL SAR protocol failed to measure a known dose. It is therefore of interest to test both MAR and MAAD protocols (Ankjaergaard *et al.*,2016) to investigate the characteristics of dose response curves built using VSL signal. The MAR and MAAD protocols measure the luminescence signal of each aliquot only twice, once for

natural/regeneration dose, and again for a test dose to normalize for the variability among aliquots (Chapot *et al*., 2012). A sensitivity-corrected MAR protocol was used to construct the MAR DRC for two samples (L0229 and L0688). Twenty seven fresh aliquots for each sample were prepared and divided into nine groups with three aliquots each. For the first group of aliquots, the natural signal $L_n/T_n$ was measured. The remaining aliquots were first bleached using VSL at 380°C for 500 s, then each group was irradiated with a range of beta doses (6, 30, 60, 125, 250, 500, 1000, 2000 Gy). The VSL signal of the aliquots was then measured and normalized to the VSL signal after a test dose of 540 Gy, and the normalized values were used to construct a MAR DRC (Figure 7). For the measured aliquots, the value of $L_n/T_n$ is always less than the $L_1/T_1$, and the DRCs were used to estimate the $D_0$ of MAR VSL protocol for studied samples. For L0229, the data point at 1000 Gy deviated from the fitting function and was considered as outlier and thus removed for the analysis.

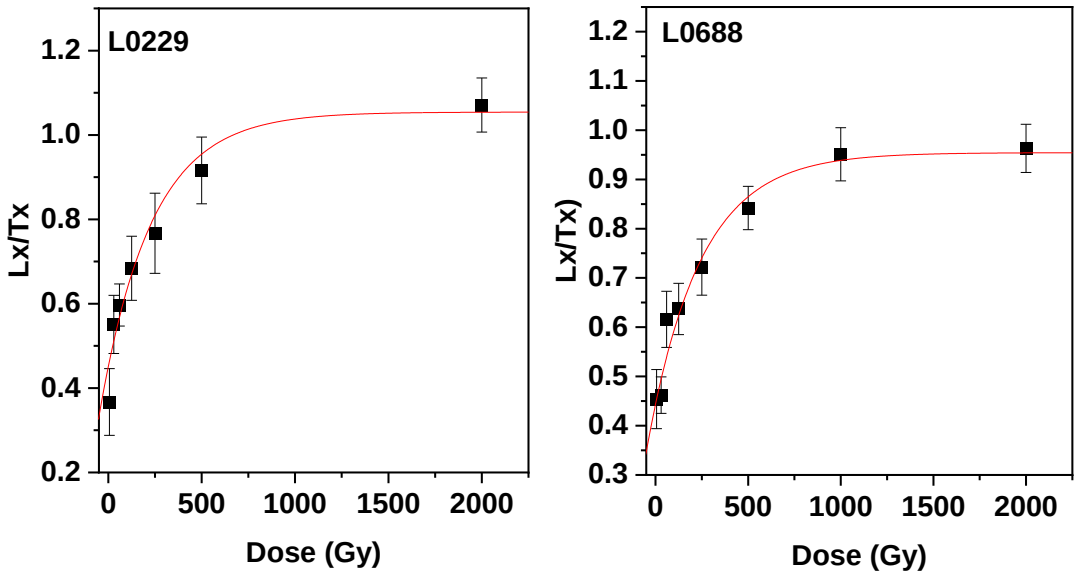


Figure 7: MAR DRC for samples L0229 and L0688 fitted with a single saturating exponential function.

The DRC for samples L0229 and L0688 can be fitted equally well with both saturating exponential and double saturating exponential functions. Resulting values of $D_0$ are presented in Table 3.

### 3.4.4.3. Multiple aliquot additive dose

The post-blue MAAD VSL protocol was applied to three samples (L0229, L0688 and L1488) following the parameters in Ankjærgaard *et al*. (2016). The main objective of this experiment is minimizing the sensitivity change that might have occurred during the high temperature VSL bleach (380°C for 500 s) before applying the MAR protocol. Fresh aliquots were given a range of doses (0, 6, 15, 30, 60, 115, 230, 460, 920, 1840, 3680 and 8100 Gy). Here, we only measured one aliquot for each dose. In this experiment, the range of doses was higher than prior experiments to investigate the maximum $D_0$ that VSL signal is able to reach for Brazilian fluvial quartz. The VSL signal of all aliquots was then measured and normalized to a VSL signal following a test dose of 540 Gy to construct the MAAD DRC (Figure 8). The double saturating exponential function fitted roughly the MAAD dose response curves for samples and the results from the fit are given in Table 3. The fitting equations also gave the same value of saturation doses ($D_{0,1}$ = $D_{0,2}$). Sample L1488 showed VSL decay curves with low signal intensity, which gave dose response curve poorly fitted by two exponential functions (Figure S4).

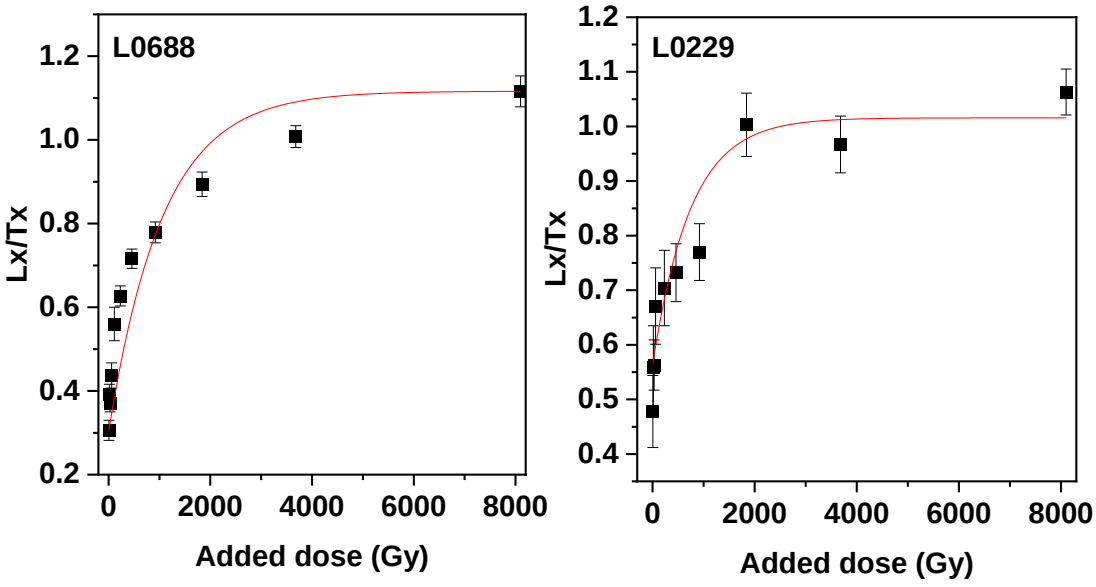


Figure 8: Dose response curves constructed from sensitivity corrected VSL signal measured after adding different laboratory doses to a natural dose fitted by a sum of two saturating exponentials.

Table 3: Values of natural doses ($D_e$) and characteristic doses ($D_0$) for studied samples. The DRC were fitted with a single saturating exponential (Exp), saturating exponential plus linear (Exp + lin) and double saturating exponential (DSE) functions. For sample L0229, DSE estimated $D_{0,2}$ with higher error of the order of power of 10.

| Sample | SAR (Exp) | | SAR (Exp + lin) | | MAR (Exp) | MAAD (DSE) |
|---|---|---|---|---|---|---|
| | $D_e$ (Gy) | $D_0$ (Gy) | $D_e$ (Gy) | $D_0$ (Gy) | $D_0$ | $D_{0,2}$ |
| L0229 | 128.8 ± 18.5 | 251.0 ± 69.4 | 92.3 ± 16.8 | 170.0 ± 122.0 | 277.9 ± 95.5 | 777.4 |
| L0688 | 85.4 ± 7.2 | 235.0 ± 28.1 | 44.4 ± 2.9 | 104.0 ± 123.0 | 287.3 ± 71.3 | 821.6 ± 489.8 |

## 3.5. Discussion

### 3.5.1. VSL signal variation

We appraised the VSL characteristics of quartz from fluvial sediment samples of different geological areas within Brazil. Samples from Western Brazil (L0229) and Southeastern Brazil (L0688) displayed a moderate natural VSL signal only after a low preheat temperature of 160°C. Samples from sedimentary deposits of the Amazon River basin, with expected minimum natural OSL dose of ~100 Gy, did not display natural VSL signal even using this low preheat temperature. However, after a high laboratory irradiation dose of the order of ~1000 Gy, low VSL signal was observed after a preheat temperature of 300°C. The potential explanation for the absence of natural VSL signal for all studied samples after a high temperature preheat (200–340°C) is that the natural VSL signal is thermally unstable over geological time scales. For this reason, thermal stability of the VSL signal was tested using a sample that displayed natural VSL signal when measured using a low preheat (160$^{o}$C).

The results using isothermal annealing experiment showed that VSL signal originates on stable trap of the depth of 2.3 eV and with a thermal lifetime of $10^{11}$ years. These values are consistent with previous reported values of VSL signal trap depth (2.02 ± 0.04 eV) and thermal lifetime (4.6 x $10^{12}$ years) for quartz from Chinese loess (Rahimzadeh *et al.*, 2021) and from the Netherlands (Ankjaergaard *et al.*, 2013) (Table 4). It is interesting to compare the lifetime obtained for the VSL signal to that of the conventional blue OSL trap, which showed E = 1.70 ± 0.01 eV s and lifetime of ~$10^9$ years of the same sample (L0229) (Mineli *et al*., 2021). Isothermal experiment showed that the VSL signals for the studied sample (L0229) originate from a deeper and more

stable trap than the OSL signal. Hence, low VSL intensity for some samples and absence of natural VSL signal for others cannot be attributed to low thermal stability of VSL signal over geological timescales.

The studied samples from the Amazon basin have quartz with moderate OSL (Sawakuchi *et al*., 2018; Mineli *et al*., 2021) and radiofluorescence sensitivities (Niyonzima *et al*., 2020) compared to the studied samples from Western and Southeastern Brazil. Hence, the observed variation of VSL characteristics could be related with the same processes leading to sensitization of quartz OSL. In Western and Southeastern Brazil, the longer lifetime of quartz grains near the surface favours the OSL sensitization through solar exposure and burial cycles. In the same way, this could also sensitize quartz VSL, which uses the same recombination center (ultraviolet emission) of OSL.

### 3.5.2. Dose response and characteristic dose

Ankjaergaard *et al.* (2016) showed that the natural VSL signal in quartz grows in the natural environment over the range from 200 to 2000 Gy, and using a modified multiple aliquots additive method they obtained ages in agreement with independent age control up to 600 ka, beyond the limit of quartz OSL dating. For the sample L0688 with low OSL $D_e$ (14 Gy), the VSL SAR protocol determined a $D_e$ of 85.4 ± 7.2 Gy, with a dose response curve showing a $D_0$ of 235.0 ± 28.1 Gy. Compared to the $D_e$ estimated by OSL (Table 2), VSL SAR overestimated the $D_e$ (sample L0688) by 60 %. For an OSL saturated sample (L0229), the SAR-VSL $D_e$ was 128.8 ± 18.5 Gy, with dose response curve presenting a $D_0$ of 251.0 ± 69.4 Gy. Some previous studies found an agreement between the estimated SAR VSL and OSL $D_e$ up to ~200 Gy (Ankjaergaard *et al*., 2013; Porat *et al*., 2018). However, other studies indicated an underestimation of 50 % or more for samples with larger naturals doses (Ankjærgaard *et al*., 2015; 2016; Colarossi *et al*., 2018; Sontag González *et al*., 2020) (Table 4). Dose recovery data obtained using the SAR VSL protocol is poor (Figure 4), considering that only data obtained with preheat at 160°C roughly produced measured-to-given dose ratio within the 0.9–1.1 range. The reason for this poor behavior is not clear but could be related to loss of VSL signal at high preheat temperature, low VSL sensitivity for the studied samples in general, and insufficient signal resetting between regenerative and test dose signal.

In the application of the MAR approaches for the studied samples, the sensitivity corrected VSL signal ($L_n/T_n$) is always less than the first regenerative point of the DRC. Here, the DRC was used to determine the $D_0$ in order to estimate the maximum dose ($2D_0$) that can be estimated by MAR VSL. The MAR DRC has $2D_0$ up to 574.6 ± 142.6 Gy when a single saturating exponential function is used. DRC from MAAD approach to minimize the sensitivity change was constructed for both samples L0229 and L0688. A $2D_{0,2}$ of 1643.2 ± 489.8 Gy (L0688) was obtained when the DRC was fitted with a double saturating exponential function. This is higher than the $2D_0$ observed for both SAR protocol (502.0 ± 138.8 Gy) and MAR protocol (574.6 ± 142.6 Gy). While the observed SAR, MAR and MAAD $2D_0$ would be an improvement relative to conventional OSL signal, they are lower than expected $2D_0$ values reported for VSL signal in the literature, which has been shown to have $2D_0$ up to 2668 ± 1008 Gy (Ankjaergaard, 2019). This indicates that the high-dose saturating VSL signal was not successfully isolated by the tested protocols or are absent in the studied quartz samples.

Fluvial sediments across Brazil usually have relatively low dose rates (~0.5-2 Gy/ka). Thus, quartz VSL could significantly increase the dating limit to the Early Pleistocene (~800 ka to 1.6 Ma for the $2D_0$ MAAD) even with the observed lower $2D_0$. Major limitation would be the absence of natural VSL signal in the studied samples from Amazon deposits.

Table 4**:** Equivalent dose, $D_e$, Characteristic doses, $D_0$, $D_{0,2}$, trap depth, E, and the thermal lifetime at 10°C for quartz samples studied using VSL signal single aliquot regenerative dose (SAR), multiple aliquots regenerative dose (MAR) and multiple aliquots additive dose (MAAD) protocols.

| **Site** | **$D_e$ (Gy)** | | **$D_0$ (Gy)** | **$2D_{0,2}$(Gy)** | **E (eV)** | **Lifetime at 10°C (years)** | **Reference** |
|---|---|---|---|---|---|---|---|
| | **(SAR)** | **(SARA)** | **(MAR)** | **(MAAD)** | | | |
| Netherland | 224 ± 26 | | | | 1.9 ±0.04 | $10^{11}$ | Ankjaergaard et al. (2013) |
| Luochuan, China | | 581 ± 130 | 1914 ± 101 | | 2.02 ± 0.04 | $10^{12}$ | Rahimzadeh et al. (2021) |
| Brooksby Quarry (UK) | 339.9 ± 67.4 | | | | | | Sontag-González et al. (2020) |
| Nahal Orvim(Israel) | 997.9 ± 36.0 | | | | 1.90 ± 0.03 | $10^{10}$ | Ankjaergaard et al. (2015) |
| Chinese Loess plateau | | | | 2668 ±1008 | | | Ankjaergaard et al. (2019) |
| KwaZulu-Natal, South africa | 93.5 ± 15.9 | 86.6 ± 28.4 | | | | | Colarossi et al. (2018) |

## 3.6. Conclusions

The VSL characteristics of quartz from sediments associated to large river systems in Brazil were investigated within the framework of improving dating range of luminescence signals. We show the presence of VSL for samples from Western and Southeastern Brazil only using a low preheat temperature (160$^{o}$C). The absence of VSL signal in samples from the Amazon fluvial deposits suggests that VSL characteristics vary in terms of the geological history of quartz. Amazon fluvial deposits have contribution of orogenic sediments from the Andes while the other studied deposits have exclusive cratonic sediment sources. Dose response curves obtained using SAR, MAR and MAAD protocols presented $2D_0$ of around 502, 574 and 1643 Gy, respectively. These values are lower than values reported for quartz from other sites, but quartz VSL could allow to extend the dating range of fluvial deposits in Brazil to the Early Pleistocene, especially in the cratonic settings where deposits are rich in quartz and dose rates are relatively low (0.5-1.0 Gy/ka). Despite the improvement in luminescence ages of Brazilian fluvial sediments using VSL signal relative to the conventional OSL signal, the behavior of VSL appears to be sample dependent, indicating the need for further studies especially applying the VSL protocol on samples of different geographical areas and depositional environments.

## 3.7. Supplementary material

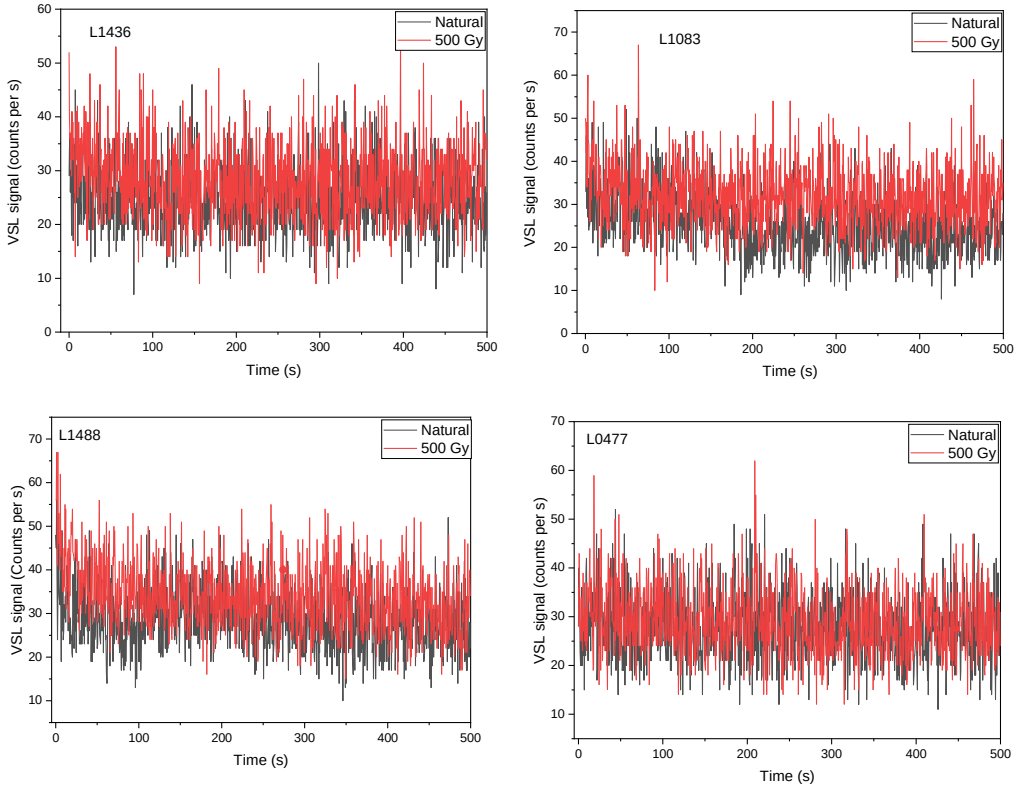


Figure S1: Selected examples of VSL decay curves of quartz of samples from Amazon River basin. The decay curves were measured before any laboratory dose and after a dose of 500 Gy.

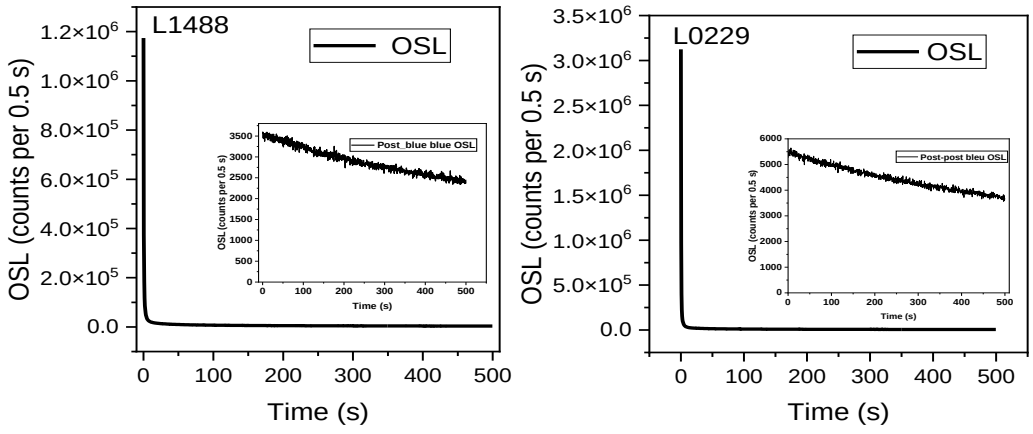


Figure S2: Comparison of blue OSL and post-blue OSL decay curves from the same aliquots measured for 500s for sample L1488 and L0229 after a preheat temperature of 160°C.

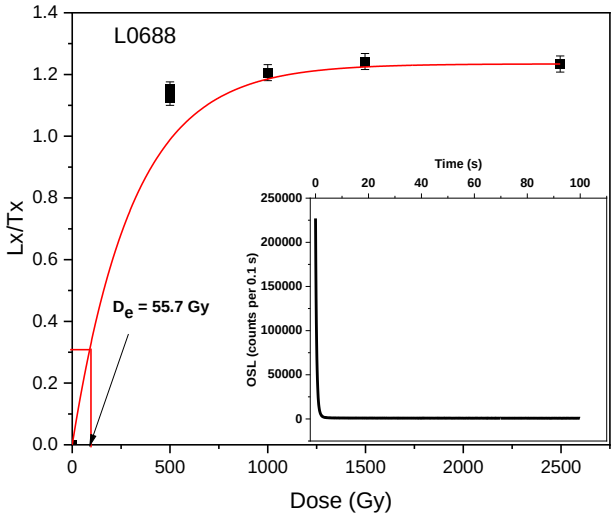


Figure S3: Dose response curve and natural decay of blue OSL signal measured before VSL signal measurement for sample L0688.

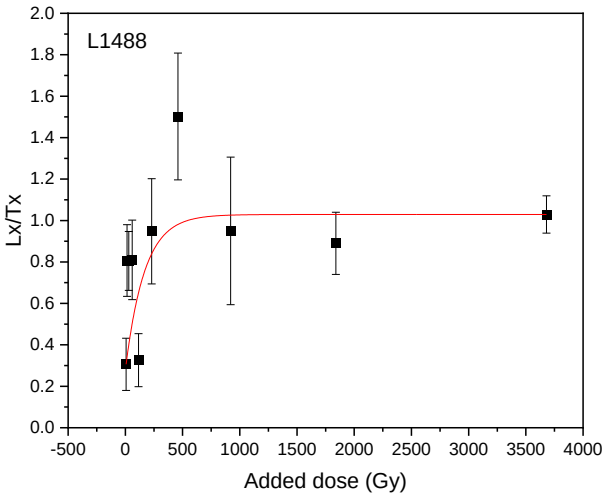


Figure S4: Dose response curve from multiple aliquots additive dose for sample L1488 fitted with sum of two exponential functions.

## 3.8. Acknowledgements

This research was supported by São Paulo Research Foundation (FAPESP grants 2016/02656-9 and 2018/23899-2). AOS and FNP are funded by Conselho Nacional de Desenvolvimento Científico e Tecnológico (CNPq grants 304727/2017-2 and #302411/2018-6). PN is grateful to National Council for Science and Technology Development (CNPq), The World Academy of Sciences (TWAS) (CNPq/TWAS grant 154507/2017-2) and The São Paulo Research Foundation (FAPESP grant 2019/04059-6) for funding his PhD fellowship at the University of São Paulo. FCGR is grateful to FAPESP for funding her PhD fellowship at the University of São Paulo (FAPESP grant 2018/12472-8).

## 3.9. References


Adamiec G., Duller G. A. T., Roberts H. M., Wintle A. G., 2010. Improving the TT-OSL SAR protocol through source trap characterisation. **Radiation Measurement**, 45: 768-777.

Aitken, M. J., 1998. An Introduction to Optical Dating: the Dating of Quaternary Sediments by the Use of Photon-Stimulated Luminescence. **Oxford University Press.**

Ankjærgaard, C., 2019. Exploring multiple-aliquot methods for quartz violet stimulated luminescence dating. **Quaternary Geochronology,** 51, 99–109.

Ankjærgaard, C., Guralnik, B., Buylaert, J-P., Reimann, T., Yi, S.W., Wallinga, J., 2016. Violet stimulated luminescence dating of quartz from Luochuan (Chinese loess plateau): Agreement with independent chronology up to ~600 ka. **Quaternary Geochronology,** 34, 33–46.

Ankjærgaard, C., Guralnik, B., Porat, N., Heimann, A., Jain, M., Wallinga, J., 2015. Violet stimulated luminescence: geo-or thermochronometer? **Radiation Measurement**, 81, 78–84.

Ankjærgaard, C., Jain, M., Wallinga, J., 2013. Towards dating quaternary sediments using the quartz violet stimulated luminescence (VSL) signal. **Quaternary Geochronology**, 18, 99–109.

Arnold, L. J., Demuro, M., María, J., Pérez-González, A., Castro, M. B. De, Carbonell, E., Arsuaga, J. L., 2015. Evaluating the suitability of extended-range luminescence dating techniques over early and Middle Pleistocene timescales: published datasets and case studies from Atapuerca, Spain. **Quaternary International**, 389, 167–190.

Bezerra, I. S. A. A., Nogueira, A. C. R., Motta, M. B., Sawakuchi, A. O., Mineli, T. D., Silva. A. Q. Silva Jr, A. G., Domingos, F. H. G., Mata, G. A. T., Lima, F. J. C., Rike, S. R. L., 2021. Incision and aggradation phases of the Amazon River in Central-Eastern Amazonia during the late Neogene and Quaternary. **Geomorphology,** 399, 108073.

Buylaert J. P., Jain M., Murray A. S., Thomsen K. J., Thiel C., Sohbati R., 2012. A robust feldspar luminescence dating method for Middle and Late Pleistocene sediments. **Boreas**, 41(3): 435–451.

Chapot, M. S., Roberts, H. M., Duller, G. A. T., Lai, Z. P., 2012. A comparison of natural and laboratory-generated dose response curves for quartz optically stimulated luminescence signals from Chinese Loess. **Radiation Measurements**, 47, 1045–1052.

Colarossi, D., Chapot, M. S., Duller, G. A., Roberts, H. M., 2018. Testing single aliquot regenerative dose (SAR) protocols for violet stimulated luminescence. **Radiation Measurements,** 120, 104–109.

Duller, G. A. T., Wintle, A. G., 2012. A review of the thermally transferred optically stimulated luminescence signal from quartz for dating sediments. **Quaternary Geochronology**, 7, 6–20.

Guedes, C. C. F., Sawakuchi, A. O., Giannini, P. C. F., DeWitt, R., Aguiar, V. A. P., 2013. Luminescence characteristics of quartz from Brazilian sediments and constraints for OSL dating. **Anais da Academia Brasileira de Ciências**, 85, 1303-1316.

Hernandez, M., Mauz, B., Mercier, N., Shen, Z., 2012. Evaluating the efficiency of TT-OSL SAR protocols. **Radiation Measurements**, 47, 669-673.

Hernandez, M., Mercier, N., 2015. Characteristics of the post-blue VSL signal from sedimentary quartz. **Radiation Measurements**, 78, 1–8.

Jain, M., 2009. Extending the dose range: probing deep traps in quartz with 3.06 eV photons. **Radiation Measurements**, 44, 445–452.

Kim, J. C., Duller, G. A.T., Roberts, H. M., Wintle, A. G., Lee, Y. I., Yi, S. B., 2009. Dose dependence of thermally transferred optically stimulated luminescence signal in quartz. **Radiation Measurements,** 44, 132-143.

Li, S. H., Chen, G., 2001. Studies of thermal stability of trapped charges associated with OSL from quartz. **Journal of Physics D: Applied Physics**, 34, 493–498.

Mineli, T. D., Sawakuchi, A.O., Guralnik, B., Lambert, R., Jain, M., Pupim, F. N.,. del Rio, I., Guedes, C. C. F., Nogueira, L., 2021. Variation of luminescence sensitivity, characteristic dose and trap parameters of quartz from rocks and sediments. **Radiation Measurements**, 144, 106-583.

Murray, A. S., Wintle, A. G., 2000. Luminescence dating of quartz using an improved single-aliquot regenerative-dose protocol. **Radiation Measurement**, 32, 57-73.

Niyonzima, P., Sawakuchi, A. O., Jain, M., Kumar, R., Minelli, T. D., del Río, I., Pupim, F. N., 2020. Radiofluorescence of quartz from rocks and sediments and its correlation with thermoluminescence and optically stimulated luminescence sensitivities. **Ancient TL,** 38 (1), 11–20.

Pickering, R., Jacobs, Z., Herries, A. I. R., Karkanas, P., Bar-Matthews, M., Woodhead, J. D., Kappen, P., Fisher, E., Marean, C. W., 2013. Paleoanthropologically significant South African sea caves dated to 1.1-1.0 million years using a combination of U-Pb, TT-OSL and paleomagnetism. **Quaternary Science Review**, 65, 39–52.

Porat, N., Duller, G. A. T., Roberts, H., Wintle, A .G., 2009. A simplified SAR protocol for TT-OSL. **Radiation Measurements**, 44, 538-542.

Porat, N., Jain, M., Ronen, A., Horwitz, L. K., 2018. A contribution to late middle Paleolithic chronology of the levant: new luminescence ages for the Atlit railway bridge site, Coastal plain. Israel. **Quaternary International**, 464, 32–42.

Pupim, F. N., Sawakuchi, A. O., Mineli, T. D., Nogueira, L., 2016. Evaluating isothermal thermoluminescence and thermally transferred optically stimulated luminescence for dating of Pleistocene sediments in Amazonia. **Quaternary Geochronology,** 36, 28-37.

Pupim, F. N., Sawakuchi, A. O., Almeida, R. P., Ribas, C. C., Kern, A. K., Hartmann, G. A., Chiessi, C. M., Tamura, L. N., Mineli, T. D., Savian, J. F., Grohmann, C. H., Bertassoli Jr, D. J., Stern, A. G., Cruz, F. W., Cracraft, J., 2019. Chronology of Terra Firme formation in Amazonian lowlands reveals a dynamic Quaternary landscape. **Quaternary Science Reviews**, 210, 154-163.

Rahimzadeh, N., Tsukamoto, S., Zhang, J., Long, H., 2021. Natural and laboratory dose response curves of quartz violet stimulated luminescence (VSL): Exploring the multiple aliquot regenerative dose (MAR) protocol. **Quaternary Geochronology**, 65, 101-194.

Sawakuchi, A. O., Jain, M., Mineli, T. D., Nogueira, L., Bertassoli Jr., D .J., Häggi, C., Sawakuchi, H. O., Pupim, F. N., Grohmann, C. H., Chiessi, C. M., Zabel, M., Mulitza, S., Mazoca, C. E. M., Cunha, D. F., 2018. Luminescence signals of quartz and feldspar indicate sediment sources and denudation rates in the Amazon River basin. **Earth and Planetary Science Letters**, 492, 152–162.

Sontag-González, M., Frouin, M., Li, B., Schwenninger, J. L., 2020. Assessing the Dating Potential of Violet Stimulated Luminescence Protocols. **Geochronometria**, DOI 10.1515/geochr-2015-0115.

Tsukamoto, S., Duller, G. A. T., Wintle, A. G., 2008. Characteristics of thermally transferred optically stimulated luminescence (TT-OSL) in quartz and its potential for dating sediments. **Radiation Measurements**, 43, 1204-1218.

Wang, X. L., Lu, Y. C., Wintle, A. G., 2006. Recuperated OSL dating of fine grained quartz in Chinese loess. **Quaternary Geochronology,** 1, 89–100.

Wintle, A. G., Adamiec, G., 2017. Optically stimulated luminescence signals from quartz: a review. **Radiation Measurements**, 98, 10–33.

Wintle, A. G., Murray, A. S., 2006. A review of quartz optically stimulated luminescence characteristics and their relevance in single-aliquot regeneration dating protocols. **Radiation Measurements**, 41, 369-391.

# Chapter 4: Luminescence dating of quartz from ironstones of the Xingu River, Eastern Amazonia

P. Niyonzima, A. O. Sawakuchi, D. J. Bertassoli. Jr, F. N. Pupim, N. Porat, M. P. Freire, A. M. Góes, F. C. G. Rodrigues

## 4.1. Abstract

This study reports on the first investigation into the potential of quartz luminescence dating to establish formation ages of ferruginous duricrust deposits (ironstones) of the Xingu River in Eastern Amazonia, Brazil. The studied ironstones comprise sand and gravel cemented by goethite (FeO(OH)), occurring as sandstones and conglomerates in the riverbed of the Xingu River, a major tributary of the Amazon River. The Xingu ironstones have a cavernous morphology and give origin to particular habitat for benthic biota in an area that hosts the largest rapids in Amazonia. So far, the Xingu ironstones have uncertain formation ages and their sedimentary origin is still poorly understood. In this way, seven samples of ironstones distributed along the lower Xingu River were collected for optically stimulated luminescence (OSL) dating of their detrital quartz sand grains. Additionally, the organic content of some samples was dated by radiocarbon ($^{14}C$) for comparison with quartz OSL ages.

The luminescence ages of the sand-sized quartz grains extracted from the ironstones were obtained from medium (100–300 grains) and small (10–20 grains) aliquots using the single aliquot regenerative-dose (SAR) protocol. Equivalent doses ($D_e$) distributions have varied overdispersion (OD) both for medium size aliquots (OD = 19–58%) and small size aliquots (OD = 29–76%). No significant trend was observed between $D_e$ and aliquot size. The studied ironstones grow over the riverbed, but stay below or above water throughout the year due to the seasonal water level variation of the Xingu River. However, the effect of water saturation in dose rates is reduced due to relatively low porosity of ironstones. Water saturated dose rates (dry sample dose rates) range from 2.70 ± 0.21 (2.79 ± 0.22) Gy/ka to 12.34 ± 0.97 (13.26 ± 1.12) Gy/ka, which are relatively high when compared to values reported for Brazilian sandy sediments

elsewhere (~1 Gy/ka). Samples with high overdispersion (> 40%) are mainly attributed to mixing of grains trapped in different time periods by goethite cementation.

The obtained OSL ages for water saturated (dry) samples range from 3.4 ± 0.3 (3.3 ± 0.4) ka to 59.6 ± 6.0 (58.1 ± 6.4) ka, using $D_e$ determined from medium size aliquots and dose response curves fitted by an exponential plus linear function. Radiocarbon ages of the bulk organic matter extracted from selected ironstone varied from ca. 4 cal ka BP to ca. 23 cal ka BP. Significant differences were observed between OSL and radiocarbon ages, suggesting asynchronous trapping of organic matter and detrital quartz within the ironstone matrix. These late Pleistocene to Holocene ages indicate that ironstones of the Xingu River result from an active surface geochemical system able to precipitate goethite and cement detrital sediments under transport. The obtained ages and differences between OSL and radiocarbon ages point out that the ironstones have multiphase and spatially heterogeneous growth across the Xingu riverbed. Our results also expand the application of luminescence dating to different sedimentary deposits.

## 4.2. Introduction

Weathering products with authigenic iron (Fe) minerals are widespread in soils and sediments of the tropical regions. However, their occurrence is peculiar in Eastern Amazonia, where fluvial sands and gravels are cemented by goethite (FeO(OH)) to form rocks (ironstones) that occur as patches over Precambrian bedrocks of the Xingu River (Sawakuchi *et al*., 2015). The ages of the Xingu ironstones are unknown and their formation process is still poorly understood despite their relevance as substrate for the aquatic ecosystems (Fitzgerald *et al*., 2018). Also, over the past decades, a growing number of studies have demonstrated the potential use of weathering clays, oxides and hydroxides as indicators of climatic changes in continental environments through mineral or isotopes markers (Giral-Kacmarcik *et al*., 1998; Girard *et al*., 2000; Girard *et al*., 2002). It has been reported that the original oxygen isotopic ratio of iron minerals such as goethite and hematite is generally preserved, thereby providing information about weathering and climate conditions prevailing at the time of ironstone formation (Giral-Kacmarcik *et al.*, 1998; Girard *et al*., 2002). Additionally, absolute dating of ironstones remains an important and challenging task for constraining the evolution of the continental surfaces as well as to support their use for paleoclimate or relief reconstructions. Different dating methods of ironstones were applied in Brazilian settings, including (U-Th)/He of goethite (Riffel *et al.*, 2016), electron paramagnetic resonance of matrix kaolinite (Allard *et al*., 2018) and cosmogenic nuclides of trapped quartz grains ($^{10}$Be) (Pupim *et al*., 2015). However, these methods are suitable to obtain ages in the hundred thousand to million years timescale and dating of ironstones is still difficult for the thousand years timescale necessary to cover the late Pleistocene and Holocene age range.

The main objectives of this work are to check the feasibility of optically stimulated luminescence (OSL) dating method on detrital quartz grains within ironstones and to shed light on the timing and processes of ironstones formation over the riverbed of the Xingu River. We focus on ironstones corresponding to sandstones and conglomerates cemented by goethite and with minor amount of organic matter and clay. We investigated the applicability of OSL dating using the single aliquot regenerative dose (SAR) protocol (Murray and Wintle, 2000; 2003) in quartz sand grains extracted from the ironstones framework. Additionally, the bulk organic matter

from selected ironstone samples was dated by radiocarbon ($^{14}C$) for independent age control. The optimal luminescence measurements conditions for obtaining equivalent dose values of the samples were then examined, with quartz OSL ages being compared to radiocarbon ages from bulk organic matter. The geochronological dataset obtained in this study is crucial to the discussion about the origin of the Xingu ironstones.

### 4.3. Study area

The Xingu River is the fifth largest tributary of the Amazon River, with a drainage area of 504,300 $km^2$ (Filizola, 1999) in Eastern Amazonia (Figure 1a,b). It is a clearwater river with a bedload dominated by fine to coarse sand, low concentration of suspended sediments (< 100 mg/l) and water pH 5 to 6 (Sioli, 1984). The rainfall is controlled by the strength of the South American Monsoon System and by shifts of the Intertropical Convergence Zone (Marengo, 2004), which promote a marked seasonality in the river water discharge. The mean annual water discharge is 9,700 $m^3/s$ (Filizola, 1999), but it ranges from 1,000 $m^3/s$ (September–October) during the dry season to 19,000 $m^3/s$ (March–April) in the wet season (Bertassoli Jr *et al*., 2019). The Xingu River shows high diversity in channel morphology, with a meandering channel at its upper catchment, a bedrock channel with multiple flow paths in the middle course, and a fluvial ria in its downstream section (Sawakuchi *et al*., 2015; Bertassoli Jr *et al*., 2019).

After the confluence with the Iriri River, the Xingu flows to northeast over Precambrian metamorphic and igneous rocks of the Brazilian shield until reaching the border of the Paleozoic-Mesozoic Amazonas sedimentary basin, where it bends to southeast and to northeast again to follow the way until the Amazon River (Figure 1c). This sector of the Xingu River is called "Volta Grande do Xingu", which has great relevance for Amazonian ecosystems due its high biodiversity and a high degree of endemism of the ichthyofauna (Nogueira *et al*., 2010). In the Volta Grande, the Xingu is a bedrock anastomosing system characterized by a 4–5 km width valley segmented into multiple interconnected crisscross channels with rapids bounding sediment bars covered by riparian vegetation and rainforest (Sawakuchi *et al*., 2015).

The morphology of the Xingu River turns to a straight, narrow and deep channel from the point that it flows over sedimentary rocks of the Amazonas basin. This zone

represents a knick point that separates the bedrock-dominated channel from the fluvial ria in its lower course (Figure 1c). The Xingu Ria can reach up to 14 km wide and 180 km long, with estuarine-like hydrodynamics due the strong influence of the backwater effect of the Amazon River, waves and tides (Meade *et al*., 1991). The studied ironstones samples were collected in sites of the Iriri and Xingu Rivers, mainly in sectors draining the Precambrian metamorphic and igneous rocks, but also in sectors over Paleozoic-Mesozoic sedimentary rocks (Figure 1c-f).

### 4.4. Samples collection and description

Seven samples representative of ironstones occurring in the lower Iriri and Xingu Rivers were collected using hammer and chisel during the dry season for luminescence dating. The location of each sample is shown in Figure 1. Three samples were also selected for radiocarbon dating of bulk organic matter. The samples were retrieved from sites lying over granitoids and sedimentary rocks that constitute the riverbed of the Iriri and Xingu Rivers in the study area (Figure 2). The Xingu ironstones have a cavernous morphology and are mainly composed of goethite matrix with detrital quartz sand grains, granules and pebbles (Figure 3).

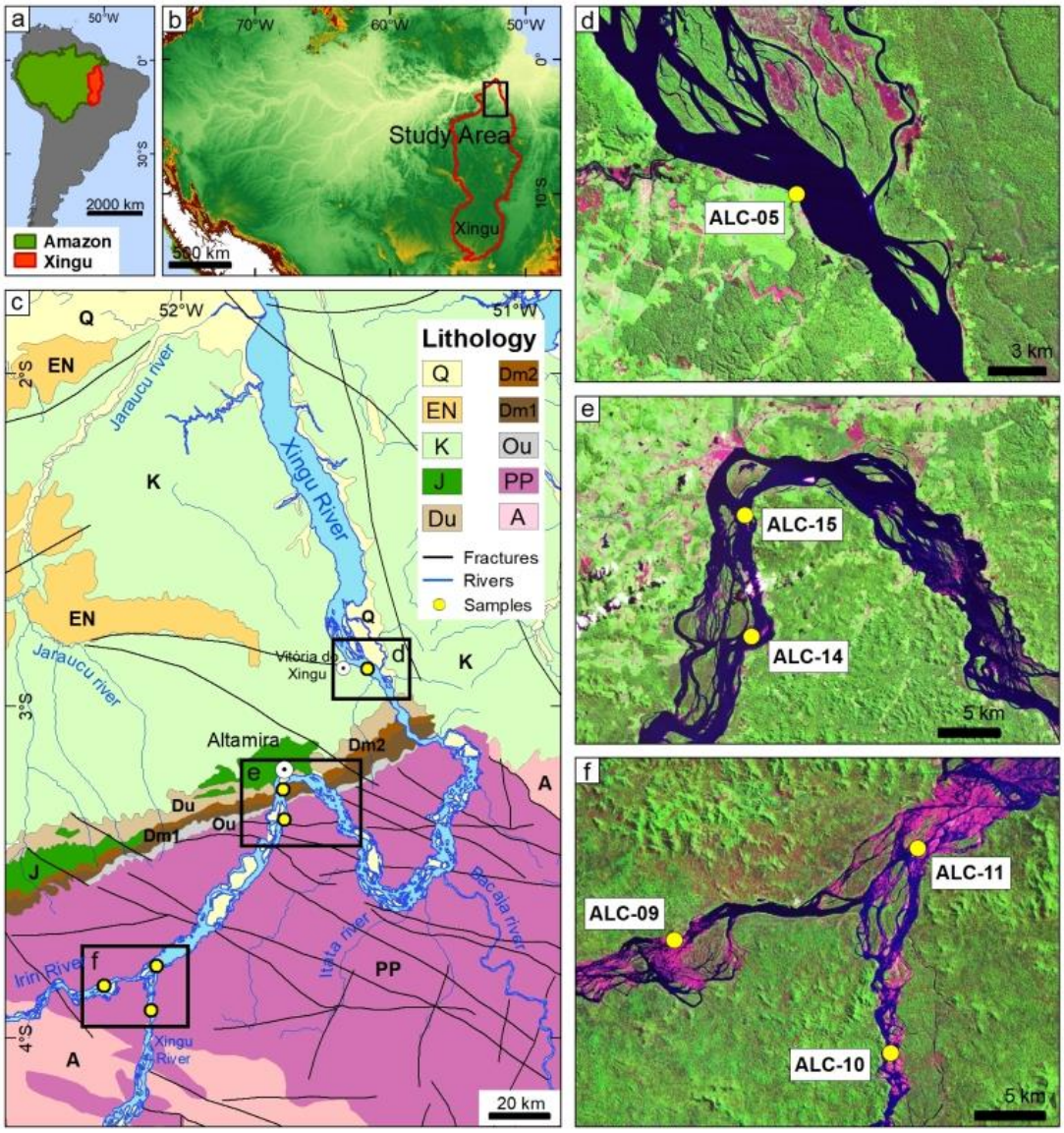


Figure 1: Location of the Xingu River basin in Eastern Amazonia (a and b). Simplified geological map (c) and location of sampling sites (yellow dots in black rectangles and in d, e and f panels) in the lower Iriri and Xingu Rivers. Lithological units of the geological map (c): (A) Archean gneisses, granodiorites and granitoids (Xingu Complex) and metavolcanic and metasedimentary rocks; (PP) Paleoproterozoic granites, granodiorites and charnockites; (Ou) Ordovician–Devonian organic-rich shales and sandstones (Trombetas Group); (Dm1–Dm2–Du) Middle–Late Devonian shales, siltstones and sandstones (Urupadi and Curuá Groups); (J) Early Triassic diabase sills (Penatecaua magmatism); (K) Cretaceous sandstones and conglomerates (Alter do Chão Formation); (EN) Eocene–Neogene undifferentiated sediments and lateritic soil crusts; (Q) Quaternary undifferentiated sediments. Lithological mapping units according to Bahia et al. (2004). Background images in d, e and f are from Landsat GeoCover 1990 (https://earthexplorer.usgs.gov/).

The textural and mineralogical characterization of sandy ironstones was performed using light polarized microscopy (LPM). All analyses were carried out at the Institute of Geosciences of the University of São Paulo (USP). Thin sections (30 μm thickness) were used for LPM analyses using a Carl Zeiss Axioplan 2 microscope, with LAS-Leica Application Suite software for imaging.


Figure 2: Field view of ironstones in the riverbed of the Xingu River exposed during the dry season. a) Rocky riverbed (migmatites and gneisses). b) Meter-scale patches of ironstones over the Xingu riverbed. c,d) Thick goethite crust with cavernous morphology.

## 4.5. Luminescence dating

### 4.5.1. Sample preparation

The preparation of detrital quartz concentrates for luminescence dating was performed under subdued orange/red light using conventional laboratory procedures (Mejdahl and Christiansen, 1994). The outer surface of each sample was removed to avoid material possibly exposed to light. This portion was kept for gamma ray spectrometry to determine radionuclides concentrations needed for dose rate calculation. The inner parts of the samples were protected from light to ensure that the sediments

retain their natural luminescence signal. This portion was carefully crushed and disaggregated to release the sand grains.

Detrital grains in the size range of 180–250 μm were recovered by wet-sieving. The target fraction was treated with hydrogen peroxide ($H_2O_2$, 27%) to remove organic matter and hydrochloric acid (HCl, 10%) to remove carbonate minerals. Heavy minerals and feldspar grains were removed by heavy liquid separation with lithium metatungstate solutions at densities of 2.75 g/cm$^3$ and 2.62 g/cm$^3$, respectively. To further purify and concentrate the quartz fraction and to remove the outer α–irradiated layer of quartz grains, the samples were etched in 38% HF for 40 min. Infrared (IR) stimulation was performed to confirm the absence of feldspar contamination in the HF-treated quartz fraction. Samples with remaining feldspar were subjected to repeated cycles of etching with 5% HF for 24 hours followed by wet sieving (180 μm) until a negligible IR signal (compared with blue stimulation signal) was achieved.

### 4.5.2. Equivalent dose measurement procedures

All luminescence measurements were carried out on an automated Risø TL/OSL DA-20 reader at the Luminescence and Gamma Spectrometry Laboratory (LEGaL) of the Institute of Geosciences, University of São Paulo. The reader is equipped with $^{90}Sr/^{90}Y$ beta source that delivers a dose rate of 0.119 ± 0.001 Gy/s, infrared (870 ± 20 nm; 145 mW/cm$^2$) and blue light-emitting diodes (470 ± 20 nm; 80 mW/cm$^2$) operating at 90% of their powers for stimulation and 7.5 mm Hoya U-340 filter for light detection in the ultraviolet band (290-340 nm) with a bialkali PM tube (Thorn EMI 9635QB) (Bøtter-Jensen *et al*., 2000). The SAR protocol proposed by Murray and Wintle (2000, 2003), as described in Table 1, was used to obtain equivalent doses ($D_e$) for all samples. The SAR sequence consisted of four regeneration doses, a recuperation (zero dose) point and a recycling point. The regeneration doses were chosen to bracket the expected $D_e$, allowing it to be evaluated by interpolation. For all aliquots used in luminescence measurements, the purity of the quartz was checked by an IR depletion ratio (Duller, 2003). Only aliquots with recycling ratio between 0.90 and 1.10, recuperation less than 5% (of the natural signal) and IR depletion ratio within 10% of unit were considered for $D_e$ estimation. The corrected OSL signal ($L_x/T_x$) was calculated using the initial 0.8 s of OSL decay curve minus the background estimated from the last 10 s of light emission.

Preheat plateau and dose recovery tests were carried out to set up the best preheat temperatures to estimate equivalent doses.

For each sample, 24 to 36 medium quartz aliquots (100–300 grains) were prepared for measurements. For better interpretation of $D_e$ distributions, two samples with high overdispersion (OD > 40%) and one sample with moderated OD (29%) were also measured using small aliquots (10–20 grains). Dose response curves (DRC) were fitted to the data with a single saturating exponential equation. However, the dosimetric behavior of OSL signals was also investigated by fitting DRCs using exponential plus linear function. For both cases, the $D_e$ was estimated by interpolating the sensitivity-corrected natural OSL signal onto the dose response curve.

The aliquots with $D_e$ greater than two times the value of characteristic dose ($2D_0$) of DRCs described by a single exponential function were also rejected for the analysis (Wintle and Murray, 2006). As fluvial sediments from different settings of Brazil are relatively well bleached (Sawakuchi *et al*., 2016; Pupim *et al*., 2016), the central age model (CAM) (Galbraith *et al*., 1999) was considered appropriate for equivalent dose estimation. Data analysis was carried out using Analyst (Duller, 2015), Origin and Luminescence R package (Kreutzer *et al*., 2012) softwares.

Table 1: The SAR protocol applied for this study (Murray and Wintle, 2003). Four regeneration doses ($D_1$ to $D_4$) were used to build the dose response curve. A constant test dose ($D_t$) was used to calculate the corrected OSL signals ($L_x/T_x$). Recuperation was calculated through the ratio between $D_5$ (0 Gy) and natural dose ($D_n$) signals. Signals from $D_6$ and $D_1$ were used to calculate recycling ratios. IR stimulation was performed before the measurement of $D_7$ signal to appraise feldspar contamination.

| Step | Treatment |
|---|---|
| 1 | Give dose, $D_x$ ($D_n$ = natural signal; $D_1<D_2<D_3<D_4$; $D_5$=0 Gy; $D_6=D_7=D_1$) |
| 2 | Preheat at 260°C for 10 s |
| 3 | Blue light stimulation for 40 s at 125°C ($L_x$) |
| 4 | Give test dose, $D_t$ |
| 5 | Cut-heat at 160°C for 0 s |
| 6 | Blue light stimulation at 125°C for 40 s ($T_x$) |
| 7 | Blue light illumination at 280°C for 40 s |
| 8 | Return to step 1 |

### 4.5.3. Determination of radionuclides concentrations and dose rate calculation

The concentrations of uranium ($^{238}$U), thorium ($^{232}$Th) and potassium ($^{40}$K) were determined using high-resolution gamma spectrometry through a high-purity germanium (HPGe) detector with a 55% relative efficiency and 2.1 keV energy resolution, encased in an ultralow background shield (Canberra industries). The outer surface of each sample was milled and 278 to 445 g of dry samples were packed in plastic containers and sealed. Gamma ray spectrometry was performed after sample storage for at least 28 days for radon to reach equilibrium with its parent radionuclides. The beta and gamma dose rates were calculated using the concentrations of $^{238}$U, $^{232}$Th and $^{40}$K and conversion factors from Guérin *et al*. (2011). The cosmic-ray dose rates were calculated according to Prescott and Hutton (1994), taking into consideration the altitude and geomagnetic latitude of the sampling site and density (Table 2) of the overlying ironstones. Average depth of 0.10 ± 0.05 m was used to calculate the cosmic dose rate for all samples, since they were retrieved from surface ironstones layers. The samples were dry rocks when collected, but they experience an underwater period during the wet season. Hence, the dose rates were calculated taking minimum (dry sample) and maximum water saturation (water weight and dry sample weight). Maximum water saturation values (Table 2) were obtained by keeping samples underwater in the laboratory.

### 4.6. Radiocarbon dating

Four samples had a significant amount of organic matter, as indicated by reaction to hydrogen peroxide ($H_2O_2$, 27%), and therefore were selected for radiocarbon dating. Fresh subsamples from the core of the selected specimens were pulverized, pretreated with HCl to ensure the absence of carbonates, and dated by Accelerator Mass Spectrometry (AMS) at Beta Analytic Laboratory, Miami, Florida, USA. Radiocarbon ($^{14}$C) ages of the bulk organic fraction were calibrated using Calib 7.1 (Stuiver *et al*., 2019) and the SHCal20 database (Hogg *et al*., 2020). Stable carbon isotopic signatures ($\delta^{13}$C) of the organic fraction were measured at the same laboratory using an Isotope Ratio Mass Spectrometer (IRMS).

## 4.7. Results

### 4.7.1. Ironstones characteristics

All studied ironstone types (sandstones, conglomeratic sandstones and conglomerates) form tabular beds irregularly covering the riverbed of the Iriri and Xingu Rivers. The sandstones have a framework (80–85% of the rock) mainly composed of quartz sand grains cemented by goethite (15–20%). The sand grains consist of monocrystalline quartz (15-35%), polycrystalline quartz (20–30%), lithic fragments of schist (5–10%), ferruginous-coated grains (15–20%) and iron oxide grains interpreted as intraclasts of ironstones matrix (1–2%) (Figure 3a,c). Conglomerates have a framework of rounded quartz pebbles and a sandy matrix cemented by goethite (Figure 3b).

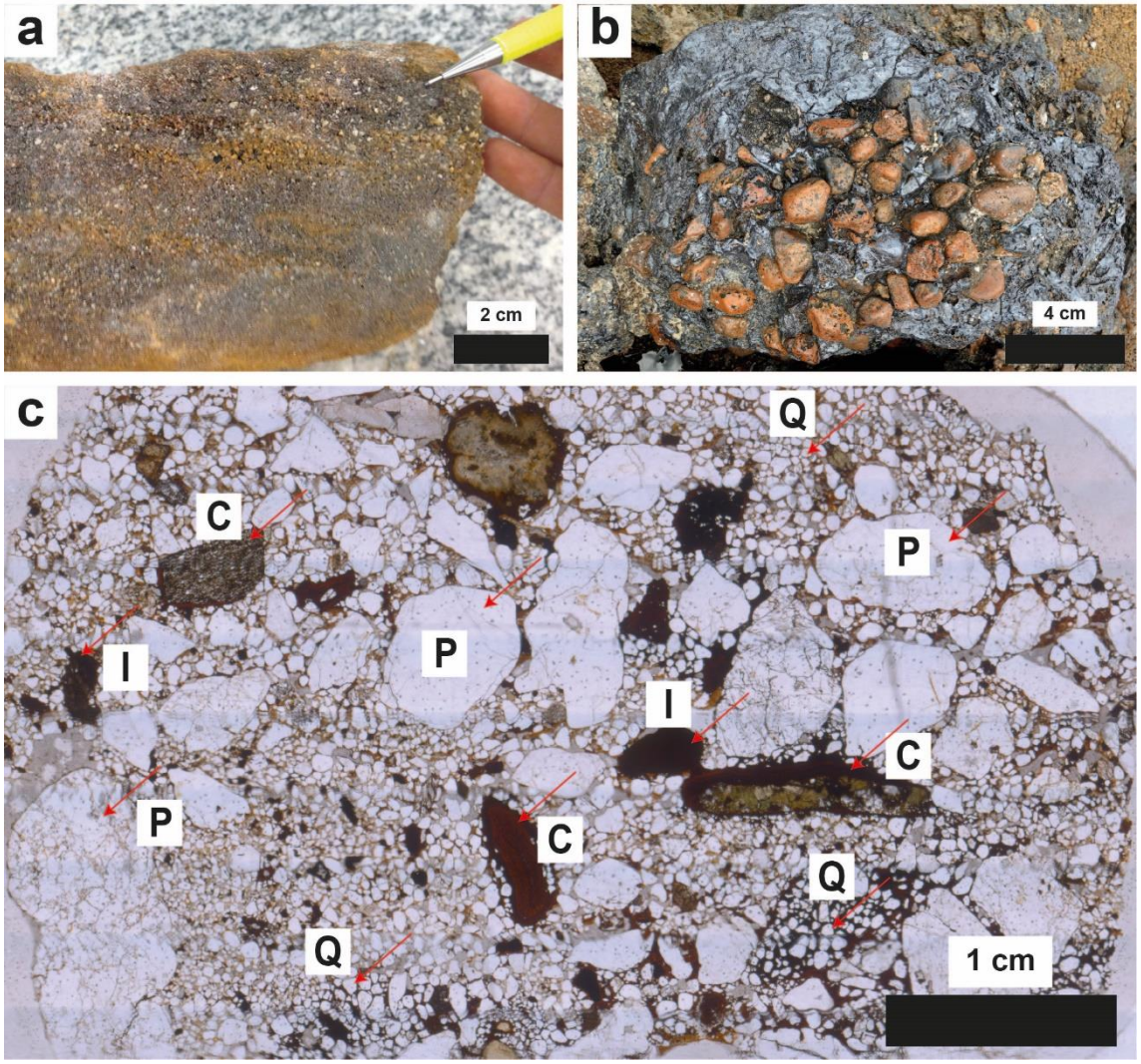


Figure 3**:** Macroscopic and microscopic views of the Xingu ironstones. a) Sandstone with goethite cement (site ALC-05). b) Conglomerate of well-rounded quartz pebbles cemented by goethite. c) Thin section view of conglomeratic sandstone (site ALC-15) with framework composed of monocrystalline quartz (Q), polycrystalline quartz (P), goethite coated grains (C) and iron oxide intraclasts (I), and cemented by goethite. Red arrows point grain types named by the respective label.

### 4.7.2. OSL and radiocarbon ages

Quartz from the ironstones of the Xingu River has high luminescence sensitivity, with OSL decay curve dominated by the fast component. The dose response curves follow a single saturating exponential function, with average $2D_0$ value up to 284.4 ± 83.4 Gy (sample L1247). Figure 4 shows examples of natural OSL decay curves and dose response curves of different aliquots from samples L1244 and L1247.

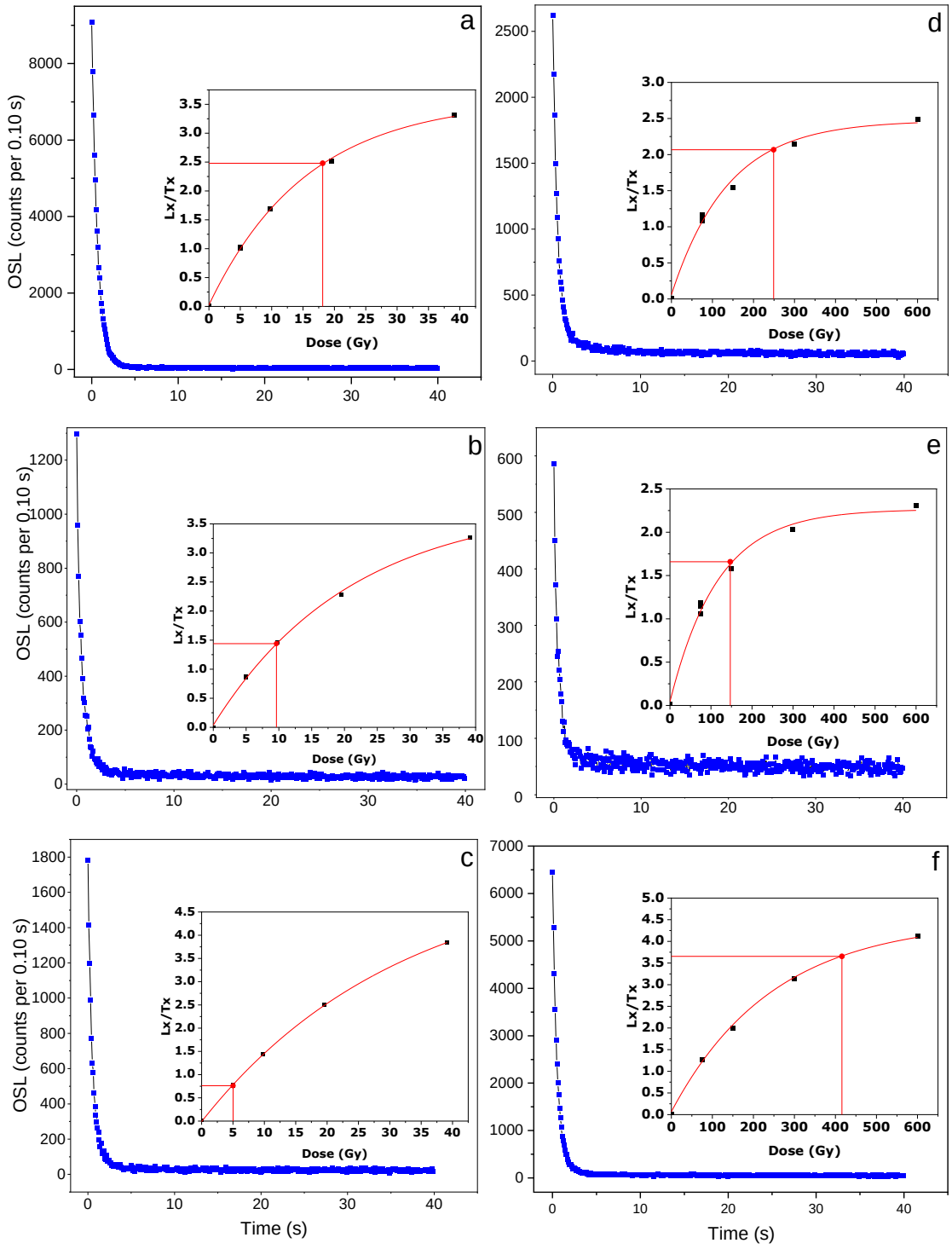


Figure 4: Representative natural OSL decay curves and corresponding sensitivity-corrected dose response curves (insets) for aliquots of samples L1244 (a, b and c) and L1247 (d, e and f). Interpolated values in dose response curves correspond to natural signals and equivalent doses.

A preheat temperature test was carried out to ensure the selection of the most suitable thermal treatment to run the SAR protocol for $D_e$ estimation. Three samples (L1244, L1245 and L1247) were used for this experiment. Three aliquots for each

sample were initially bleached for 100 s at 25 °C using blue LEDs at 90% power to remove the natural signal. The bleached aliquots were then irradiated with a beta dose of 50 Gy and sensitivity-corrected OSL signals were measured at various preheat temperatures ranging from 180 ºC to 300 ºC (20 °C intervals) with cut-heat at 160 °C. The sensitivity-corrected OSL signal for the given dose of 50 Gy was plotted in function of different preheat temperatures (Figure 5), indicating that corrected OSL signals for our samples did not change significantly for preheat temperatures ranging from 200 °C to 260 °C.

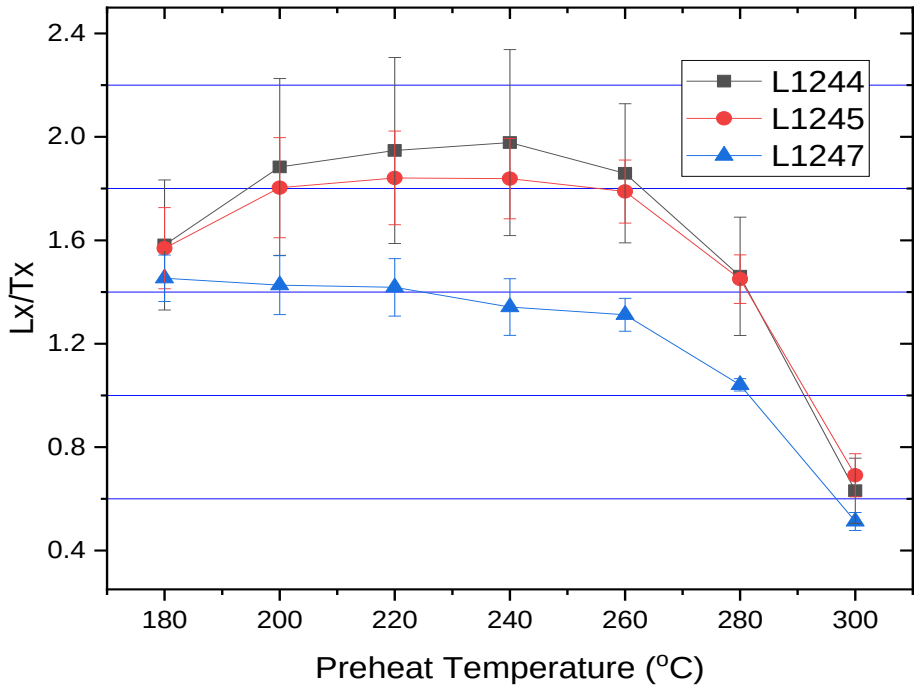


Figure 5: Sensitivity-corrected OSL signal ($L_x/T_x$) from a given dose of 50 Gy against the preheat temperature between 180°C and 300 °C. Each data point represents the average of three aliquots with its respective standard deviation as error bars.

We performed dose recovery tests on quartz aliquots of samples L1244, L1245 and L1266 using given beta doses of 15, 50, 100 and 200 Gy. This dose range was selected from a preliminary set of $D_e$ measurements made on each of the studied samples. Aliquots were firstly bleached using a blue LED stimulation at room temperature (~25°C) for 300 s before irradiation. Afterwards, dose recovery tests for a given dose of 50 Gy were carried out on aliquots of samples L1245 and L1245 using the protocol described in Table 2, with the preheat temperatures between 180°C and 280°C. Calculated-to-given ratios were between 0.83 ± 0.02 and 1.05 ± 0.07 (Figure 6).

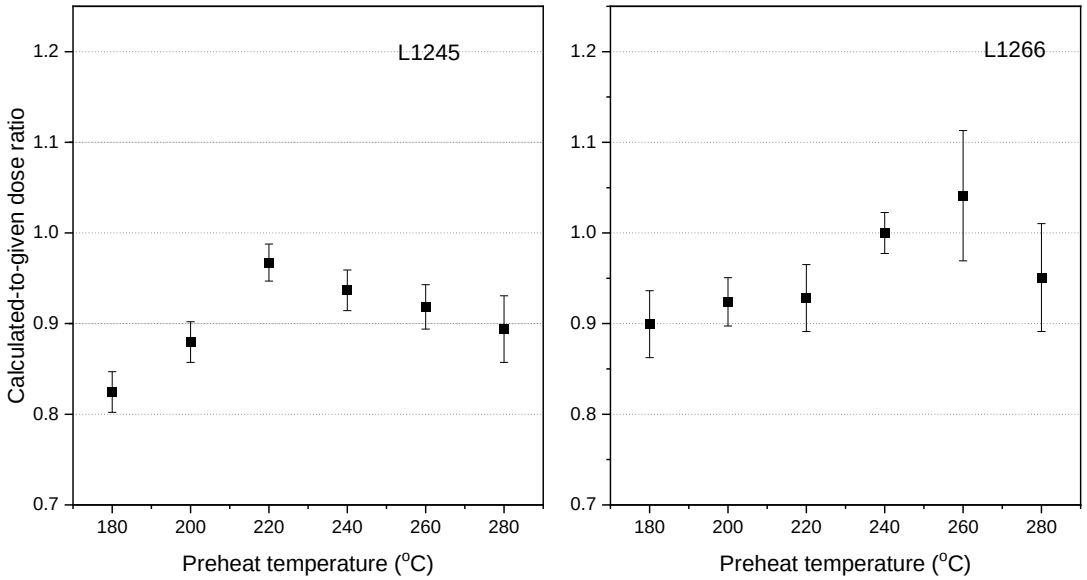


Figure 6: Calculated-to-given dose ratios obtained through dose recovery tests using samples L1245 and L1266. Three aliquots were measured for each data point using a given dose of 50 Gy. The equivalent doses were calculated using the Central Age Model (CAM) and 1 σ was used as error bar.

The preheat temperature of 260°C represents the best performance on dose recovery tests performed for a given dose of 50 Gy, considering not only the calculated-to-given dose ratios of 0.92 ± 0.02 (L1245) and 1.05 ± 0.07 (L1266), but also the recycling ratios closer to unity and lower recuperation values. Thus, additional dose recovery tests were carried out on sample L1244 using given doses of 15, 50, 100 and 200 Gy and preheat temperature of 260°C (Figure 7). For this purpose, sixteen aliquots of sample L1244 were firstly bleached using a solar simulator for 24 hours and four aliquots were used for each given dose. In this test, doses were estimated through fitting the DRCs by both saturating single exponential and exponential plus linear functions. Similar equivalent doses were obtained from DRCs described by single saturating exponential and exponential plus linear functions (Figure 7).

The calculated-to-given dose ratios obtained using a single saturating exponential DRC were 0.98 ± 0.07, 0.91 ± 0.05, 0.89 ± 0.08 and 0.85 ± 0.18 for given doses of 15, 50, 100 and 200 Gy, respectively. We observed increasing $D_e$ underestimation for given doses of 100 and 200 Gy using both fitting functions. For doses up to 50 Gy, calculated-to-given dose ratios are within 10% of unity. These dose recovery experiments supported the choice of 260°C preheat temperature to estimate $D_e$ in the studied ironstone samples.

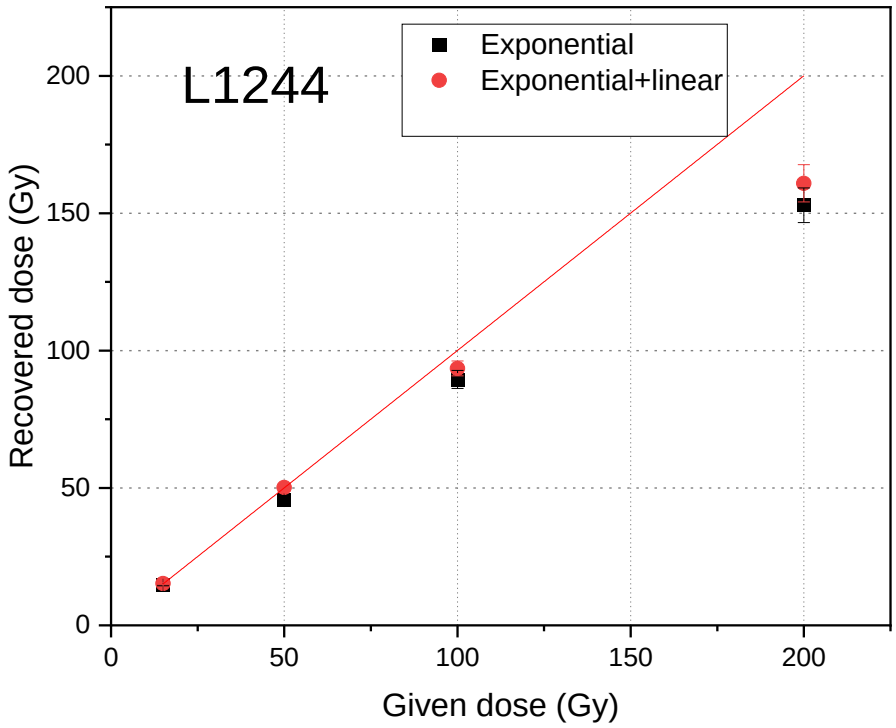


Figure 7: Given dose against recovered dose for quartz aliquots from sample L1244. Four aliquots were measured for each given dose (15, 50, 100 and 200 Gy). The recovered doses were calculated using the Central Age Model (CAM) with its standard error at 1 σ as error bar. The unity line was added for easy evaluation of given and recovered doses.

### 4.7.3. Dose rates, equivalent doses and ages

The ironstone samples have densities from 2.41 to 2.87 g/cm$^3$ and maximum water saturation up to 6.4% (Table 2). Cosmic dose rates are relatively uniform, with values of 0.23 and 0.24 Gy/ka (Table 3). The Xingu ironstones have large variation in radionuclides concentrations, with $^{238}$U and $^{232}$Th concentrations respectively reaching up to 19 and 122 ppm (Table 3). The high $^{238}$U and $^{232}$Th concentrations give relatively high dose rates up to ~13 Gy/ka (Table 4). Since the exact time that the samples spend under water is unknown, a range of total dose rates were calculated assuming water saturated samples and dry samples. Thus, water saturated and dry dose rates (Table 3) of each sample were used in the age calculation.

Table 2**:** Geographical coordinates and altitude of the sampling sites and densities and maximum water saturation of studied samples.

| Field code | Lab code | Longitude | Latitude | Altitude (m) | Density (g/cm$^3$) | Maximum water saturation (%) |
|---|---|---|---|---|---|---|
| ALC-11-1 | L1244 | -3°46′56.81″ | -52°34′19.21″ | 117 | 2.62 | 3.2 |
| ALC-09-2 | L1245 | -3°50′32.10″ | -52°43′50.17″ | 126 | 2.41 | 6.4 |
| ALC-15-1 | L1246 | -3°15′03.52″ | -52°11′37.28″ | 86 | 2.35 | 3.4 |
| ALC-05-04 | L1247 | -2°53′19.12″ | -51°56′25.36″ | 2 | 2.50 | 3.4 |
| ALC-10-1A | L1264 | -3°55′00.21″ | -52°35′23.67″ | 126 | 2.24 | 3.0 |
| ALC-15-1A | L1265 | -3°15′03.52″ | -52°11′37.28″ | 86 | 2.87 | 3.0 |
| ALC-14 | L1266 | -3°20′29.03″ | -52°11′20.24″ | 92 | 2.87 | 1.5 |

Table 3**:** Summary of radionuclides concentrations, dry and water saturated (WS) gamma and beta dose rates and cosmic dose rates (DR) for the studied samples. Field codes are in Table 2.

| Lab code | $^{238}$U (ppm) | $^{232}$Th (ppm) | K (%) | $^{232}$Th/$^{238}$U | Dry gamma DR (Gy/ka) | WS gamma DR (Gy/ka) | Dry beta DR (Gy/ka) | WS beta DR (Gy/ka) | Cosmic DR (Gy/ka) |
|---|---|---|---|---|---|---|---|---|---|
| L1244 | 9.12 ± 0.41 | 19.98 ± 0.63 | 0.38 ± 0.02 | 2.2 | 2.07 ± 0.05 | 1.99 ± 0.23 | 1.93 ± 0.06 | 1.85 ± 0.23 | 0.23 ± 0.02 |
| L1245 | 15.89 ± 0.55 | 122.17 ± 3.37 | 0.54 ± 0.02 | 7.7 | 7.76 ± 0.17 | 7.23 ± 0.78 | 5.27 ± 0.12 | 4.88 ± 0.58 | 0.23 ± 0.02 |
| L1246 | 6.52 ± 0.23 | 29.35 ± 0.86 | 0.42 ± 0.01 | 4.5 | 2.24 ± 0.05 | 2.16 ± 0.24 | 1.84 ± 0.04 | 1.77 ± 0.22 | 0.23 ± 0.02 |
| L1247 | 19.88 ± 0.68 | 0.29 ± 0.09 | 0.01 ± 0.01 | 0.01 | 2.24 ± 0.08 | 2.15 ± 0.25 | 2.57 ± 0.93 | 2.47 ± 0.31 | 0.23 ± 0.02 |
| L1264 | 4.70 ± 0.18 | 12.13 ± 0.40 | 1.13 ± 0.05 | 2.6 | 1.39 ± 0.03 | 1.34 ± 0.15 | 1.76 ± 0.05 | 1.70 ± 0.21 | 0.24 ± 0.02 |
| L1265 | 4.92 ± 0.18 | 16.85 ± 0.53 | 0.17 ± 0.01 | 3.4 | 1.40 ± 0.03 | 1.35 ± 0.15 | 1.15 ± 0.03 | 1.11 ± 0.14 | 0.23 ± 0.02 |
| L1266 | 7.12 ± 0.25 | 55.35 ± 1.56 | 0.23 ± 0.01 | 7.8 | 3.50 ± 0.08 | 3.44 ± 0.39 | 2.37 ± 0.05 | 2.32 ± 0.29 | 0.23 ± 0.02 |

The $D_e$ values determined using the CAM for medium aliquots are relatively higher than values from small aliquots, but there is no clear relationship between aliquot size and overdispersion (OD) of equivalent dose distributions (Table 4). Abanico plots for both medium and small size aliquots for samples L1246, L1247 and L1266 are presented on Figure 8. Abanico plots for other samples (L1244, L1245, L1264 and L1265) are also presented on Figure 9. The medium size aliquots gave $D_e$ values ranging from 13.6 ± 0.9 Gy to 230.5 ± 13.1 Gy when the DRCs are fitted by single saturating exponential function, with OD values ranging from 19% to 58%. However, in the dose range beyond 100 Gy, DRCs are better fitted by exponential plus linear function, which gave $D_e$ values higher than the values, obtained using the single saturating exponential function (Table 5). Ages calculated from water saturated dose rates and exponential plus linear function $D_e$ vary between 3.4 ± 0.3 and 59.9 ± 6.0 ka. Ages calculated using dry or water saturated dose rates overlap by their errors. Table 5 presents a summary of $D_e$, dose rates and calculated ages.

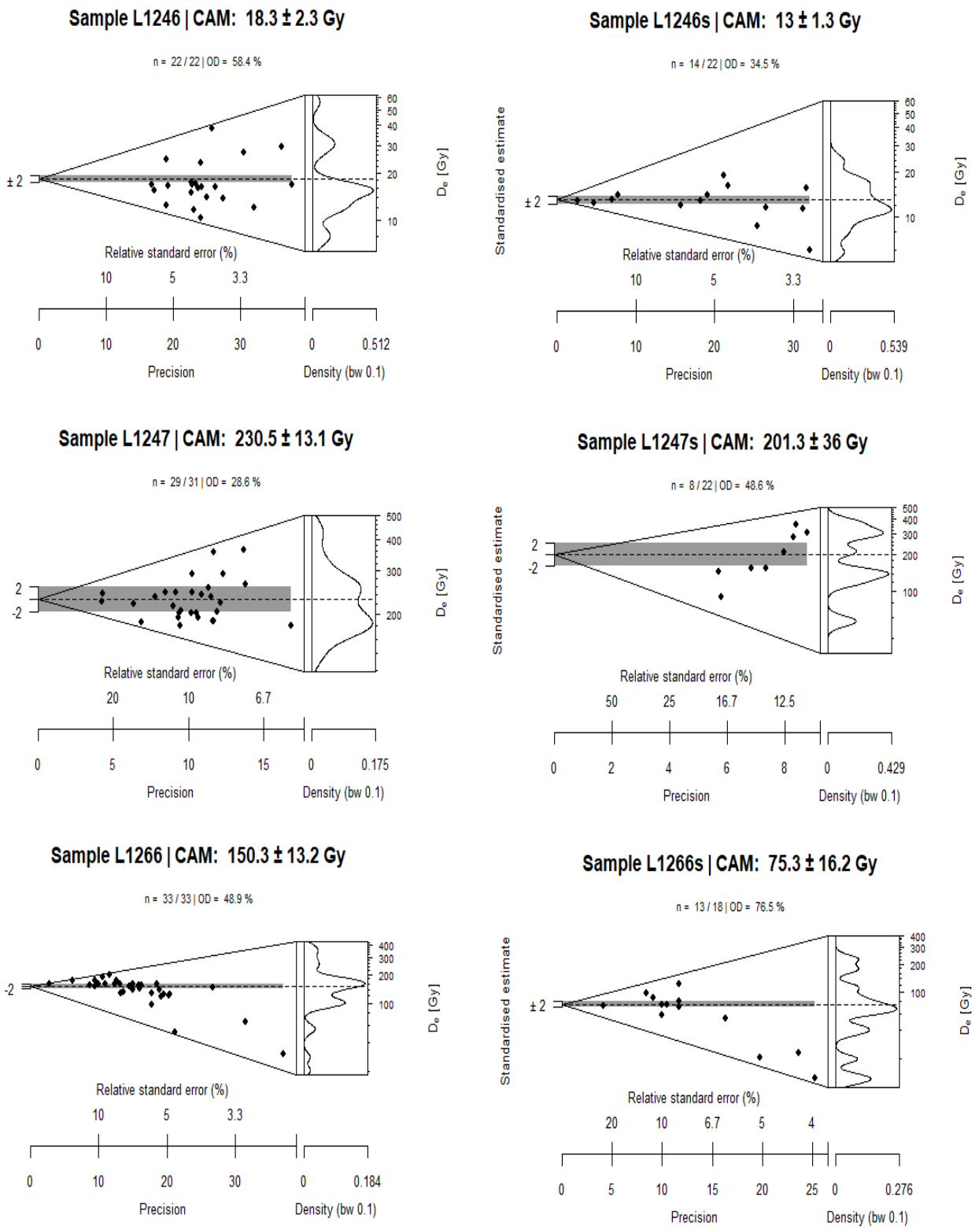


Figure 8: Abanico plots of $D_e$ values obtained using medium (left column) and small (right column) size aliquots for selected samples. The "s" in samples codes (L1246s, L1247s and L1266s) identifies equivalent dose distributions from small aliquots. The numbers of accepted and measured aliquots are indicated by "n". The samples equivalent dose (CAM) is indicated by the dashed line. The grey shaded band shows $D_e$ range within its 2σ.

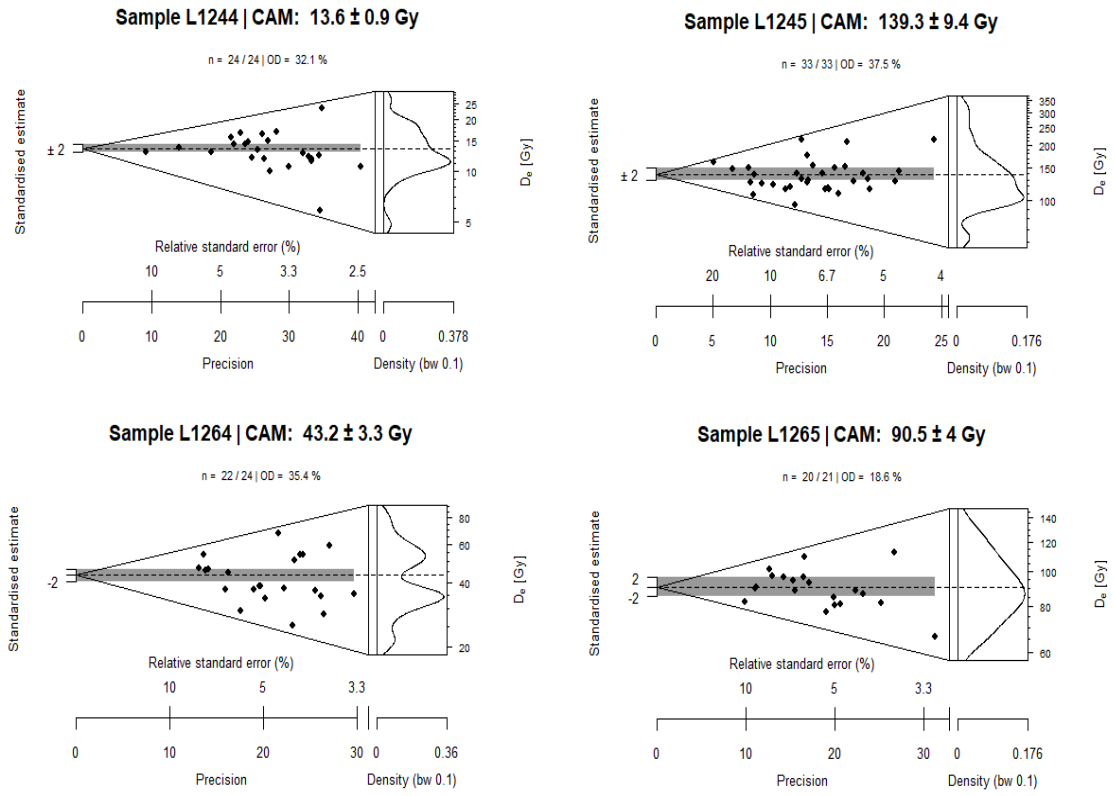


Figure 9: Abanico plots showing $D_e$ distributions from medium aliquots of samples L1244, L1245, L1264 and L1265. The numbers of accepted and measured aliquots are indicated by "n". The samples equivalent dose (CAM) is indicated by the dashed line. The grey shaded band shows $D_e$ range within its 2σ.

Table 4: Equivalent doses ($D_e$) and overdispersion (OD) values calculated using the Central Age Model (CAM) for medium and small size aliquots from selected samples. Dose response curves were fitted by a single saturating exponential function. Field codes are presented in Table 2.

| Lab code | Medium aliquots | | Small aliquots | |
|---|---|---|---|---|
| | $D_e$ (Gy) | OD (%) | $D_e$ (Gy) | OD (%) |
| L1246 | 18.3 ± 2.3 | 58 | 13.0 ± 1.3 | 34 |
| L1247 | 230.5 ± 13.1 | 29 | 201.3 ± 35.9 | 49 |
| L1266 | 150.3 ± 13.2 | 49 | 73.3 ± 16.2 | 76 |

Table 5: Equivalent doses ($D_e$) and ages calculated using the Central Age Model (CAM) for medium size aliquots by fitting the DRCs with both single saturating exponential (Exp) and exponential plus linear functions (Exp + lin). OSL ages were calculated using maximum water saturation (WS) and dry sample (DS) dose rates (DR). Field codes are presented in Table 2.

| Lab code | Exp $D_e$ (Gy) | Exp + lin $D_e$ (Gy) | Total WS DR (Gy/ka) | Total DS DR (Gy/ka) | WS Exp OSL age (ka) | DS Exp OSL age (ka) | WS Exp + lin OSL age (ka) | DS Exp + lin OSL age (ka) |
|---|---|---|---|---|---|---|---|---|
| L1244 | 13.6 ± 0.9 | 14.0 ± 0.9 | 4.08 ± 0.32 | 4.22 ± 0.35 | 3.4 ± 0.3 | 3.2 ± 0.3 | 3.4 ± 0.4 | 3.3 ± 0.4 |
| L1245 | 139.3 ± 9.4 | 163.8 ± 17.4 | 12.34 ± 0.97 | 13.26 ± 1.12 | 11.3 ± 1.2 | 10.5 ± 1.2 | 13.3 ± 1.8 | 12.4 ± 1.7 |
| L1246 | 18.3 ± 2.3 | 18.4 ± 2.5 | 4.17 ± 0.33 | 4.31 ± 0.36 | 4.4 ± 0.7 | 4.3 ± 0.7 | 4.4 ± 0.4 | 4.3 ± 0.7 |
| L1247 | 230.5 ± 13.1 | 290.8 ± 16.6 | 4.85 ± 0.40 | 5.03 ± 0.43 | 47.6 ± 4.8 | 45.8 ± 4.7 | 59.9 ± 6.0 | 58.1 ± 6.4 |
| L1264 | 43.2 ± 3.3 | 46.3 ± 3.9 | 3.27 ± 0.26 | 3.38 ± 0.28 | 13.2 ± 1.5 | 12.8 ± 1.4 | 14.2 ± 1.6 | 13.9 ± 1.8 |
| L1265 | 90.5 ± 4 | 88.8 ± 4.6 | 2.70 ± 0.21 | 2.79 ± 0.22 | 33.6 ± 3.0 | 32.5 ± 2.9 | 33.0 ± 3.1 | 32.3 ± 3.9 |
| L1266 | 150.3 ± 13.2 | 164.5 ± 16.4 | 6.00 ± 0.50 | 6.09 ± 0.51 | 25.1 ± 3.1 | 24.7 ±3.0 | 27.5 ± 3.5 | 27.1 ± 3.6 |

Calibrated radiocarbon ages of organic matter extracted from samples L1244, L1264, L1245 and L1265 range between ca. 4.5 and 23 cal ka BP. OSL ages were older or younger than radiocarbon ages obtained in the corresponding samples. Calibrated ages and conventional radiocarbon ages, $\delta^{13}C$ values of organic matter and OSL ages are presented in Table 6.

Table 6: Conventional and calibrated ages and $\delta^{13}C$ of bulk organic matter from selected samples. Ages were calibrated with Calib 7.1 using the SHCal13 calibration curve (Stuiver *et al*. 2019; Hogg *et al*. 2020). OSL ages from water saturated (WS) dose rates and exponential (Exp) or exponential plus linear (Exp+lin) dose response curves are showed for comparison. Field codes are presented in Table 2.

| Lab code | Lab ID | Conventional age (ka BP) | IRMS $\delta^{13}C$ (‰) | Calibrated age (cal ka BP, 2σ) | WS Exp OSL age (ka) | WS Exp+lin OSL age (ka) |
|---|---|---|---|---|---|---|
| L1244 | Beta-533270 | 20.68 ±- 0.07 | -24.1 | 23.17–22.68 | 3.4 ± 0.3 | 3.4 ± 0.4 |
| L1245 | Beta-537938 | 14.22 ± 0.05 | -25.9 | 15.44–15.13 | 11.3 ± 1.2 | 13.3 ± 1.8 |
| L1264 | Beta-537939 | 16.10 ± 0.05 | -23.6 | 17.59–17.26 | 12.8 ± 1.4 | 14.2 ± 1.6 |
| L1265 | Beta-537940 | 5.59 ± 0.03 | -23.7 | 4.49–4.34 | 32.5 ± 2.9 | 33.0 ± 3.1 |

## 4.8. Discussion

### 4.8.1. OSL ages uncertainties

#### 4.8.1.1. Sources of overdispersion in the equivalent dose distributions

The $D_e$ distributions for medium and small size aliquots of the analyzed samples clearly show a varied scatter, with OD values between 19 and 76%. For $D_e$ distributions obtained using medium size aliquots, sample L1265 has low OD of 19%, pointing to a single population of grains with doses centered on the weighted mean $D_e$ value. Another sample (L1266) has $D_e$ distributions with high OD up to 67%. However, most of our samples have $D_e$ with OD values in the range of 29–35%, consistent with the commonly reported range for heterogeneous, but relatively well-bleached sediments, i.e, majority of grains was fully bleached and not affected by post-depositional mixing (Arnold *et al*., 2007; Arnold and Roberts, 2009).

For medium aliquots (100–300 grains), at least part of resulting OSL signals will be affected by averaging effects (Arnold and Roberts, 2009). Thus, measurements using small aliquots were performed in order to minimize averaging effects, highlighting $D_e$ variations among grains of the same sample. In the studied samples, small aliquots (10–20 grains) show $D_e$ distributions with lower or higher OD (up to 76%), but presenting

systematically lower $D_e$ values when compared to medium aliquots (Table 4). This suggests that the contribution of grains with higher $D_e$ increases from small to medium aliquots. The variation in $D_e$ due to aliquot size as well as the high OD of some samples point out to significant $D_e$ variability among quartz grains hosted in ironstones.

The most likely interpretation of high OD in $D_e$ distributions from fluvial sediments is that grains were incompletely and heterogeneously bleached prior to deposition (Wallinga, 2002; Rodnight *et al*., 2005). This interpretation is not supported for the studied river by the fact that quartz grains from fluvial sediments of the Xingu River (Pupim *et al*., 2016) and of other cratonic rivers in Brazil are well bleached (Sawakuchi *et al*., 2016). Post-depositional sediment mixing due to the movement of grains by natural processes such as bioturbation and pedogenesis is another potential source of variability in $D_e$ distributions (David *et al*., 2007; Jacobs and Roberts, 2007). However, the high degree of cementation of the studied samples makes post-depositional grain mixing negligible. The scatter in $D_e$ distributions can also be attributed to intrinsic differences in the luminescence sensitivity of different measured aliquots (Tsakalos *et al*., 2018), but this effect should be minimal in the studied samples due to the high sensitivity of their quartz grains. Heterogeneities in density of sedimentary matrix (Nathan *et al*., 2003) and small-scale variations in the beta radiation dose rate to which the samples have been exposed during burial (Jacobs and Roberts, 2007) are also potential factors contributing to overdispersion in $D_e$ distributions from quartz sand grains. Dose rate heterogeneities would be more important in conglomeratic ironstones, where quartz pebbles can promote zones of low dose rate compared to the goethite matrix, which concentrates $^{238}U$ and $^{232}Th$. Thus, quartz sand grains laying nearby quartz pebbles would be submitted to lower dose rate field compared to quartz grains immersed in the goethite matrix. The break up of granules or pebbles during sample preparation could also contribute for $D_e$ variation within sample. In this case, fragments derived from the inner portion of granules or pebbles should have saturated OSL signals, contributing to a high dose tail of the $D_e$ distributions. However, this possibility is reduced as saturated aliquots were not observed in the younger samples.

The studied ironstones would be formed by successive phases of goethite precipitation and trapping of quartz grains through a timespan. This could explain the significant variation of $D_e$ from aliquots of the same sample as well as the differences between ages of detrital organic matter and quartz grains. Thus, mixing of grains

trapped during different time periods could be a major source of dispersion in $D_e$ distributions from the studied ironstones. In this case, $D_e$ determined using multigrain aliquots and CAM would represent the average population of grains trapped in the sampled ironstone layer. In the studied samples, the use of a relatively thin ironstone layer (~10 cm thickness) for extraction of quartz grains should minimize this effect. However, we recommend further studies using a single grain dating approach combined with petrographic methods to discriminate specific goethite cementation and grain trapping phases.

### 4.8.1.2. OSL signal saturation

The upper limit of the OSL dating on quartz is defined by signal saturation, and by assuming first order kinetics whereby a single electron trap/recombination center is involved in OSL signal used for dating. In this case, a single saturating exponential function would be expected to fit an OSL dose response curve and the recommended upper dose limit is defined by two times the characteristic dose ($2D_0$) (Wintle and Murray, 2006). The average $2D_0$ of the studied quartz is 284.4 ± 83. 9 Gy, which is relatively high, but within the range of values reported in the literature (Mineli *et al*., 2021). Additional linear function is predicted for doses greater than 125 Gy (Wintle and Murray, 2006), however processes that influence the dosimetric characteristics of OSL are still unknown for this high dose linear component (Timar-Gabor *et al*., 2012).

In our study, DRCs for samples with high $D_e$ (> 100 Gy) are best fitted by exponential plus linear function. Nevertheless, both single saturating exponential and exponential plus linear functions show dose underestimation as demonstrated by dose recovery tests (Figure 7). Thus, age underestimation should be considered for samples L1245, L1247 and L1266, which presented $D_e$ beyond 100 Gy (Table 5). In this way, the ages reported for these samples should be considered as minimal.

### 4.8.1.3. Dose rate considerations

The Xingu ironstones have relatively high radionuclides concentrations and most samples have dose rates higher than 4 Gy/ka, with a dry sample reaching a dose rate of 13 Gy/ka (Table 5). The overall dose rates are high compared to the doses rates

commonly found in Brazilian sediments, which are mostly in the range of 0.4 to 3.1 Gy/ka (Pupim *et al*., 2016, 2019; Guedes *et al*., 2013, Sawakuchi *et al*. 2008; 2016; Soares *et al*. 2010; Ribeiro *et al*. 2015). Hence, the relatively high dose rate implies upper age limit of approximately ~71 ka for quartz OSL dating, considering maximum dose of around 284 Gy ($2D_0$) and dose rate of 4 Gy/ka. Despite the fact that the high dose rate results in faster OSL signal saturation of quartz grains within the ironstones, it allows the dating of young sediments, possibly in a few years age range (< 25 years), assuming the estimation of $D_e$ lower than 0.1 Gy and dose rate of 4 Gy/ka.

The unusual dose rates of the Xingu ironstones are related to the high concentrations of $^{238}U$ and $^{232}Th$. The Xingu watershed has headwaters draining sandstones of the Parecis sedimentary basin, but most of the watershed drains granitoid rocks of the Brazilian shield, which host minerals rich both in $^{238}U$ and $^{232}Th$. Typical $^{232}Th/^{238}U$ ratios in most upper crustal rocks are between 3.5 and 4.0, and in sedimentary rocks, $^{232}Th/^{238}U$ values greater than 4.0 may indicate intense weathering in source areas or sedimentary recycling i.e., derivation from old sedimentary rocks (Asiedu *et al.*, 2000). In most cases, elevation in the $^{232}Th/^{238}U$ ratio is associated to the loss of $^{238}U$ due to weathering (Asiedu *et al.*, 2000; Pupim *et al*., 2016). The studied ironstones are composed mainly of quartz sand grains, granules or pebbles immersed in a goethite matrix. In this case, goethite should be the main host of $^{238}U$ and $^{232}Th$. The studied ironstones have $^{232}Th/^{238}U$ ratios with moderate values around 2.2–3.4 to relatively high $^{232}Th/^{238}U$ ratios in the range of 4.5–7.8 (Table 3). The source rocks of sediments supplied to the Xingu River are under heavy and long chemical weathering due low denudation rates in the drainage basin (Wittmann *et al*., 2010). This could contribute to surface waters and/or fine-grained suspended sediments rich in $^{238}U$ and $^{232}Th$, which are further concentrated by authigenic goethite precipitation as cement of the Xingu River sediments. The variation of $^{232}Th/^{238}U$ ratios also suggests that goethite from ironstones of the Xingu River is precipitated from waters draining source areas with different weathering degree or source rock composition. However, detailed mineral chemistry studies are needed to understand the relatively high concentration of $^{238}U$ and $^{232}Th$ in the ironstones and their controlling variables.

The studied ironstones are formed underwater during fluvial sediment deposition followed by goethite precipitation, but experiences seasonal dry phases or long term dry periods due to shifts in the riverbed. Hence, variations in water saturation through play a

role for dose rate assessment and should be considered in age uncertainties. The studied samples were water saturated in the laboratory to appraise the maximum range of variation in dose rate. In this way, dose rates were estimated from water saturated and dry samples, showing similar results (Table 5) because of the intense cementation and low porosity of ironstones. Thus, water variation during wet and dry seasons has minor effect on our dating results, assuming that goethite cements are stable after precipitation. However, detailed petrological studies are still needed to evaluate phases of pore filling or generation respectively due to crystallization or dissolution of cements.

### 4.8.1.4. Ironstones ages and formation processes

In this section, we consider a range of OSL ages based on CAM $D_e$ from the medium size aliquots, exponential plus linear dose response function and dose rates from both dry and water saturated samples. In this way, the OSL ages of the studied ironstones ranged from ~60 ka to 3 ka (Table 5). The radiocarbon ages fall in the interval of 17.63–4.46 cal ka BP (Table 6). OSL and radiocarbon ages would indicate the trapping time of detrital quartz and organic matter into the goethite matrix of the ironstones, respectively. Thus, both methods would indicate ironstone formation ages through cementation of terrigenous sediments deposited in the Xingu riverbed. Considering individual samples, we observed a significant age offset between the OSL and radiocarbon ages, which highlight the asynchronous trapping of terrigenous sediments during ironstone formation. As there is no discernible pattern for the offsets, and radiocarbon ages are not systematically younger or older than the OSL ages, it is difficult to hypothesize a specific single cause for the observed difference. Effects related to the OSL ages, pre-aging of organic matter and permeation of young organic carbon into the rock pores could all contribute to this offset. As discussed, processes affecting OSL ages can be related to incomplete bleaching, mixing of grains continuously trapped through time or dose rate microheterogeneities. However, the relatively low overdispersion (<30%) observed in $D_e$ distributions of some samples would exclude the contribution of both incomplete bleaching, mixing of grains and dose rate microheterogeneities effects. In this case, the high overdispersion of some samples could be attributed to multiple episodes of sediment trapping, thus, suggesting that ironstones growth is a multiphase process. However, a single grain approach coupled with detailed microscopic characterization is recommended to appraise if overdispersion

in $D_e$ distributions is related with populations of quartz grains trapped during different phases of ironstones growth.

The organic fraction of the studied ironstones is enriched in $^{13}C$ ($\delta^{13}C$ = -25.9 to -23.6, Table 6) in comparison to organic matter from riverbed sediments ($\delta^{13}C$ = -31.04 to -27.49 ‰) of the lowermost part of the Xingu River (Bertassoli *et al*., 2017). This could be caused by post-depositional effects (e.g. degradation) and by significantly higher percentages of autochthonous material (e.g., microbial) or C4 plants in the bulk organic matter trapped during the formation of the ironstones. Thus, the organic matter within the ironstones differs from the organic matter of detrital sediments under transport in the Xingu River. The uptake of autochthonous (aquatic) organic matter by ironstones could be favored by the widespread growth of benthic algae over the rocky substrates of the Xingu riverbed (Zualaga-Gómez *et al.*, 2016).

Despite the discussed age uncertainties, the OSL and radiocarbon ages greatly improve our knowledge about the growth timespan of the Xingu ironstones. According to the obtained OSL and radiocarbon ages, the ironstones of the Xingu River are younger than goethite crusts found in upland terrains from Amazonia (e.g., Allard *et al*., 2018) or in other regions in Brazil (Riffel *et al*., 2016), which should have an origin related to tropical soil development. The studied ironstones are restricted to the Xingu River channel, in areas permanently or seasonally inundated and with lotic water conditions. This environment somehow promotes conditions suitable for authigenic goethite crystallization and cementation of terrigenous sediments transported by the Xingu River. The OSL ages suggest that this system has been functioning for a thousand years, at least since the late Pleistocene, creating specific habitats for the aquatic biota adapted to turbulent flows in clear water Amazonian rivers (Zuluaga-Gómez *et al*., 2016). However, we highlight that the presented OSL and radiocarbon ages should represent minimum ages for the Xingu ironstone system because our sampling was restricted to the uppermost layer of ironstones lying over the riverbed as well as because of the low preservation potential of ironstones in the long term due the high erosion capacity of the Xingu rapids. The climate and geochemical controls on this system is still unknown, but the OSL ages give the first timescale to shed light on formation processes of the Xingu ironstones.

## 4.9. Conclusions

This is the first application of quartz OSL dating to Quaternary ironstones. However, the high dose rates observed in the studied goethite-cemented ironstones limit the quartz OSL dating to around 71 ka. For some studied samples, $D_e$ distributions with low OD suggest grains that quartz grains are well bleached prior to deposition while samples with $D_e$ distributions showing high OD are attributed to the presence of quartz grains populations trapped through time.

The $^{232}Th/^{238}U$ ratio values indicate that most of the studied ironstones comprise sediments sourced from rocks under intense weathering conditions. The OSL ages are between ~60 ka and 3 ka, indicating a Late Pleistocene and Holocene system responsible for ironstone formation in the Xingu River. The OSL ages improve the understanding of the genesis of ironstones, suggesting they are related with the Quaternary hydrology of the Xingu River. Future luminescence dating studies are recommended to extend the age limit and establish a regional chronological framework of the Xingu River ironstones in order to achieve a better understanding of their geochemical and/or hydrological controls.

## 4.10. Acknowledgments

We are grateful to the anonymous reviewers and Editor Frank Preusser for the critical and careful comments, which decisively improved the quality of our manuscript. This research was supported by São Paulo Research Foundation (FAPESP grants 2016/02656-9 and 2018/23899-2). AOS and FNP are funded by Conselho Nacional de Desenvolvimento Científico e Tecnológico (CNPq grants 304727/2017-2 and #302411/2018-6). DJB was supported by FAPESP (grants 2016/11141-2, 2018/15123-4, 2019/24349-9 and 2019/24977-0). PN is grateful to National Council for Science and Technology Development (CNPq), The World Academy of Sciences (TWAS) (CNPq/TWAS grant 154507/2017-2) and The São Paulo Research Foundation (FAPESP grant 2019/04059-6) for funding his PhD fellowship at the University of São Paulo. FCGR is grateful to FAPESP for funding her PhD fellowship at the University of São Paulo (FAPESP grant 2018/12472-8). We would like to thank Thays Desirée Mineli and Ian del Río for their assistance during luminescence measurements and data analysis.

## 4.11. References


Allard, T., Gautheron, C., Riffel, S. B., Balan, E., Soares. B. F., Pinna-Jamme, R., Derycke, A., Morin, G., Bueno, G. T., do Nascimento, N., 2018. Combined dating of goethites and kaolinites from ferruginous duricrusts. Deciphering the Late Neogene erosion history of Central Amazonia. **Chemical Geology,** 479, 136–150.

Arnold, L. J., Bailey, R. M., Tucker, G. E., 2007. Statistical treatment of fluvial dose distributions from southern Colorado arroyo deposits. **Quaternary Geochronology,** 2, 162–167.

Arnold, L. J., Roberts, R. G., 2009. Stochastic modeling of multi-grain equivalent dose ($D_e$) distributions: implications for OSL dating of sediment mixtures. **Quaternary Geochronology,** 4, 204–230.

Asiedu, D. K., Suzuki, S., Nogami, K., Shibata, T., 2000. Geochemistry of lower cretaceous sediments, inner zone of southwest Japan. Constraints on provenance and tectonic environment. **Geochemical Journal,** 34, 155–173.

Bahia, R. B. C., Faraco, M. T. L., Monteiro, M. A. S., and Oliveira, M. A. O., 2004. Folha SA.22-Belém. In: Carta Geológica do Brasil ao Milionésimo. Sistema de Informações Geográficas. Programa Geologia do Brasil, edited by Schobbenhaus, C., Gonçalves, J. H., Santos, J. O. S., Abram, M. B., Leão Neto, R., Matos, G. M. M., Vidotti, R. M., Ramos, M. A. B., and Jesus, J. D. A. de, CPRM, Brasilia, CD-ROM.

Bertassoli Jr, D. J., Sawakuchi, A. O., Chiessi, C. M., Schefuβ, E, Hartmann, G. A., Häggi, C., Cruz, F. W., Zabel, M., McGlue, M., Santos, R. A., Pupim, F. N., 2019. Spatiotemporal variations of riverine discharge within the Amazon basin during the Late Holocene coincide with extratropical temperature anomalies. **Geophysical Research Letters,** 46(15), 9013–9022.

Bertassoli Jr, D. J., Sawakuchi, A. O., Sawakuchi, H. O., Pupim, F. N., Hartmann, G. A., McGlue, M. M., Chiessi, C. M., Zabel, M., Schefuß, E., Pereira, T. S., Santos, R. A., Faustino, S. B., Oliveira, P. E., Bicudo, D. C., 2017. The fate of carbon in sediments of the Xingu and Tapajós Clearwater Rivers, Eastern Amazon. **Frontiers in Marine Science**, 4. https://doi.org/10.3389/ fmars.2017.00044.

Bøtter-Jensen, L., Bulur, E., Duller, G. A. T., Murray, A. S., 2000. Advances in luminescence instrument systems. **Radiation Measurements,** 32, 523–528.

David, B., Roberts, R. G., Magee, J., Mialanes, J., Turney, C., Bird, M., White, C., Fifield, L. K., Tibby, J., 2007. Sediment mixing at Nonda Rock: investigations of stratigraphic integrity at an early archaeological site in northern Australia and implications for the human colonisation of the continent. **Journal of Quaternary Science,** 22, 449–479.

Duller, G. A. T., 2003. Distinguishing quartz and feldspar in single grain luminescence measurements. **Radiation Measurements,** 37, 161–165.

Duller, G. A. T., 2015. The Analyst software package for luminescence data: overview and recent improvements. **Ancient TL,** 33, 35–42.

Filizola, N. P., 1999. O fluxo de sedimentos em suspensão nos rios da bacia Amazônica Brasileira. **Publicação ANEEL, Brasília**, 63 pp.

Fitzgerald, D. B., Sabaj Perez, M. H., Sousa, L. M., Gonçalves, A. P., Rapp Py-Daniel, L., Lujan, N. K., Zuanon, J., Winemiller, K. O., Lundberg, J. G., 2018. Diversity and community structure of rapids-dwelling fishes of the Xingu River: Implications for conservation amid large-scale hydroelectric development. **Biological Conservation,** 222, 104–112.

Galbraith, R. F., Roberts, R. G., Laslett, G. M., Yoshida, H., Olley, J. M., 1999. Optical dating of single and multiple grains of quartz from Jinmium rock shelter, Northern Australia: part I, experimental design and statistical models. **Archaeometry,** 41, 339–364.

Giral-Kacmarkcik, S., Savin, S. M., Nahon, D., Girard, J.-P., Lucas, Y., and Abel, L., 1998. Oxygen isotope geochemistry of kaolinite in laterite-forming processes, Manaus, Amazonas, Brazil. **Geochimica et Cosmochimica Acta,** 62, 1865–1879.

Girard, J. P., Freyssinet, P., Morillon, A. C., 2002. Oxygen isotope study of Cayenne duricrust paleosurfaces: implications for past climate and laterization processes over French Guiana. **Chemical Geology,** 191, 329–343.

Girard, J.-P., Freyssinet, P., Chazot, G., 2000. Unraveling climatic changes from intraprofile variation in oxygen and hydrogen isotopic composition of goethite

and kaolinite in laterites: an integrated study from Yaou, French Guiana. **Geochimica et Cosmochimica Acta,** 64 (3), 409–426.

Guedes, C. C. F., Sawakuchi, A. O., Giannini, P. C. F., DeWitt, R., Aguiar, V. A. P., 2013. Luminescence characteristics of quartz from Brazilian sediments and constraints for OSL dating. **Anais da Academia Brasileira de Ciências,** 85, 1303–1316.

Guerin, G., Mercier, N., Adamiec, G., 2011. Dose-rate conversion factors: update. **Ancient TL,** 29, 5–8.

Hogg, A. G., Heaton, T. J., Hua, Q., Palmer, J. G., Turney, C. S. M., Southon, J., Bayliss, A., Blackwell, P. G., Boswijk, G., Ramsey, C. B., Pearson, C., Petchey, F., Reimer, P., Reimer, R., Wacker, L., 2020. SHCal20 Southern hemisphere calibration, 0–55,000 years Cal BP. **Radiocarbon,** 62(4), 759–778.

Jacobs, Z., Roberts, R. G., 2007. Advances in Optically Stimulated Luminescence Dating of Individual Grains of Quartz from Archeological Deposits. **Evolutionary Anthropology,** 16, 210–223.

Kreutzer, S., Schmidt, C., Fuchs, M. C., Dietze, M., Fischer, M., Fuchs, M., 2012. Introducing an R package for luminescence dating analysis. **Ancient TL,** 30, 1–8.

Marengo, J. A., 2004. Interdecadal variability and trends of rainfall across the Amazon basin. **Theoretical and Applied Climatology,** 78, 79–96.

Meade, R. H., Rayol, J. M., Conceição, S. C., Natividade, J. R. G., 1991. Backwater effects in the Amazon river basin of Brazil. **Environmental Geology and Water Sciences,** 18, 105–114.

Mejdahl, V., Christiansen, H. H., 1994. Procedures used for luminescence dating of sediments. **Quaternary Science Reviews,** 13, 403–406.

Mineli, T. D., Sawakuchi, A. O., Guralnik, B., Lambert, R., Jain, M., Pupim, F. N., del Río, I. A. G., Nogueira, L., 2021. Variation of luminescence sensitivity, characteristic dose and trap parameters of quartz from rocks and sediments. **Radiation Measurements,** 144, 106583.

Murray, A. S., Wintle, A. G., 2000. Luminescence dating of quartz using an improved single-aliquot regenerative-dose protocol. **Radiation Measurements,** 32, 57–73.

Murray, A. S., Wintle, A. G., 2003. The single aliquot regenerative dose protocol: potential for improvements in reliability. **Radiation Measurements,** 37(4–5), 377–381.

Nathan, R. P., Thomas, P. J., Jain, M., Murray, A. S., Rhodes, E. J., 2003. Environmental dose rate heterogeneity of beta radiation and its implications for luminescence dating: Monte Carlo modelling experimental validation. **Radiation Measurements,** 37, 305–313.

Nogueira, C., Buckup, P. A., Menezes, N. A., Oyakawa, O. T., Kasecker, T. P., Neto, M. B. R., da Silva, J. M. C., 2010. Restricted-range fishes and the conservation of Brazilian freshwaters. **PLOS ONE,** 5(6), 1–10.

Prescott, J. R., Hutton, J. T., 1994. Cosmic ray contributions to dose rates for luminescence and ESR dating: large depths and long-term time variations. **Radiation Measurements,** 23, 497–500.

Pupim, F. N., Bierman, P. R., Assine, M. L., Rood, D. H., Silva, A., Merino, E. R., 2015. Erosion rates and landscape evolution of the lowlands of the Upper Paraguay River basin (Brazil) from cosmogenic $^{10}$Be. **Geomorphology,** 234, 151–160.

Pupim, F. N., Sawakuchi, A. O., Almeida, R. P., Ribas C. C., Kern, A. K., Hartmann, G. A., Chiessi, C. M., Tamura L. N., Mineli, T. D., Savian, J .F., Grohmann, C. H., Bertassoli Jr, D. J., Stern, A. G., Cruz, F. W., Cracraft, J., 2019. Chronology of Terra Firme formation in Amazonian lowlands reveals a dynamic Quaternary landscape. **Quaternary Science Reviews,** 210, 154–163.

Pupim, F. N., Sawakuchi, A. O., Mineli, T. D., Nogueira, L., 2016. Evaluating isothermal thermoluminescence and thermally transferred optically stimulated luminescence for dating of Pleistocene sediments in Amazonia. **Quaternary Geochronology,** 36, 28–37.

Ribeiro, L. M. A. L., Sawakuchi, A. O., Wang, H., Sallun Filho, W., Nogueira, L., 2015. OSL dating of Brazilian fluvial carbonates (tufas) using detrital quartz grains. **Quaternary International,** 362, 146–156.

Riffel, S. B., Vasconcelos, P. M., Carmo, I. O., Farley, K. A., 2016. Goethite (U–Th)/He geochronology and precipitation mechanisms during weathering of basalts. **Chemical Geology,** 446, 18–32.

Rodnight, H., Duller, G. A. T., Tooth, S., Wintle, A. G., 2005. Optical dating of a scroll-bar sequence on the Klip River, South Africa, to derive the lateral migration rate of a meander bend. **The Holocene,** 15, 802–811.

Sawakuchi, A. O., Hartmann, G. A., Sawakuchi, H. O., Pupim, F. N., Bertassoli Jr., D. J., Parra, M., Antinao, J. L., Sousa, L. M., Sabaj Perez, M. H., Oliveira, P. E., Santos, R. A., Savian, J. F., Grohmann, C. H., Medeiros, V. B., McGlue, M. M., Bicudo, D. C., Faustino, S. B., 2015. The Volta Grande do Xingu: Reconstruction of past environments and forecasting of future scenarios of a unique Amazonian fluvial landscape. **Scientific Drilling,** 20, 21–32.

Sawakuchi, A. O., Kalchgruber, R., Giannini, P. C. F., Nascimento, Jr. D. R., Guedes, C. C. F., Umisedo, N. K., 2008. The development of blowouts and foredunes in the Ilha Comprida barrier (Southeastern Brazil): the influence of Late Holocene climate changes on coastal sedimentation. **Quaternary Science Reviews,** 27, 2076–2090.

Sawakuchi, A. O., Mendes, V. R., Pupim, F. N., Mineli, T. D., Ribeiro, L. M. A. L., Zular, A., Guedes, C. C. F., Giannini, P. C. F., Nogueira, L., Sallun Filho, W., Assine, M. L., 2016**.** Optically stimulated luminescence and isothermal thermoluminescence dating of high sensitivity and well bleached quartz from Brazilian sediments: from Late Holocene to beyond the Quaternary? **Brazilian Journal of Geology,** 46(1), 209–226.

Sioli, H., 1984. The Amazon: Limnology and Landscape Ecology of a Mighty Tropical River and its Basin, **Kluwer Academic Publishers, ed. Dordrecht, Boston**.

Soares, E. A. A., Tatumi, S. H., Riccomini, C., 2010. OSL age determination of Pleistocene fluvial deposits in Central Amazonia. **Anais da Academia Brasileira de Ciências,** 82, 691–699.

Stuiver, M., Reimer, P. J., and Reimer, R. W., 2019, CALIB 7.1 [WWW program] at http://calib.org, accessed 2019-12-18.

Timar-Gabor, A., Vasiliniuc, S¸, Vandenberghe, D. A. G., Cosma, C., Wintle, A. G., 2012. Investigations into the reliability of SAR-OSL equivalent doses obtained for quartz samples displaying dose response curves with more than one component. **Radiation Measurements,** 47, 740–745.

Tsakalos, V., Dimitriou, E., Kazantzaki, M., Anagnostou, C., Christodoulakis, J., Filippaki, E., 2018. Testing optically stimulated luminescence dating on sand-sized quartz of deltaic deposits from the Sperchios delta plain, central Greece. **Journal of Palaeogeography,** 7, 130–145.

Wallinga, J., 2002. On the detection of OSL age overestimation using single-aliquot techniques. **Geochronometria,** 21, 17–26.

Wintle, A. G., Murray, A. S., 2006. A review of quartz optically stimulated luminescence characteristics and their relevance in single aliquot regeneration dating protocols. **Radiation Measurements,** 41, 369–391.

Wittmann, H., von Blanckenburg, F., Maurice, L., Guyot, L., Filizola, N., Kubik, P. W., 2010. Sediment production and delivery in the Amazon River basin quantified by in situ-produced cosmogenic nuclides and recent river loads. **Geological Society of America Bulletin B,** 30317–1.

Zuluaga-Gómez, M. A., Fitzgerald, D. B., Giarrizzo, T., Winemiller, K. O., 2016. Morphologic and trophic diversity of fish assemblages in rapids of the Xingu River, a major Amazon tributary and region of endemism. **Environmental Biology of Fishes,** 99, 647–658.

## Chapter 5: Summary conclusions

Chapters 2, 3 and 4 of this study provide characteristics of different luminescence signals (RF, VSL and OSL) of quartz from Brazilian fluvial rocks (ironstones) and sediments. All characteristics confirmed the use of the luminescence signals for provenance, first estimation of fluvial ironstones formation ages using existing luminescence method (SAR OSL) and the appraisal of the recently proposed VSL method to extending the dating range of Brazilian sediments using samples dated using existing OSL methods.

The general observation the work presented in chapter 2, is that the RF intensity differs between quartz from rocks and sediments, and among quartz from sediments with different provenances. The observed linear correlation between OSL, TL sensitivities and UV-RF emission intensity improved the understanding that the sensitization processes in nature might be due to the changes in recombination processes rather than changes in the charge trapping probability. From this correlation, this work also suggested for the first time the use of UV-RF emission intensity for provenance analysis in addition to other provenance proxies. It also supports the suggestion that a single process is involved in sensitization of both TL and OSL. However, further studies are recommended using samples from different provenances in order to confirm the use of the UV-RF signal as provenance proxy.

Chapter 3 investigates the characteristics of VSL signals of quartz from major fluvial systems within Brazil and the use of VSL signals in extending luminescence dating range of Brazilian sediments. VSL protocols used in this study showed that VSL signal of quartz could extend the dating range of fluvial deposits in Brazil especially in the cratonic settings where dose rates are relatively low. Here, it is recommended to use more samples as we observed the dependence of VSL signal on samples. In chapter 4, the OSL dating method was found to be feasible in dating ironstones deposits and the OSL ages are between ~60 ka and 3 ka. The estimated OSL ages of quartz improve the understanding of the genesis of ironstones and suggest that they are related with the Quaternary hydrology of the Xingu River. We recommend the use of single grain approach to determine the time of specific grain trapping, minimize the averaging effect and investigate the possible source of high overdispersion observed for same samples